D4

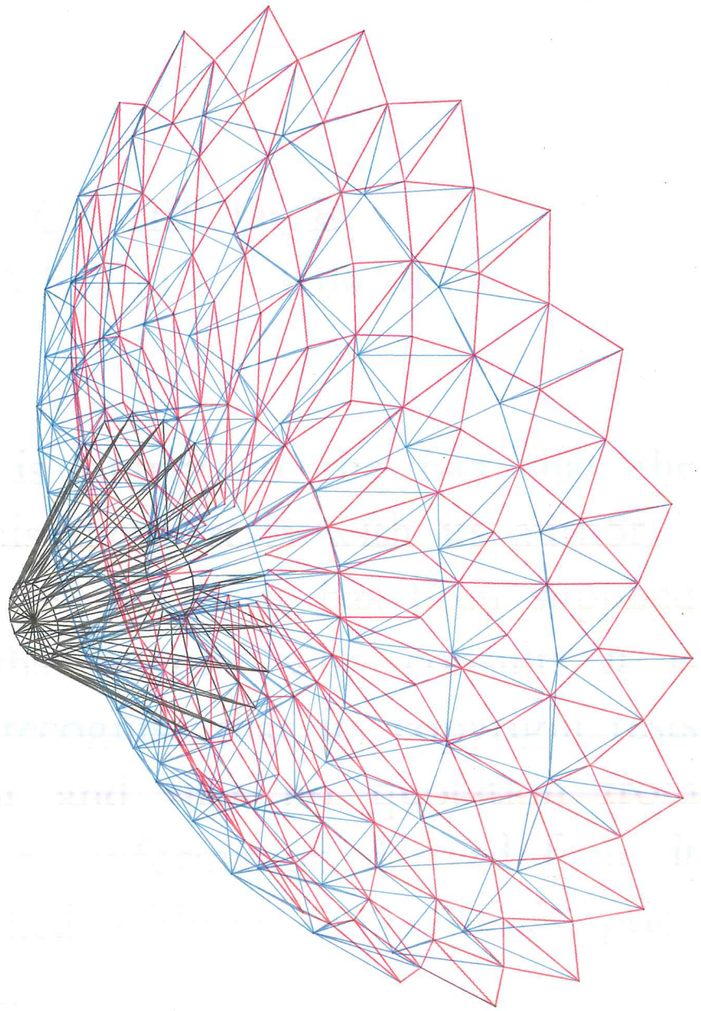

An early version of the homologically deforming cyclically symmetric dish structure for the U.K. Millimetre wave telescope.

PhD 11960

The Design of Homologically Deforming Cyclically Symmetric Structures

by

Timothy Smithers

A Dissertation submitted to the University of Cambridge for the degree of Doctor of Philosophy.

Darwin College
Cambridge

March, 1981

UNIVERSITY LIBRARY CAMBRIDGE

To Julie

Preface

The work presented here was carried out by the author between October 1977 and December 1980, while at the Cambridge University Engineering Department. The help and guidance of Dr R.K. Livesley, who supervised the work, is gratefully acknowledged, together with the support and encouragement received from Dr R.E. Hills of the Radio Astronomy Group at the Cavendish Laboratory, Cambridge - at whose suggestion the work was started - and Messrs. B. Colyer and A. Middleton of the Rutherford and Appleton Laboratories, Chilton, Oxfordshire. Thanks is also due to Mr K.N. Warner, who as manager of the computer used for much of the work presented here, gave constant help and advice on all computing matters. The author considers it a privilege to have been given the opportunity to work with such able people. Lastly, the financial support of the Science Research Council and the Engineering Department Rex Moir Fund is gratefully acknowledged.

In accordance with the statutes, it is declared that the contents of this thesis are original, except where reference is made to the work of others. No part is collaborative, nor has it been, or is it being, submitted, in part or in whole, for any other degree at this or any other University.

[redacted]

Darwin College
Cambridge

March 1981

Summary

It can be shown that for a given diameter of a radio telescope, whose structure is designed to be as stiff as possible, there is a minimum wavelength at which it can operate. Below this limit the distortion of the parabolic reflecting surface, produced by the gravitational deformation of the surface supporting structure, becomes too large for it to act as a sufficiently good reflector. One way of passing this gravitational wavelength limit is to design a surface supporting structure which deforms homologically, as the telescope is tilted. In other words, the surface supporting structure is designed so that its gravitational deformation is such that a parabolic reflecting surface is always maintained. An interactive computer supported design procedure, for homologically deforming millimetre wave telescope structures is presented, and demonstrated. It uses an iterative improvement scheme to deal with the non-linear and mixed continuous-discontinuous variable problem created by the design of practical homologically deforming millimetre wave telescope structures.

The most suitable form for a potentially homologically deforming telescope structure is a purely cyclically symmetric one. However, for millimetre wave telescopes this form of structure presents practical difficulties, so a region of structural non-cyclic symmetry is introduced. To enable the complete telescope structure to be analysed, yet still to take advantage of its high degree of cyclic symmetry, to reduce the size of the analysis problem, an analytical method is presented which is able to deal with a cyclically symmetric structure having a region of structural non-cyclic symmetry and which is subjected to general non-cyclically symmetric loads.

Contents

List of Symbols

D - Parabolic antenna or telescope diameter

λ_g - Gravitational wavelength limit

k - Active/Passive weight ratio

w_{ps} - Passive antenna or telescope structure weight

w_{ac} - Active antenna or telescope structure weight

α - Antenna or telescope elevation (pointing) angle

Δf - Focal length change

x_o - x-direction shift of paraboloid origin

z_o - z-direction shift of paraboloid origin

ϕ - Paraboloid axis tilt

} homology parameters

n - Order of structural cyclic symmetry

$\bar{a}^k = \exp\{-i2\pi k/n\} = \cos(2\pi k/n) - i \sin(2\pi k/n)$

$a^k = \exp\{i2\pi k/n\} = \cos(2\pi k/n) + i \sin(2\pi k/n)$

(x_i, y_i, z_i) - ith segment co-ordinate axes

$\underline{P}_i^{(j)}$ - ith segment load vector relative to the jth segment co-ordinate system

$\underline{d}_i^{(j)}$ - ith segment displacement vector relative to the jth segment co-ordinate system

$\underline{K}_{ij}^{(k)}$ - The stiffness matrix of connections between the ith and jth segments relative to the kth segment co-ordinate system

$\underline{T}_{mn}$ - The transformation matrix from the mth segment co-ordinate system to the nth segment co-ordinate system

$\underline{P}_{\tau_i}$ - ith segment transformed load vector

$\underline{d}_{\tau_i}$ - ith segment transformed displacement vector

$\underline{K}_{\tau_{ij}}$ - The ijth transformed stiffness matrix

$\underline{\underline{P}}$ - Real space super load vector

$\underline{\underline{d}}$ - Real space super displacement vector

$\underline{\underline{K}}$ - Real space super stiffness matrix

$\underline{\underline{P}}_\tau$ - Transformed, Complex Fourier space super load vector

$\underline{\underline{d}}_r$ - Transformed, Complex Fourier space super displacement vector

$\underline{\underline{K}}_r$ - Transformed, Complex Fourier space super stiffness matrix

$\underline{\underline{S}}$ - Super transformation matrix

A symbol with a bar over the top represents the complex conjugate of the unbarred symbol.

n_{sy} - The number of surface support points per cyclic segment

C_z - The number of conditions which must be satisfied for the support points of one cyclic segment to lie on a zenith pointing parabolic surface

C_h - The number of conditions which must be satisfied for the support points of one cyclic segment to lie on a horizon pointing parabolic surface

P_y - The number of joints per cyclic segment

D_f - The number of available design variables (per cyclic segment)

G - The gain of a parabolic reflector

G_o - The no error gain

ε - The r.m.s. signal path length variation

η_s - The reflector surface efficiency ($= G/G_o$)

ε_s - The r.m.s. signal path length variation produced by the surface supporting structure alone

σ_z - Zenith pointing r.m.s. signal path change error

σ_h - Horizon pointing r.m.s. signal path length change error

σ_o - The overall r.m.s. signal path length change error, or homology error

List of Figures

List of Tables

Key words

Homological Deformation

Millimetre wave telescopes

Radio telescopes

Cyclic Symmetry

Computer Aided Design

Structural Design

Chapter One - Introduction and Background

1.0 - Introduction

In recent years, interest has arisen in the development of parabolic antenna systems capable of receiving and transmitting very high frequency radio waves. This interest reflects the advances sought in a number of different but related areas which include: high density radio communication links, high resolution radar, long range tracking of space craft and, in particular, millimetre wave astronomy.

The problems associated with the design and construction of antenna systems which operate at very short wavelengths, can be divided into two areas: that of building suitable electronic receiving, amplification and control equipment, and the design and construction of the filled aperture antennae required. It is with certain aspects of this second structural area that the work presented here is concerned, particular attention being given to the problem of designing millimetre wave radio telescope structures.

The technology for building large fully steerable parabolic antennae, of the filled aperture type, was first developed for the construction of the 76.2 m (250 ft.) radio telescope at Jodrell Bank [1] in 1958. Considerable improvements in the methods of design and construction have since been made as the number of large steerable telescopes designed and built throughout the world has increased [2,3]. These developments have led to telescopes having improved accuracy and efficiency, which has enabled astronomers to observe at shorter and shorter wavelengths.

The limits of these conventional methods of design and construction have now been reached. Therefore, new ways of dealing with the problems created by the very high surface accuracy requirements

UNIVERSITY LIBRARY CAMBRIDGE

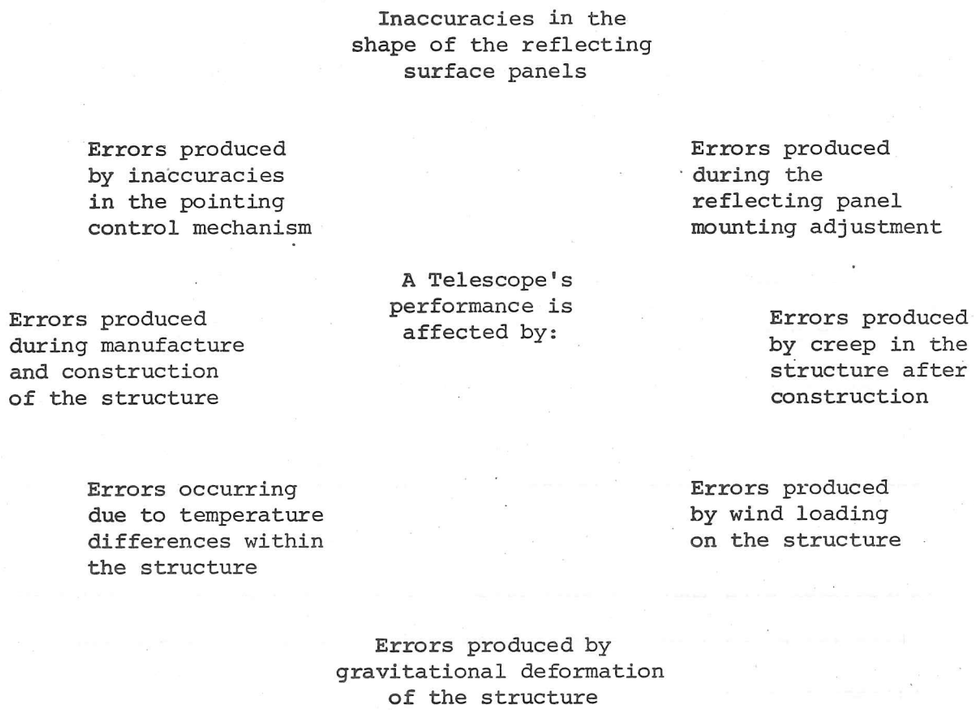

Fig.1.1.1 - Structural factors affecting the performance of a Radio Telescope

of millimetre wave antennae, are having to be developed.

1.1 - Structural Aspects of Radio Telescopes

The fundamental aim in the design of any telescope is to obtain as high a sensitivity and resolving power as possible. For parabolic radio antennae the sensitivity is proportional to the reflector diameter 'D', and its resolving power is proportional to D^2 (for a given wave length). Therefore the aim of radio telescope designers has been to build the largest structure which can support a sufficiently accurate reflecting surface. The surface accuracy requirement is governed by the frequency range in which the telescope is to operate.

Although designs do vary, radio telescope structures can generally be described as having a circular, framework type, dish structure, onto which a large number of individual panels are mounted to form the parabolic reflecting surface. This dish structure is supported, by a secondary structure, in such a way that it can be pointed in any direction - this often takes the form of a two point elevation axis mounting (see reference [1] for example). The reflecting surface is formed from individual panels because of the impracticality of building it as one continuous reflector (as in optical reflecting telescopes), even for quite small dishes.

The overall performance of these telescope structures are affected by many different factors (see fig.1.1.1), all of which must be adequately accounted for in any final design. Now the errors introduced by most of these structural factors can be (and indeed have been) reduced by using improved manufacturing and construction techniques and new materials and measuring instruments. However, there is one factor which cannot be reduced in this way, and that is the effect of gravity - in other words, the deformation of the telescope structure under its

own weight - which directly affects the performance of the reflecting surface.

1.2 - Gravitational Deformation and the Observable Wavelength Limit

For a radio telescope of a given diameter, which depends on the stiffness of its structure to maintain an accurate reflecting surface, a lower limit on the observable wavelength is set by the gravitational deformation it suffers. This is because the gravitational deformation changes the shape of the surface, formed by the reflecting panels, as the telescope is tilted (in elevation), and so the individual reflecting panels are not kept on the required parabolic surface. Failure to maintain the panels on a parabolic surface distorts the phase front of the reflected signals which causes deviations in the desired radiation pattern of the antenna. This effect can be quantified in terms of an r.m.s. surface error. Now for a given r.m.s. surface error, there is a minimum wavelength, or maximum frequency, at which the surface will behave as a coherent reflector and at which the telescope can be considered useful.

Von Hoerner [4] has shown that for a given wavelength there is a telescope diameter above which no structure can be made sufficiently stiff for its gravitationally induced surface errors to be small enough for useful operation of the telescope to be possible. In other words, a minimum observable wavelength λ_g (mm) can be defined for a telescope of diameter D (m), and is given by:

$$\lambda_g \text{ (mm)} = 53\ k\ \left(\frac{D \text{ (m)}}{100}\right)^2, \qquad (1.2.1)$$

where k is the active/passive weight ratio.

1.3 - The Active/Passive Weight Ratio

The active/passive weight ratio, k, is a measure of how much of the total telescope structure contributes to the stiffness of the surface support structure. It is important because the greater the weight of the parts which do not directly oppose the surface deformations, the greater the gravitational wavelength limit. k is therefore defined as:

$$k = \frac{W_{ps} + W_{ac}}{W_{ac}} , \qquad (1.3.1)$$

where W_{ps} - the passive weight - is the weight of structural components which do not oppose the gravitational deformation, and W_{ac} - the active weight - is the weight of those components which do. In practice it is difficult to obtain a value of k below 1.3 and it is more typically in the range 1.4 to 4.3 [5]. Figure 1.3.1 presents the variation of λ_g for a range of values of D as predicted by equation (1.2.1), using a k value of two.

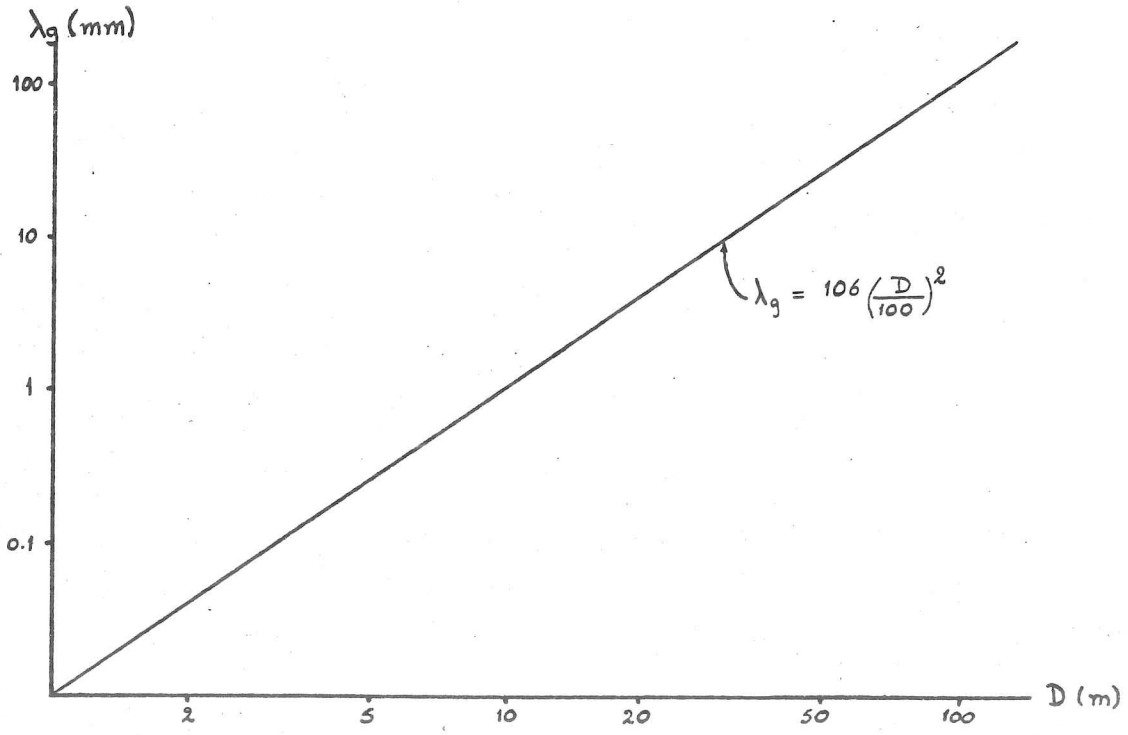

Fig.1.3.1 - The variation of λ_g with D for a k value of two.

1.4 - The Gravitational Diameter Limit and Methods of Exceeding it

When considering the structural aspects of radio telescope design, the gravitational wavelength limit (for a given diameter), see equation (1.2.1), is more usefully thought of as a gravitational diameter limit (for a given wavelength). It can therefore be seen that the gravitational deformation of a telescope structure places an upper limit on its resolving power and sensitivity at a given wavelength by limiting its diameter. For telescopes designed to observe in the metre and high centimetre wavelength range, this gravitational diameter limit does not represent a practical limitation, since other factors impose smaller limits, such as the financial cost. However, as the wavelength at which the telescope is to operate becomes shorter, so the gravitational wavelength limit becomes significant. This means that some means of exceeding this diameter limit must be found before a telescope's resolving power and sensitivity can be improved.

A number of methods for passing this diameter limit (or the wavelength limit) have been proposed [6,7,8,9,10,11]. These can be described either as a means of artificially increasing the stiffness of a structure, by compensating for, or correcting, the gravitational deformation; or the use of homological deformation to maintain a parabolic surface. 'Homological deformation' is a term first used by von Hoerner [4] to describe the behaviour of a structure which deforms in such a way as it is tilted, that at any angle of elevation the surface panels will lie on a perfect paraboloid. In other words, the surface support structure is designed to continuously deform the reflecting panels from one paraboloid into another (having a different axis and focal length), as it is tilted in elevation.

A comparison of the basic requirements of artificial methods for maintaining an accurate reflecting surface beyond the gravitational

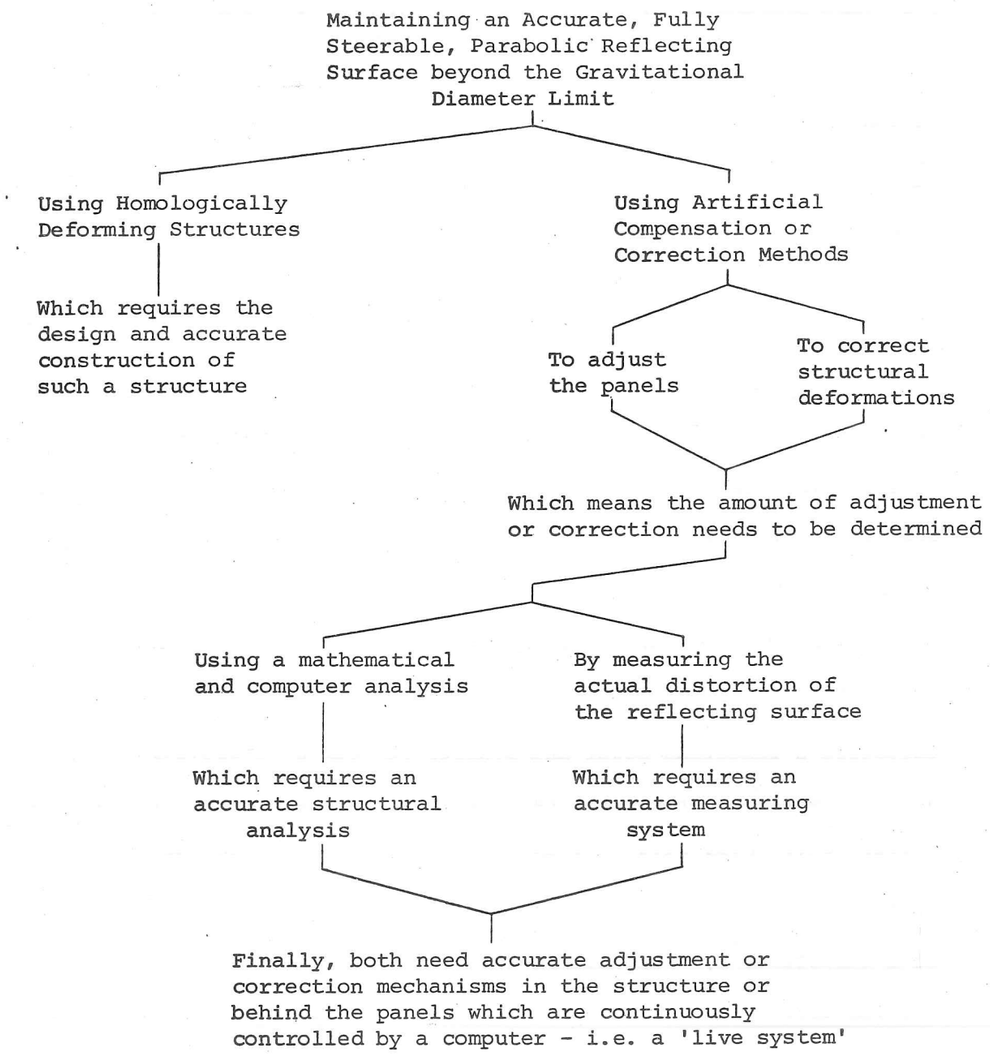

Fig.1.4.1 - Methods for exceeding the gravitational diameter limit.

diameter limit and the method of homological deformation, is presented in figure 1.4.1. The automatic adjustment of the reflecting panels, by controlled jacks placed at their support points, is referred to as 'displacement compensation'. And the use of variable prestress, produced by means of control cables or hydromechanical devices, to correct the deformation of the panel support structure, is referred to as 'force compensation'.

From the comparison made in figure 1.4.1, it can be seen that an artificial method of maintaining an accurate reflecting surface presents a much greater problem, in terms of the mechanical and electronic components required, than the use of a homologically deforming structure. Although the technological capability exists for building a telescope using one of the artificial methods, it has yet to be demonstrated that they can be made to work in practice. Indeed, of the several projects started, which planned to use such techniques, none has been successful - the main reason being the failure to devise a satisfactory system to continuously monitor the reflecting surface. In any case, artificial methods do not present as elegant a solution to the problem of passing the gravitational diameter limit, as a homologically deforming structure does - which requires no external mechanisms of continuous control system. This method takes advantage of the fact that it is not really the deformations of the panel support points themselves that matter, but their deviation from a parabolic surface. In other words, it is not necessary to maintain the support points (and thus the panels) on the same paraboloid, as the telescope is tilted, which is what the artificial methods attempt to do. Changes of focal length and pointing direction, during homological deformation, can easily be allowed for by adjustment of the feed or secondary reflector (in the case of a Cassegrain arrangement).

1.5 - Homologically Deforming Radio Telescope Structures

The homological deformation of radio telescope structures is not new. In fact it can be said that all parabolic dish antennae possess some degree of homological behaviour. However, it was not until von Hoerner's early work [4] in 1967 that it was formally defined and proposed as a principle to be used in the design of telescopes exceeding the gravitational diameter limit. The problem with designing a homologically deforming structure is that it is not possible (without considerable experience of their design and some luck) to design a structure, whose homological deformation behaviour is sufficiently good, for it not to need improving. This situation is further complicated by the fact that there is not a linear relationship between structural alterations and the effect they have on the homological behaviour of the reflecting surface. Methods for designing such structures will therefore usually contain some form of iterative improvement procedure.

The method developed by von Hoerner [12], initially for the design of very large radio telescopes of 100 m (300 ft) diameter and more [4,10], is based on an automatic iteration procedure which is performed using a computer. This linearized iterative method has first to be given an initial structure which represents a 'guess' at the final solution - the structure being assumed to be of a pin-jointed, tubular framework type. In each iteration step the cross-sections of all the members are changed simultaneously by such amounts that the deviation of the supported reflecting surface, from a best-fit paraboloid, becomes zero. So that the problem is uniquely defined, the method selects (out of all the possible homology solutions) that solution which is most similar to the first guess. It uses a generalized 'Newton's method' for finding the zero point of a function, the quantity whose zero is required being the r.m.s. deviation of the

surface support points from the best-fit paraboloid. The combined task of achieving homology and selecting the solution closest to the initial structure is then solved using the method of Lagrangean multipliers.

The important distinction between a mathematical and a physical solution is also introduced - a physical solution being defined as one in which all the cross-sections are positive. This is necessary because it can be shown that all stable structures have mathematical solutions which do not necessarily contain only positive cross-section values - negative and complex values also being possible.

Further work has been published by Zarghame [13] and Kowaleski and Ziebrath [14], who propose that for small telescopes of 25 m (80 ft) diameter, or less, the reflecting surface should be fixed to the supporting structure (rather than mounted on it), thus enabling it to contribute to the overall stiffness of the structure. However, both these pieces of work have remained as purely theoretical contributions, neither of them being implemented in a complete telescope structure design procedure comparable to von Hoerner's.

Although von Hoerner has used his automatic search procedure to produce complete telescope structure designs having diameters ranging from 100 m to 25 m , none of these has actually been built - largely due to lack of funds rather than any other reason. It will also be shown that simply varying all the member cross-sections, to obtain a homologically deforming solution, leads to some practical difficulties in the case of small dishes (15 - 30 m diameter) , designed for millimetre wave observations. However, an impressive demonstration of the feasibility of a large homologically deforming telescope, for centimetre wave observations, is the 100 m dish at the Max-Plank Institut fur Radioastronomie, just outside Bonn, West Germany [15,16]. This is the first Radio Telescope to be designed and built using the

principle of homological deformation and is also the world's largest fully steerable dish. Although it is a very large structure, it is quite a simple design - to which much of its success may be attributed. The surface supporting dish structure is formed from 24 identical radial cantilevered ribs which are held together by a series of ring beams and cross-bracing members. It is perhaps best likened to an open umbrella which has been blown inside out - thus forming a dish, rather than a dome as intended. Like an umbrella, this cyclically symmetric dish structure is held at two points on the axis of cyclic symmetry. This, on axis, two point support is achieved using an octahedron type structure which provides the secondary reflector support (tetrapod) and elevation circle structure - the elevation bearings being placed at two corners of the octahedron (see ref.15). The major advantage of such an on axis support, is that it removes the non-homological astigmatism [17] produced by supporting a dish at two elevation points off the axis, as is the case in many previous designs - Jodrell Bank being a good example (see ref.1). By varying the cross-sections of single members and groups of members of an initial design, the deviation of the surface deformation from the required homological form was reduced to a sufficiently small value. Although similar to von Hoerner's approach for finding homological solutions, this cross-section variation procedure was carried out by hand - rather than automatically.

1.6 - Homologically Deforming Millimetre Wave Telescopes

In order to achieve high resolution a millimetre wave telescope does not need a dish nearly as large as those of telescopes which observe at the longer centimetre and metre wavelengths. However, for a telescope structure designed using the conventional 'stiffest structure' philosophy, the gravitational deformation still imposes an

unacceptably small diameter limit, and thus resolving power. Now although the principle of homological deformation was first used in the design of large radio telescopes, for observations in the low centimetre wavelength range (see table 4, ref.10), it also provides a means by which high resolution millimetre wave telescopes may be built. The problems encountered in the design and construction of a homologically deforming millimetre wave telescope are, however, rather different from those of a large dish - like the one at Bonn. This is mainly because the accuracy of the reflecting surface required for successful millimetre wave observations is at least an order of magnitude greater than that required by telescopes observing centimetre waves.

The work presented here is therefore primarily concerned with the design of homologically deforming millimetre wave telescope structures and was started at the suggestion of members of the U.K. Millimetre Wave Telescope Project. This project's aim is to design and build a 15 m diameter dish which is capable of observing waves as short as 0.35 mm - the shortest waves in the millimetre range to penetrate the earth's atmosphere (in good observing conditions). It is to be built on Las Palma in the Canary Islands at a height of 2400 m - to get above most of the water vapour in the atmosphere which absorbs millimetre waves - as part of the Northern Hemisphere Observatory. A diameter of 15 m for the parabolic reflector was chosen in order to give good resolution at 3 mm wavelength observations (and so compete with existing telescopes), but not to make the goal of efficient operation in the submillimetre range (0.8 - 0.35 mm) too difficult.

As a measure of how much such a telescope would depend on homological deformation to achieve the required reflecting surface accuracy, the diameter of 15 m can be compared to the gravitational

diameter limit of 6.4 m at a wavelength of 0.35 mm , assuming a k value of 1.6 (from equation 1.2.1). Apart from the gravitational deformation, there are other environmental conditions, such as wind loading and temperature differences (which occur in the structure as a result of differential heating and cooling), that can significantly affect the accuracy of the reflecting surface. These effects may be removed, or at least substantially reduced, by placing the telescope in a Radome or some other form of protective housing (similar to optical telescopes) - which is what is proposed for the U.K. millimetre wave telescope. This then leaves the gravitational deformation to be dealt with, and so what follows is a method for designing homologically deforming millimetre wave telescope structures.

1.7 - References

1. Husband, H.C. - The Jodrell Bank Radio Telescope, Proc.Inst.Civ.Engrs. Paper no. 6370, Jan. 1958, pp.65-86.

2. Hey, J.S. - The Evolution of Radio Astronomy, Elek Science, London, 1973.

3. Mar, J.W. and Liebowitz, H. (Eds.) - Structures Technology for Large Radio and Radar Telescope Systems, MIT Press, 1969.

4. Von Hoerner, S. - Design of Large Steerable Antennae, Astronomical J., vol.72, no.1, Feb. 1967.

5. Calculated using information in table 1, page 32 of reference [3] - Weiss, H.G.

6. Rothman, H. and Chang, F.K. - Maintaining Surface Accuracy of Large Radio Telescopes by Active Compensation, see ref.[3], page 273.

7. Weidlinger, P. - Control of RMS Surface Error in Large Antenna Structures, see ref.[3], page 287.

8. Weiss, H.G. - Design Studies for a 440 ft Diameter Radio and Radar Telescope, see ref.[3], page 29.

9. Weiss, H.G., Fanning, W.R., Folino, F.A. and Muldoon, R.A. - Design of the Haystack Antenna and Raydome, see ref.[3], page 151.

10. Von Hoerner, S. - Homologus Deformation of Tiltable Telescopes, see ref.[3], page 311.

11. Von Hoerner, S. - Radio Telescopes for Millimetre Wavelengths, Astron. & Astrophys., vol.2, 1975, pp.1-6.

12. Von Hoerner, S. - Homologus Deformation of Tiltable Telescopes, J.Struct.Div. Proc. A.S.C.E., ST.5, Oct. 1967, pp.461-485.

13. Zarghame, H.S. - Minimum Weight Design of Enclosed Antennae, J.Struct.Div. Proc. A.S.C.E., ST.6, June 1969, pp.1139-1152.

14. Kowaleski, J.F. and Zeibrath, H.A. - Homologus Deformation of Stiffened Shells for Radio Telescope Structures, J. AGARD, Conf.Proc. n.123, Nov. 1973.

15. Hachenberg, O. - The 100 m Radio Telescope of the Max-Plank Institute for Radio Astronomy in Bonn, see ref.[3], pp.13-27.

16. Hachenberg, O., Graht, B.H. and Wielebinski, R. - The 100 metre Radio Telescope at Effelsberg, Proc. IEEE, vol.61, no.9, Sept. 1973, pp.1288-1295.

17. Von Hoerner, S. - Gravitational Deformation and Astigmatism of Tiltable Radio Telescopes, IEEE Trans. on Aut. & Prop., AP-23, 1975, p.689.

Chapter Two - A Preliminary Look at the Problem

2.0 - Introduction

As with all engineering problems, a preliminary look at the nature of the problem to be solved is necessary. This is so that the various components of its solution may be identified. A complete solution may then be obtained (or at least attempted) via the solving of a number of smaller, more manageable, problems. Now the problem considered here may be generally defined as: the formulation of a method for designing a homologically deforming structure to support the reflecting surface panels of a parabolic reflector, within the practical constraints imposed by having to accurately build such a structure. Before considering what form this design method should take however, it is worth considering in some detail the nature of the loading and type of structures involved.

2.1 - Structural Loading

The loading to which a surface supporting structure is subjected can be divided into two types: unpredictable environmental loads (arising from wind forces and temperature differences occurring within the structure), and the predictable gravitational (self weight) loads. Now a structure cannot be expected to deform homologically when subjected to unpredictable loads, but it can when predictable loads are acting on it. Thus, only the structural deformation arising from the gravitational loading can reasonably be considered in deciding how close to homological a particular structure's behaviour is. The unpredictable loads must be accounted for by placing minimum strength requirements on the overall design, together with the use of highly reflective paint and the avoidance of large differences of thermal mass

in the structure - to reduce the temperature differences that occur within a structure, especially when working in direct sunlight. Alternatively, as has been mentioned, for small telescopes they can be removed, or at least greatly reduced, by placing the telescope in a Radome or protective housing.

When in use a telescope may be required to point in any direction from the zenith (straight up) to horizon pointing (or a few degrees above in practice). As a result, the gravitational loading will vary from being parallel with the telescope dish axis, at zenith pointing, to being perpendicular to it at horizon pointing. Now for any other pointing direction, between zenith and horizon, the gravitational loading can be resolved into components parallel with, and perpendicular to, the telescope axis (see fig.2.1.1). Thus, the gravitational

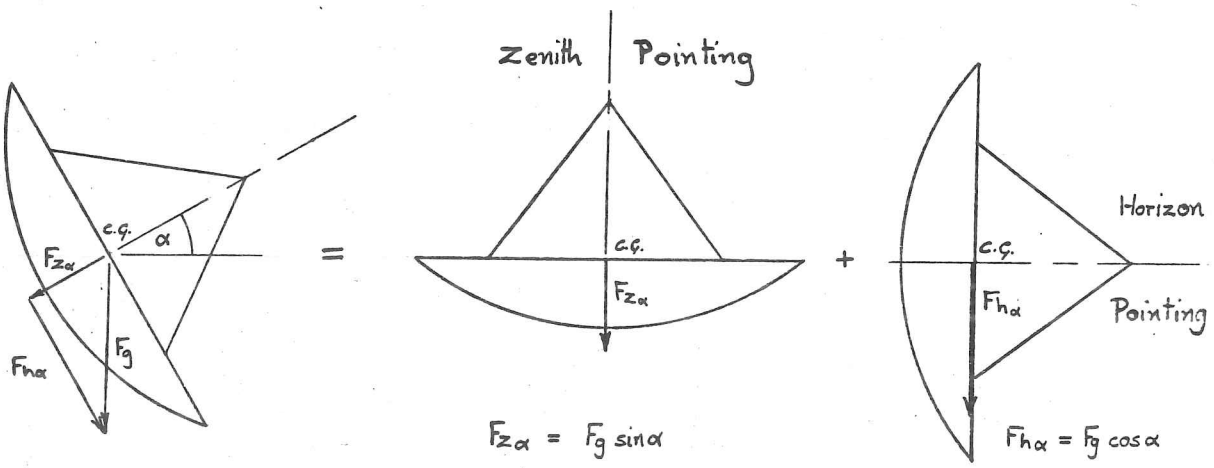

Fig.2.1.1 - Zenith and Horizon pointing components of the gravitational loading at an angle of elevation α.

deformation at any pointing direction can be resolved into zenith and horizon pointing components (assuming linear elastic behaviour of the structure). This means that if a structure can be designed to deform homologically in the two cases of zenith pointing and horizon pointing,

it will deform homologically at any other pointing direction. It is therefore only necessary to consider the two cases of zenith and horizon pointing in the deformation analysis of a surface supporting structure.

Having established the form of the loading under which a structure must satisfy the homology condition, the next stage is to decide what type of structure will deform in a 'potentially' homological way for both zenith and horizon pointing load cases. In other words, for what type of initial structure will the required degree of homological behaviour be most easily obtained by making small alterations to it. To discover this, the form of what constitutes perfect homological deformation for each loading case must be defined.

2.2 - Homological Deformation and Structural Form

Consider first the zenith pointing case. Here the gravitational loads act vertically downward, parallel with the parabolic dish axis. Now under this loading, the simplest form of deformation of the parabolic surface, which gives a new parabolic surface, is one which results in a downward shift of the origin and an increase in focal length. In other words, one in which an opening out of the initial (gravity off) parabolic surface and a downward displacement of its origin occurs (see fig.2.2.1). Thus, for a structure supporting a reflecting surface consisting of individual panels arranged in a number of identical segments, this implies a cyclically symmetric deformation pattern of the panel support points.

The most obvious form that a structure can take, which is required to deform cyclically symmetrically when subjected to a cyclically symmetric loading (as the zenith pointing gravitational loads are), is a cyclically symmetric one. This structural cyclic symmetry can most

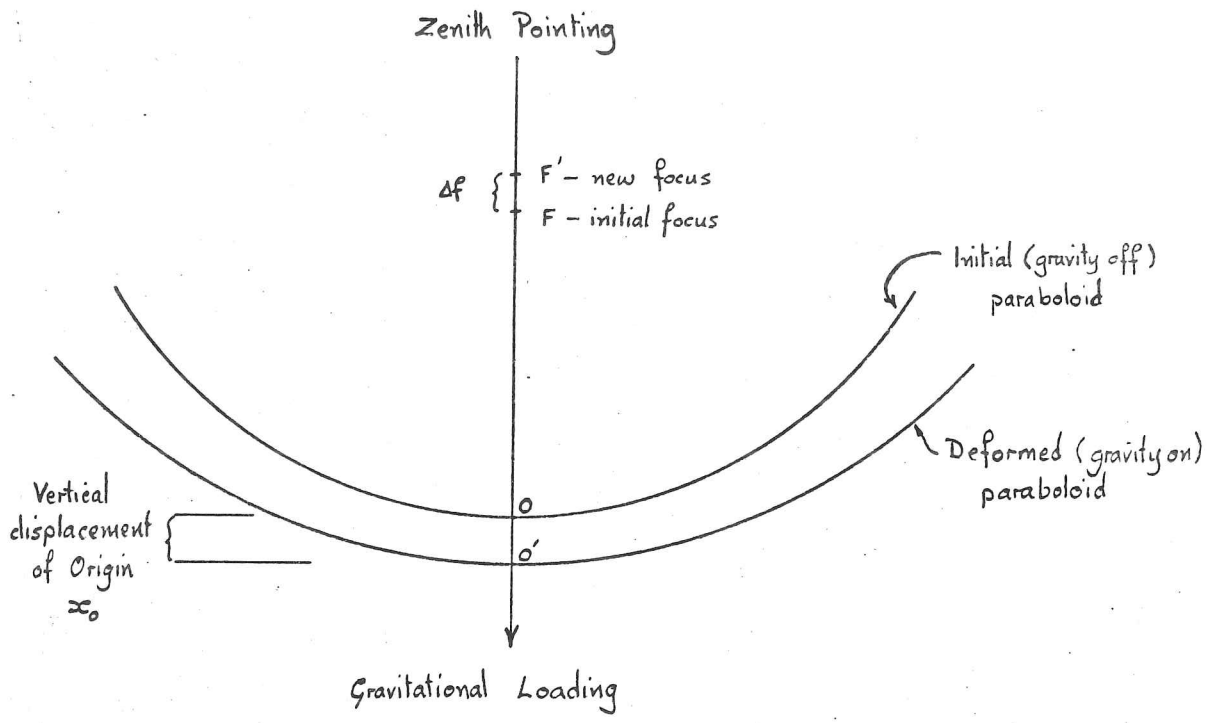

Fig.2.2.1 - The zenith pointing gravitational loads produce an increase in the focal length and a vertical shift of the origin (which may be up or down depending on the particular telescope structure) for perfect homological deformation.

conveniently be achieved using a large number of identical, cross-braced, cantilevered trusses, each one supporting an identically panelled reflector surface segment, and all connected at points on the central axis - from where the complete dish structure must be mounted to preserve the cyclic symmetry.

Consider now the horizon pointing case, where again the gravitational loading acts vertically downward, but this time perpendicular to the initial paraboloid axis. The loading is thus anti-symmetric about a horizontal plane through the initial paraboloid axis. It follows from this, that the deformation of the structure above this horizontal plane has the opposite z-directional displacement to that of the structure below the plane. In this case, the simplest form of reflector surface deformation, which gives a new paraboloid, is one in which there is a downward tilting of the initial paraboloid axis,

plus downward shift of its origin (see fig.2.2.2). For this form of

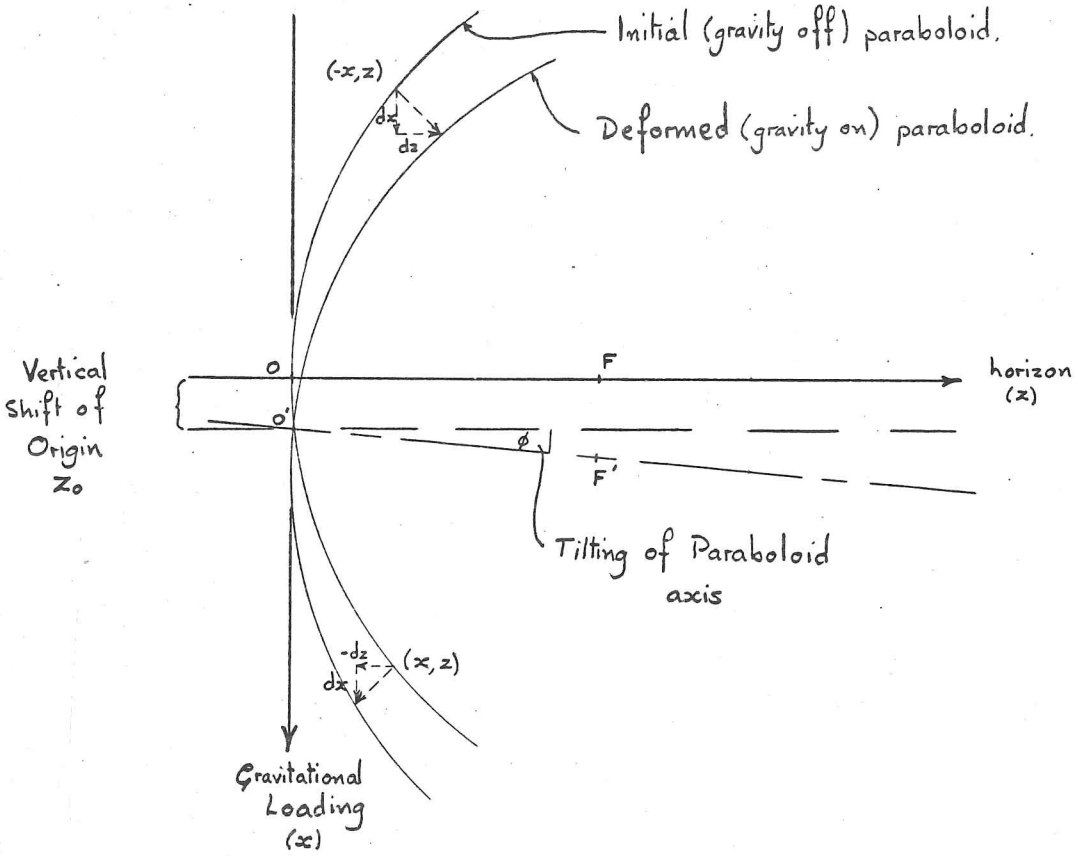

Fig.2.2.2 - The horizon pointing gravitational load produces a vertical shift (up or down) of the origin and a tilting of the initial paraboloid axis, for perfect homological deformation.

deformation to occur, surface points in the vertical plane through the origin must remain in that plane during deformation, and surface points in the horizontal plane through the origin must remain in a plane perpendicular to the initial paraboloid axis. Now it can be shown (see Appendix 2.1) that a cyclically symmetric radial cantilever type structure, held at points on its axis, also deforms in this way when subjected to an anti-symmetric loading, and so represents a 'potentially' homologically deforming structure. From the description of the 100 m Bonn Telescope given earlier, it can be seen that this is also the reasoning behind its cyclically symmetric dish design. This practical demonstration of the successful use of this type of structure in the

UNIVERSITY LIBRARY CAMBRIDGE

design of a homologically deforming telescope provides further justification for its use in smaller millimetre wave telescope structures.

There is, however, an important difference between large radio telescopes and the smaller millimetre telescopes, which results from having to place the receiving equipment at the centre of a millimetre wave telescope structure, behind the primary reflecting surface (see fig.2.2.3). This is because the receiving equipment used for millimetre

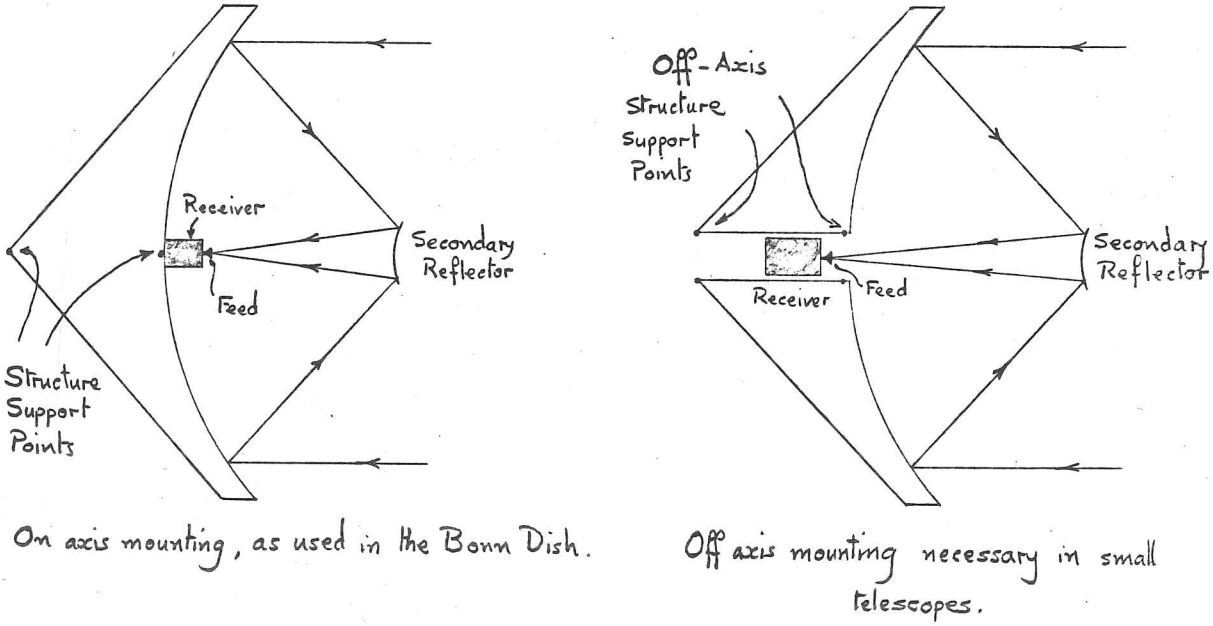

Fig.2.2.3 - The different Cassegrain reflector arrangements necessary to place receivers in the middle of the telescope structure.

wave reception, is rather more bulky than that used for longer wavelength observations. Providing a large enough space behind the reflector to do this means that the surface supporting dish structure can no longer be mounted at two points on the telescope axis - as should ideally be the case. A further problem arises from the fact that in order to provide the reflector surface accuracy required for good millimetre wave observations, the deformation of the elevation mounting structure, though small, has also to be taken into account when assessing the homological performance of a structure. Now, if this problem, and that

of not being able to use a two point on axis mounting for the dish structure, is not to introduce unacceptable non-homological deformation effects, this particular part of the structure will have to be very carefully designed. This means that a design procedure which enables the cyclically symmetric, homologically deforming, surface support structure, and the (non-cyclically symmetric) central elevation mounting structure, to be analysed as one structure, should prove superior to those that require them to be considered separately.*

2.3 - An Outline for a Design Procedure

Having established that a sufficient condition for homological deformation at any angle of elevation (pointing direction) is that the surface support structure deforms homologically in the two cases of zenith and horizon pointing, and also having decided on the most suitable form of such a structure, an outline for a design procedure may now be formulated.

In section 1.5 it was explained that the design of a homologically deforming structure was essentially a matter of trial and error and that any method for their design should contain some form of iterative, first guess, improvement scheme. In other words, the problem of designing a homologically deforming structure is, in common with many engineering problems, one of trying to improve an initial design. The design procedure must therefore contain a loop which has an entry point for the initial design and an exit point for the design which satisfies the homology requirement. Figure 2.3.1 presents such a design loop in the form of a flow diagram.

---

*Which is how many of the existing designs for millimetre wave telescopes have been produced.

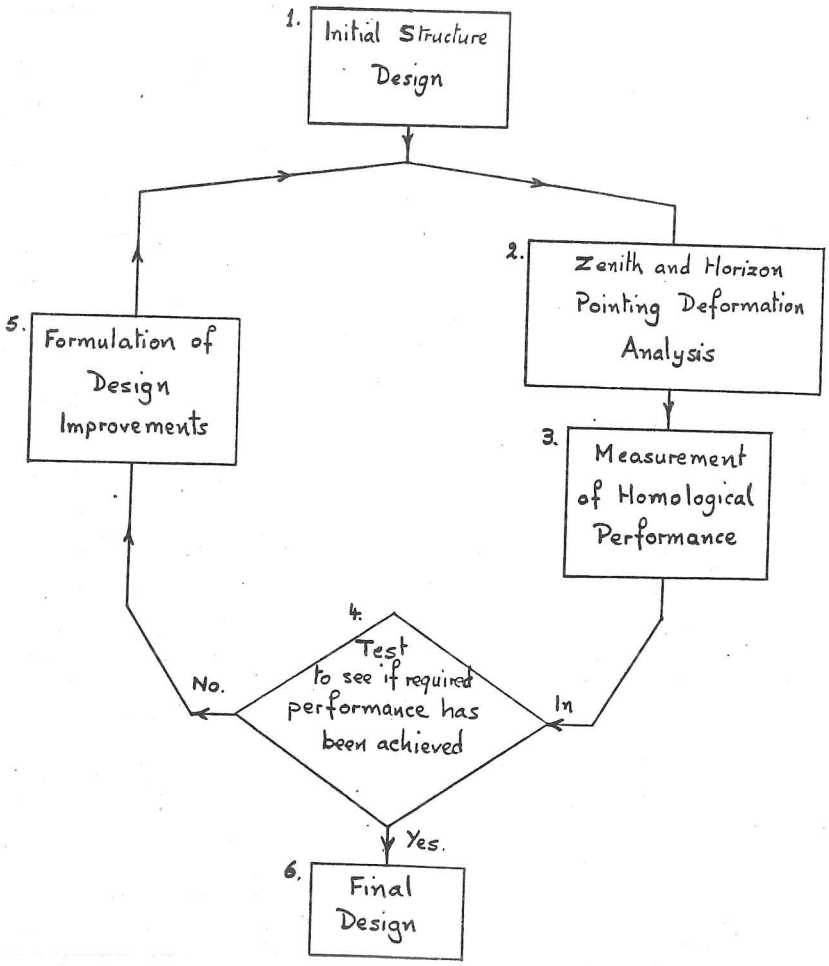

Fig.2.3.1 - Homologically Deforming Structure Design Procedure.

As a result of the need to produce an initial guess at the solution, it is important that the design procedure not only carries out the five stages of the design loop accurately, but also that it does this in as short a time as possible. This is so that a designer can use the same design procedure to gain the necessary experience of what constitutes good potentially homologically deforming structures, before attempting a final design. Now the stage which is likely to take the longest time to complete in each cycle of the loop is number five - the formulation of design improvements. However, since the time taken at this stage is largely dependent on the user of the design procedure, it is not possible to reduce the cycle time of the loop (stages 2, 3, 4 and 5) at this stage. It is possible to do this though,

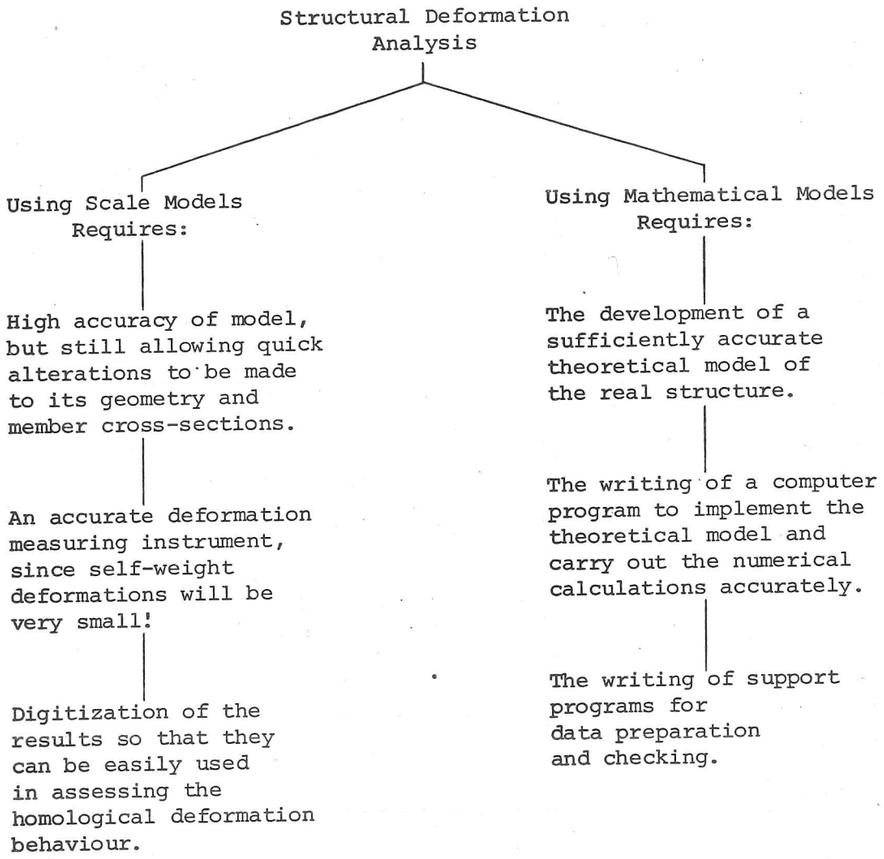

Fig.2.4.1 - Details of Scale Model and Mathematical Model Deformation Analysis Methods.

with the other three stages - 2, 3 and 4. Of these the one which will take the longest to complete is stage two - the zenith and horizon pointing deformation analysis. It is therefore desirable that the quickest suitable means of carrying out this stage is found.

2.4 - Structural Deformation Analysis

There are basically two ways of determining the gravitational deformation of a structure: by the testing of scale models or the use of mathematical modelling techniques. The details of what is involved in using each of these methods are summarized in figure 2.4.1.

It can be seen from figure 2.4.1 that the use of scale models does not lend itself to a fast design loop situation. Another disadvantage is the difficulty of successfully modelling self weight conditions - although this could be overcome by placing the model in a large centrifuge. However, this would considerably increase the already difficult instrumentation problem. This method can, therefore, only really be considered as a possible means of checking a final design, before actually building it.

We turn now to the use of mathematical modelling techniques, such as the finite element method, which, with the very large store capacities and high central processor speeds of modern digital computers, presents a more suitable means of determining the gravitational deformation of a structure fast enough to meet the design loop requirements. Another advantage of using mathematical modelling techniques is that the numerical analysis task may be considerably reduced by taking advantage of the high degrees of cyclic symmetry possessed by the surface supporting dish structures. Although there are such analytical methods available in a number of the large finite element computer packages, it was found that none of these could be

applied to a structure having any non-cyclically symmetric component - such as the elevation mounting structure which supports the cyclically symmetric dish structure. To take advantage of the cyclic symmetry of the dish structure, using one of the available analysis package facilities, would therefore mean the analysis and design of the elevation mounting structure and surface supporting dish structure would have to be carried out separately - which, as has already been pointed out, is not a very satisfactory approach to designing a millimetre wave telescope structure. Now because of this situation, and the fact that the proposed design procedure largely depends on a fast but accurate deformation analysis stage, it was decided that an analytical method should be developed, which is able to deal with a non-cyclically symmetric region in an otherwise cyclically symmetric structure, while still taking advantage of this cyclic symmetry to reduce the analysis task. The results of this work are presented in the next two chapters; chapter three containing the theoretical development of the analysis method, and chapter four a description of the computer program written to implement it.

2.5 - Completing the Design Loop

Having determined the form of the gravitational deformation of a structure, the next stage (see fig.2.3.1) is to measure how near to the desired homological form it is. This is done at stage three of the design procedure, by finding a best-fit paraboloid to all the deformed surface support points using a least squares method. The homological performance is then measured by calculating the r.m.s. error arising from the deviation of each surface support point from the best-fit paraboloid - which thus presents a measure of the deviation of the deformed reflecting surface from the required parabolic surface form.

Since perfect homological deformation is not a practical goal, an acceptable r.m.s. deviation error must be established below which the design may be considered good enough, and therefore a final design. This acceptable value depends largely on the wavelength of the radiation to be observed and is found from a theoretical consideration of a parabolic reflector antenna's performance and the factors which affect it. The current r.m.s. deviation error is then tested against the required accuracy at stage four. If a current design fails to pass this homological performance test, the next stage (five) is to formulate a set of structural alterations which will improve its performance - thus producing a new structure to be analysed, and so on round the loop until an acceptable final design is reached. These remaining stages, together with the development of the theoretical conditions which must be satisfied for a structure to be potentially homologically deforming (in theory at least), are considered in detail in chapter five.

In order to test the various components of the proposed design procedure, as well as to test the procedure as a whole, it has been used for the design of a 15 m diameter telescope structure whose homological deformation behaviour is good enough for sub-millimetre wavelength observations. The results and details of this test are presented in chapter six, together with a review of the problem of how the resulting design might actually be built.

A final discussion of aspects of the work presented here, with a set of conclusions and recommendations, forms the last chapter.

2.6 - References

1. Hachenberg, O. - The 100 m Radio Telescope of the Max Plank Institute for Radio Astronomy in Bonn,
Structures Technology for Large Radio and Radar Telescope Systems,
Ed. Mar, J.W. and Liebowitz, H., MIT Press, 1969, pp.13-27.

2. Hachenberg, O., Grahl, B.H. and Wielebinski, R. - The 100-meter Radio Telescope at Effelsberg,
Proc. IEEE, vol.61, no.9, Sept. 1973, pp.1288-1295.

3. Hills, R.E. and Colyer, B.D. - Computation of the Gravitational Deflections of a Radially Symmetric Telescope Structure,
Internal U.K. millimetre wave project technical note, Aug. 1976.

Chapter Three - The Analysis of Cyclically Symmetric Structures

3.0 - Introduction

In the next two chapters we will move away from the problem of homologically deforming structures to consider the more general problem of analysing a cyclically symmetric structure having a non-cyclically symmetric central region.

First, a review of the development of the methods for analysing cyclically symmetric structures is presented, in which the absence of a method capable of dealing with any structural non-cyclic symmetry is shown. The theoretical formulation of a method that is able to do this follows. The implementation of this method, in a computer program, is then described in chapter four.

3.1 - Review

The development of methods for analysing cyclically symmetric structures, which take advantage of their cyclic symmetry to reduce the analysis task, does not have an easily traceable or continuous historical path. As with other aspects of structural analysis more has been done in this area since the advent of electronic computers - especially since the appearance of large finite element structural analysis packages. However, a surprising fact revealed by this survey is the relatively small amount of work which has been done. None of the currently available cyclically symmetric structural analysis procedures are able to deal with any degree of structural non-cyclic symmetry, even though the ability to do so must have been considered desirable for some time. Large aircraft and radio telescope structures, whose analysis would have been considerably simplified (and speeded up) by such a facility, have existed for many years.

The first person to take advantage of the cyclic symmetry of a structure, to reduce the problem of its analysis, appears to have been Southwell [1], who in 1932 was concerned with the design of large dirigible airship structures. A similar method of using symmetric and anti-symmetric loads in various combinations to synthesize a general load applied to a cyclically symmetric structure, thus reducing the analysis problem to a number of more manageable ones, was published by Newell [2] a few years later, although he draws on earlier work done in Germany [3]. Another piece of isolated work was published by Renton [4] in 1963 on the buckling of cyclically symmetric framework structures.

Nooshin and Butterworth [5] developed an analytical method for the analysis of purely cyclically symmetric structures subjected to purely cyclically symmetric loads, which, although rather limited in its application, is significant in being the first formal setting out of the reduced analysis which can be developed by taking advantage of the cyclic symmetry of a structure. Their method also allows the existence of nodes (framework joints) on the axis about which the structure is cyclically symmetric - a facility not found in any subsequent analysis method. Another useful concept introduced by Nooshin and Butterworth, and again used in the development of the analysis method presented here, is that of segments whose boundaries do not pass through nodes, and which each have their own (segment) co-ordinate system.

The ability to deal with cyclically symmetric structures subjected to non-cyclically symmetric loads - the obvious development of Nooshin and Butterworth's method - became available the following year in the form of a special facility in the large general finite element package NASTRAN [6]. The method draws on theoretical work published by Fortescue [7] (in 1918), on the analysis of polyphase electrical

circuits, to transform a general load pattern into a set of cyclically symmetric load components. As mentioned earlier, it is surprising that this development did not take place sooner and also that it was not extended to deal with structural non-cyclic symmetry - especially since structures which would have benefitted from such a development were being analysed using the conventional NASTRAN facilities at the time [8].

Another computer package implementation of a method for analysing cyclically symmetric structures subjected to non-cyclically symmetric loading, is contained in ASKA-CS [9]. Although this method is theoretically equivalent to that used by NASTRAN, it is based on a complex finite Fourier transformation technique. A further computer implementation of a method which takes advantage of structural cyclic symmetry to reduce the analysis task, has been developed by Colyer [10] at the Rutherford and Appleton Laboratory. However, it is not a general purpose program, being written specifically to analyse purely cyclically symmetric radio telescope structures which are only subjected to symmetric and anti-symmetric gravitational loadings.

This then, was the position at the start of the work presented here concerning the analysis of cyclically symmetric structures. It is by an extension of the application of Fortescue's Symmetric Components (Fortescue's original term was 'symmetric co-ordinates', but 'symmetric components' is usually used now) and the use of concepts introduced by Nooshin and Butterworth that an analytical method able to deal with non-cyclically symmetric loadings and a region of structural non-cyclic symmetry, has been developed.

It is interesting to note that this is not the first time electrical engineering methods have been applied to the analysis of structures. Kron [11], an electrical engineer, often used electrical

analogies when talking about structures and their analysis. He was also the first person to present Fortescue's method of symmetric components in matrix form [12]. Furthermore it seems he too missed an opportunity to apply the method to the analysis of cyclically symmetric structures - especially since he later developed a method for solving complex structures in easy stages [13], which can be likened to present sub-structuring methods, of which cyclic symmetry analysis methods are a particular type.

3.2 - Cyclically Symmetric Structures

A structure is said to be cyclically symmetric, if there exists an axis about which repeated turns of the structure, through a constant angle, result in structure configurations which are coincident with the original structure position. The axis about which a structure is cyclically symmetric is referred to as 'the axis of cyclic symmetry' and the smallest angle through which it can be turned, to obtain coincidence of the structure with the original position, is called the 'angle of cyclic symmetry'. An example of a high order cyclically symmetric structure is a Terry's Chocolate Orange, which consists of a number of identical segments all equally spaced round a central core to which they are each joined.

By taking advantage of the geometric properties of cyclically symmetric structures, a considerable reduction in the amount of analytical computation, otherwise necessary in the analysis of such structures, may be achieved. Although the main reasons for wanting to do this are obviously to save time and money, an important reason, as far as the numerical computation is concerned, is that cyclically symmetric structures analysed conventionally (by modelling the whole, or large parts of the structure) using finite elements, produce

sparse, wide banded, stiffness matrices, which are not very amenable to fast accurate numerical analysis.

3.3 - Symmetric Components

In problems of analysis success can largely depend on the choice of co-ordinate system used in defining the problem. By the selection of a suitable system, aspects of a problem, which at first may elude comprehension, can be, if not simplified, at least rendered more amenable to analysis. For example, a system of three co-planar concurrent vectors may at first appear to be simply a group of three arbitrary vectors, which is only fully defined when their magnitudes and angular positions, relative to some fixed direction, are given. Such a system may be said to have six degrees of co-ordinate freedom - since each vector may vary in both magnitude and angular position without regard to the others. If, however, we impose the condition that the vectors must be of equal magnitude, we find that with the direction of one vector given, the other two are completely defined when only their directions are given. The system has therefore lost two degrees of co-ordinate freedom by imposing the above condition or constraint. If we now impose a further condition - that the vectors be symmetrically placed about their common origin - the system is reduced to one of only two degrees of co-ordinate freedom.

It is evident from this example that a more general system of n co-planar concurrent vectors may have $2n$ degrees of co-ordinate freedom, and that a system of n co-planar concurrent symmetrically spaced vectors, of equal magnitude, has two degrees of co-ordinate freedom. Thus, it should be possible, by means of a transformation, to define a system of n arbitrary concurrent vectors by n other systems of concurrent vectors which are placed symmetrically about

sparse, wide banded, stiffness matrices, which are not very amenable to fast accurate numerical analysis.

3.3 - Symmetric Components

In problems of analysis success can largely depend on the choice of co-ordinate system used in defining the problem. By the selection of a suitable system, aspects of a problem, which at first may elude comprehension, can be, if not simplified, at least rendered more amenable to analysis. For example, a system of three co-planar concurrent vectors may at first appear to be simply a group of three arbitrary vectors, which is only fully defined when their magnitudes and angular positions, relative to some fixed direction, are given. Such a system may be said to have six degrees of co-ordinate freedom - since each vector may vary in both magnitude and angular position without regard to the others. If, however, we impose the condition that the vectors must be of equal magnitude, we find that with the direction of one vector given, the other two are completely defined when only their directions are given. The system has therefore lost two degrees of co-ordinate freedom by imposing the above condition or constraint. If we now impose a further condition - that the vectors be symmetrically placed about their common origin - the system is reduced to one of only two degrees of co-ordinate freedom.

It is evident from this example that a more general system of n co-planar concurrent vectors may have $2n$ degrees of co-ordinate freedom, and that a system of n co-planar concurrent symmetrically spaced vectors, of equal magnitude, has two degrees of co-ordinate freedom. Thus, it should be possible, by means of a transformation, to define a system of n arbitrary concurrent vectors by n other systems of concurrent vectors which are placed symmetrically about

their common point. These n symmetrical systems so obtained are called 'symmetric co-ordinates', or 'symmetric components' (the term used from now on) of the first system of arbitrary vectors, and completely define it. In other words, our original example of three arbitrary concurrent vectors may also be fully defined by three sets of three symmetrically spaced vectors of equal magnitude.

To demonstrate this transformation of an arbitrary co-planar system of three concurrent vectors into its symmetric components, consider the set of three vectors defined in figure 3.3.1.

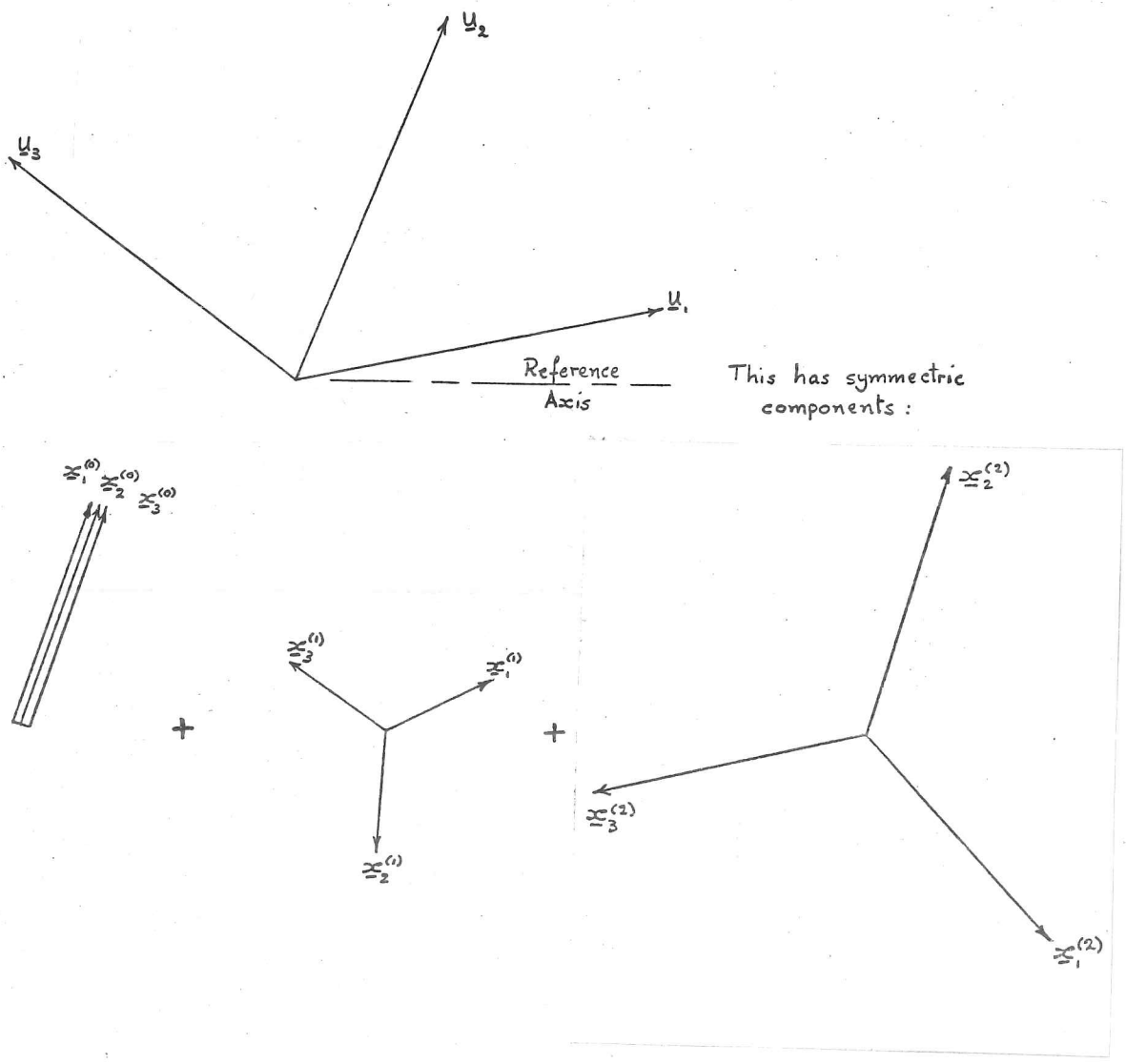

Fig.3.3.1 - An arbitrary set of three concurrent vectors and its symmetric components.

By the theory of symmetric components:

$$\left.\begin{aligned} \underline{u}_1 &= \underline{x}_1^{(0)} + \underline{x}_1^{(1)} + \underline{x}_1^{(2)} \\ \underline{u}_2 &= \underline{x}_2^{(0)} + \underline{x}_2^{(1)} + \underline{x}_2^{(2)} \\ \underline{u}_3 &= \underline{x}_3^{(0)} + \underline{x}_3^{(1)} + \underline{x}_3^{(2)} \end{aligned}\right\} \quad (3.3.1)$$

Since the operator i $(=\sqrt{-1})$ rotates a vector through $\pi/2$ rad. in an anti-clockwise direction, it can be shown that:

$$\left.\begin{aligned} \underline{x}_2^{(1)} &= \underline{x}_1^{(1)}\cos(2\pi/3) - i\,\underline{x}_1^{(1)}\sin(2\pi/3) \\ \underline{x}_3^{(1)} &= \underline{x}_1^{(1)}\cos(4\pi/3) - i\,\underline{x}_1^{(1)}\sin(4\pi/3) \\ \underline{x}_2^{(2)} &= \underline{x}_1^{(2)}\cos(4\pi/3) - i\,\underline{x}_1^{(2)}\sin(4\pi/3) \\ \underline{x}_3^{(2)} &= \underline{x}_1^{(2)}\cos(2\pi/3) - i\,\underline{x}_1^{(2)}\sin(2\pi/3) \end{aligned}\right\} \quad (3.3.2)$$

Also, since $\underline{x}_2^{(0)} = \underline{x}_3^{(0)} = \underline{x}_1^{(0)}$

$$\left.\begin{aligned} \underline{u}_1 &= \underline{x}_1^{(0)} + \underline{x}_1^{(1)} + \underline{x}_1^{(2)} \\ \underline{u}_2 &= \underline{x}_1^{(0)} + \underline{x}_1^{(1)}[\cos(2\pi/3) - i\sin(2\pi/3)] + \underline{x}_1^{(2)}[\cos(4\pi/3) - i\sin(4\pi/3)] \\ \underline{u}_3 &= \underline{x}_1^{(0)} + \underline{x}_1^{(1)}[\cos(4\pi/3) - i\sin(4\pi/3)] + \underline{x}_1^{(2)}[\cos(2\pi/3) - i\sin(2\pi/3)] \end{aligned}\right\} \quad (3.3.3)$$

which may be rewritten in the form:

$$\left.\begin{aligned} \underline{u}_1 &= \underline{x}_1^{(0)} + \underline{x}_1^{(1)} + \underline{x}_1^{(2)} \\ \underline{u}_2 &= \underline{x}_1^{(0)} + \bar{a}\,\underline{x}_1^{(1)} + \bar{a}^2\underline{x}_1^{(2)} \\ \underline{u}_3 &= \underline{x}_1^{(0)} + \bar{a}^2\underline{x}_1^{(1)} + \bar{a}\,\underline{x}_1^{(2)} \end{aligned}\right\} \quad (3.3.4)$$

where $\bar{a} = e^{-i2\pi/3} = \cos(2\pi/3) - i\sin(2\pi/3)$

and $\bar{a}^2 = e^{-i4\pi/3} = \cos(4\pi/3) - i\sin(4\pi/3)$

By inverting equation (3.3.4) to give $\underline{x}_1^{(0)}$, $\underline{x}_1^{(1)}$ and $\underline{x}_1^{(2)}$ in terms of $\underline{u}_1$, $\underline{u}_2$ and $\underline{u}_3$, we obtain the transformation required to find the symmetric co-ordinates of the initial system; $\underline{x}_1^{(0)}$, $\underline{x}_1^{(1)}$ and $\underline{x}_1^{(2)}$.

Thus:

$$\left.\begin{aligned} \underline{x}_1^{(0)} &= \tfrac{1}{3}(\underline{u}_1 + \underline{u}_2 + \underline{u}_3) \\ \underline{x}_1^{(1)} &= \tfrac{1}{3}(\underline{u}_1 + a\,\underline{u}_2 + a^2\underline{u}_3) \\ \underline{x}_1^{(2)} &= \tfrac{1}{3}(\underline{u}_1 + a^2\underline{u}_2 + a\,\underline{u}_3) \end{aligned}\right\} \quad (3.3.5)$$

where $a = e^{i2\pi/3} = \cos(2\pi/3)+i\sin(2\pi/3)$

and $a^2 = e^{i4\pi/3} = \cos(4\pi/3)+i\sin(4\pi/3)$

The matrix form of this transformation, for the three-fold cyclic symmetric example is thus given by:

$$\left.\begin{bmatrix} \underline{x}_i^{(0)} \\ \underline{x}_i^{(1)} \\ \underline{x}_i^{(2)} \end{bmatrix} = \frac{1}{3}\begin{bmatrix} \underline{I} & \underline{I} & \underline{I} \\ \underline{I} & a\underline{I} & a^2\underline{I} \\ \underline{I} & a^2\underline{I} & a\underline{I} \end{bmatrix}\begin{bmatrix} \underline{u}_1 \\ \underline{u}_2 \\ \underline{u}_3 \end{bmatrix}.\right\} \quad (3.3.6)$$

This idea of symmetric components will now be applied to the problem of analysing cyclically symmetric structures having a non-cyclically symmetric central region and subjected to non-cyclically symmetric loadings, to reduce the problem to one of analysing a set of purely cyclically symmetric structures subjected to purely cyclically symmetric loadings.

3.4 - Properties of the Load-Displacement Relationship for a Cyclically Symmetric Structure

The properties of the load-displacement stiffness relationship for a cyclically symmetric structure, will be demonstrated by considering a three-dimensional framework structure, having four-fold cyclic symmetry. This structure, whose geometry is arbitrary, and which has a central region of structural non-cyclic symmetry, may be represented by its central region and cyclic segment boundaries - see figure 3.4.1. The segment boundaries are drawn such that they do not pass through any structure joints, thus uniquely defining to which segment each joint belongs. The z-axis of each segment co-ordinate system coincides with the axis of cyclic symmetry. Also, the co-ordinate system of the central region (which contains joints which lie on the axis of cyclic symmetry, or do not form part of the cyclically

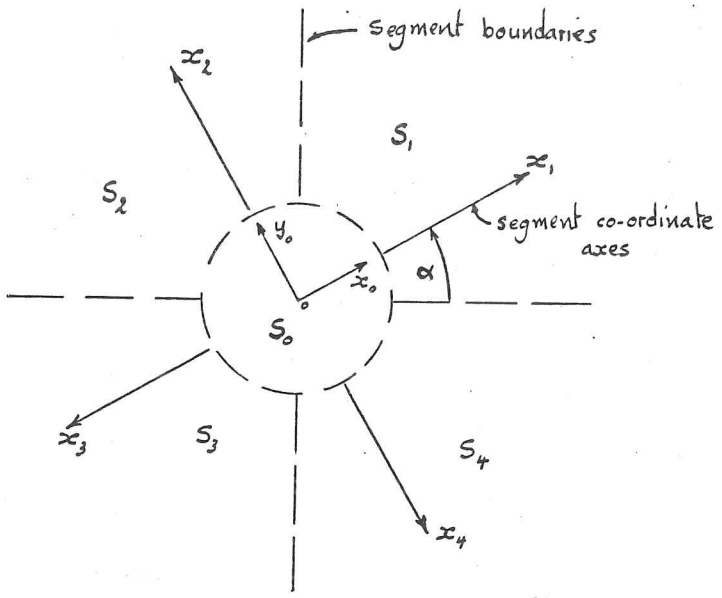

Fig.3.4.1 - A four-fold cyclically symmetric structure represented by its segment boundaries. The z_o, z_1, z_2, z_3, and z_4 axes coincide at the origin 'O' and are directed out of the page.

symmetric structure) and the co-ordinate system of the first cyclic segment coincide.

Instead of describing the overall structure load pattern in terms of one complete global load vector, as is usual, it will be divided into a series of segment load vectors, one for the central region and each cyclic segment, defined with respect to their corresponding co-ordinate systems. Now by considering each cyclic segment load vector as a line vector, from the co-ordinate system origin to a point in p-dimensional space, where p is the number of degrees of (joint) freedom per cyclic segment, a series of arbitrary, but concurrent vectors is obtained. On transforming this set of four vectors (in the example considered here) into four cyclically symmetric vector sets, by the method described in the previous section, the symmetric load components are obtained. The problem then becomes one of a cyclically symmetric structure having a non-cyclically symmetric

central region, subjected to a set of four different cyclically symmetric load patterns. The central region load vector is dealt with by dividing it equally amongst the cyclically symmetric loadings.

The four joint displacement solutions, obtained from applying each symmetric load component, will not necessarily be themselves cyclically symmetric, due to the structural non-cyclic symmetry of the central region. However, by describing the overall joint displacement solution in terms of segment displacement vectors (defined with respect to their corresponding segment co-ordinate systems), and interpreting them in the same way as the segment load vectors, a system of independent, concurrent, p-dimensional 'displacement' vectors is obtained. As with the load vector system, this displacement vector system can be transformed into its symmetric components, which will be a set of four cyclically symmetric joint displacement vector sets. Because the joint displacement solution is assumed to be linearly related to the applied loading, via the structural stiffness matrix, the symmetric component transformation will be the same for both the segment load vector and displacement vector systems.

Thus, by also transforming the joint displacement solution into its symmetric components, the problem becomes one of analysing a set of four purely cyclically symmetric structures, each subjected to a purely cyclically symmetric loading. This follows because by transforming the load and displacement vectors into their symmetric components, the structural stiffness relationship must also be transformed in order to preserve the same linear relationship between loads and displacements.

The structural stiffness relationship will now be developed for the four-fold cyclically symmetric structure having a non-cyclically symmetric central region and subjected to non-cyclically symmetric

loadings. The symmetric component transformation will then be applied.

First, each segment stiffness relationship is expressed in terms of a global co-ordinate system (coincident with the co-ordinate system of the central region and first cyclic segment). By applying appropriate co-ordinate transformations these segment stiffness equations may be expressed in terms of their respective co-ordinate systems - to which, after some simplification, the symmetric component transformation is applied.

Thus the structural stiffness relationship for the cyclically symmetric structure defined in figure 3.4.1 is given by:

$$\left.\begin{aligned}
\underline{P}_0^{(1)} &= \underline{K}_{00}^{(1)}\underline{d}_0^{(1)} + \underline{K}_{01}^{(1)}\underline{d}_1^{(1)} + \underline{K}_{02}^{(1)}\underline{d}_2^{(1)} + \underline{K}_{03}^{(1)}\underline{d}_3^{(1)} + \underline{K}_{04}^{(1)}\underline{d}_4^{(1)} \\
\underline{P}_1^{(1)} &= \underline{K}_{10}^{(1)}\underline{d}_0^{(1)} + \underline{K}_{11}^{(1)}\underline{d}_1^{(1)} + \underline{K}_{12}^{(1)}\underline{d}_2^{(1)} + \underline{0} + \underline{K}_{14}^{(1)}\underline{d}_4^{(1)} \\
\underline{P}_2^{(1)} &= \underline{K}_{20}^{(1)}\underline{d}_0^{(1)} + \underline{K}_{21}^{(1)}\underline{d}_1^{(1)} + \underline{K}_{22}^{(1)}\underline{d}_2^{(1)} + \underline{K}_{23}^{(1)}\underline{d}_3^{(1)} + \underline{0} \\
\underline{P}_3^{(1)} &= \underline{K}_{30}^{(1)}\underline{d}_0^{(1)} + \underline{0} + \underline{K}_{32}^{(1)}\underline{d}_2^{(1)} + \underline{K}_{33}^{(1)}\underline{d}_3^{(1)} + \underline{K}_{34}^{(1)}\underline{d}_4^{(1)} \\
\underline{P}_4^{(1)} &= \underline{K}_{40}^{(1)}\underline{d}_0^{(1)} + \underline{K}_{41}^{(1)}\underline{d}_1^{(1)} + \underline{0} + \underline{K}_{43}^{(1)}\underline{d}_3^{(1)} + \underline{K}_{44}^{(1)}\underline{d}_4^{(1)}
\end{aligned}\right\} \quad (3.4.1)$$

The notation used here, and in what follows, is based on the general forms $\underline{P}_i^{(j)}, \underline{K}_{mn}^{(l)}$ and $\underline{d}_u^{(v)}$, where $\underline{P}_i^{(j)}$ is the load vector for segment 'i' defined with respect to segment co-ordinate system 'j', $\underline{K}_{mn}^{(l)}$ is the stiffness matrix of connections between segments 'm' and 'n' defined with respect to segment co-ordinate system 'l' and $\underline{d}_u^{(v)}$ is the displacement vector for segment 'u' defined with respect to segment co-ordinate system 'v'. Also, it has been assumed (for this example) that only adjacent segments are connected by structural members.

By defining the load and displacement vector co-ordinate transformations:

$$\left.\begin{aligned}
\underline{P}_m^{(n)} &= \underline{T}_{mn}\underline{P}_m^{(m)} \\
\underline{d}_m^{(n)} &= \underline{T}_{mn}\underline{d}_m^{(m)}
\end{aligned}\right\} \quad (3.4.2)$$

where $\underline{P}_m^{(n)}, \underline{P}_m^{(m)}, \underline{d}_m^{(n)}$ and $\underline{d}_m^{(m)}$ are defined as above and $\underline{T}_{mn}$ is the co-ordinate transformation matrix from segment co-ordinate system 'm' to segment co-ordinate system 'n', equation (3.4.1) may be rewritten in terms of segment load and displacement vectors defined with respect to their own co-ordinate systems. Thus:

$$\left.\begin{aligned}
\underline{P}_0^{(1)} &= \underline{K}_{00}^{(1)}\underline{d}_0^{(1)} + \underline{K}_{01}^{(1)}\underline{d}_1^{(1)} + (\underline{K}_{02}^{(1)}\underline{T}_{21})\underline{d}_2^{(2)} + (\underline{K}_{03}^{(1)}\underline{T}_{31})\underline{d}_3^{(3)} + (\underline{K}_{04}^{(1)}\underline{T}_{41})\underline{d}_4^{(4)} \\
\underline{P}_1^{(1)} &= \underline{K}_{10}^{(1)}\underline{d}_0^{(1)} + \underline{K}_{11}^{(1)}\underline{d}_1^{(1)} + (\underline{K}_{12}^{(1)}\underline{T}_{21})\underline{d}_2^{(2)} + \underline{0} + (\underline{K}_{14}^{(1)}\underline{T}_{41})\underline{d}_4^{(4)} \\
\underline{P}_2^{(2)} &= (\underline{T}_{21}^{T}\underline{K}_{20}^{(1)})\underline{d}_0^{(1)} + (\underline{T}_{21}^{T}\underline{K}_{21}^{(1)})\underline{d}_1^{(1)} + (\underline{T}_{21}^{T}\underline{K}_{22}^{(1)}\underline{T}_{21})\underline{d}_2^{(2)} + (\underline{T}_{21}^{T}\underline{K}_{23}^{(1)}\underline{T}_{31})\underline{d}_3^{(3)} + \underline{0} \\
\underline{P}_3^{(3)} &= (\underline{T}_{31}^{T}\underline{K}_{30}^{(1)})\underline{d}_0^{(1)} + \underline{0} + (\underline{T}_{31}^{T}\underline{K}_{32}^{(1)}\underline{T}_{21})\underline{d}_2^{(2)} + (\underline{T}_{31}^{T}\underline{K}_{33}^{(1)}\underline{T}_{31})\underline{d}_3^{(3)} + (\underline{T}_{31}^{T}\underline{K}_{34}^{(1)}\underline{T}_{41})\underline{d}_4^{(4)} \\
\underline{P}_4^{(4)} &= (\underline{T}_{41}^{T}\underline{K}_{40}^{(1)})\underline{d}_0^{(1)} + (\underline{T}_{41}^{T}\underline{K}_{41}^{(1)})\underline{d}_1^{(1)} + \underline{0} + (\underline{T}_{41}^{T}\underline{K}_{43}^{(1)}\underline{T}_{31})\underline{d}_3^{(3)} + (\underline{T}_{41}^{T}\underline{K}_{44}^{(1)}\underline{T}_{41})\underline{d}_4^{(4)}
\end{aligned}\right\} \quad (3.4.3)$$

Now is can be shown that:

$\underline{T}_{21}^{T}\underline{K}_{22}^{(1)}\underline{T}_{21} = \underline{K}_{22}^{(2)}$, $\underline{T}_{31}^{T}\underline{K}_{33}^{(1)}\underline{T}_{31} = \underline{K}_{33}^{(3)}$ and $\underline{T}_{41}^{T}\underline{K}_{44}^{(1)}\underline{T}_{41} = \underline{K}_{44}^{(4)}$, also

$\underline{K}_{01}^{(1)} = (\underline{K}_{10}^{(1)})^{T}$, $\underline{K}_{02}^{(1)}\underline{T}_{21} = (\underline{T}_{21}^{T}\underline{K}_{20}^{(1)})^{T}$, $\underline{K}_{03}^{(1)}\underline{T}_{31} = (\underline{T}_{31}^{T}\underline{K}_{30}^{(1)})^{T}$, $\underline{K}_{04}^{(1)}\underline{T}_{41} = (\underline{T}_{41}^{T}\underline{K}_{40}^{(1)})^{T}$,

$\underline{K}_{12}^{(1)}\underline{T}_{21} = (\underline{T}_{21}^{T}\underline{K}_{21}^{(1)})^{T}$, $\underline{K}_{14}^{(1)}\underline{T}_{41} = (\underline{T}_{41}^{T}\underline{K}_{41}^{(1)})^{T}$,

$\underline{T}_{21}^{T}\underline{K}_{23}^{(1)}\underline{T}_{31} = (\underline{T}_{31}^{T}\underline{K}_{32}^{(1)}\underline{T}_{21})^{T}$, and $\underline{T}_{31}^{T}\underline{K}_{34}^{(1)}\underline{T}_{41} = (\underline{T}_{41}^{T}\underline{K}_{43}^{(1)}\underline{T}_{31})^{T}$.

As a result of the cyclic symmetry of the structure, further simplifications may be made as follows:

$\underline{K}_{11}^{(1)} = \underline{K}_{22}^{(2)} = \underline{K}_{33}^{(3)} = \underline{K}_{44}^{(4)}$,

$\underline{K}_{12}^{(1)}\underline{T}_{21} = (\underline{K}_{14}^{(1)}\underline{T}_{41})^{T}$,

$\underline{K}_{12}^{(1)}\underline{T}_{21} = \underline{T}_{21}^{T}\underline{K}_{23}^{(1)}\underline{T}_{31} = \underline{T}_{31}^{T}\underline{K}_{34}^{(1)}\underline{T}_{41}$

Using the above relationships, equations (3.4.3) may be rewritten in the form:

$$
\left.
\begin{aligned}
\underline{P}_0^{(1)} &= \underline{K}_{00}^{(1)}\underline{d}_0^{(1)} + \underline{K}_{01}^{(1)}\underline{d}_1^{(1)} + (\underline{K}_{02}^{(1)}\underline{T}_{21})\,\underline{d}_2^{(2)} + (\underline{K}_{03}^{(1)}\underline{T}_{31})\,\underline{d}_3^{(3)} + (\underline{K}_{04}^{(1)}\underline{T}_{41})\,\underline{d}_4^{(4)} \\
\underline{P}_1^{(1)} &= (\underline{K}_{01}^{(1)})^T\underline{d}_0^{(1)} + \underline{K}_{11}^{(1)}\underline{d}_1^{(1)} + (\underline{K}_{12}^{(1)}\underline{T}_{21})\,\underline{d}_2^{(2)} + \underline{0} + (\underline{K}_{12}^{(1)}\underline{T}_{21})^T\underline{d}_4^{(4)} \\
\underline{P}_2^{(2)} &= (\underline{K}_{02}^{(1)}\underline{T}_{21})^T\underline{d}_0^{(1)} + (\underline{K}_{12}^{(1)}\underline{T}_{21})^T\underline{d}_1^{(1)} + \underline{K}_{11}^{(1)}\underline{d}_2^{(2)} + (\underline{K}_{12}^{(1)}\underline{T}_{21})\,\underline{d}_3^{(3)} + \underline{0} \\
\underline{P}_3^{(3)} &= (\underline{K}_{03}^{(1)}\underline{T}_{31})^T\underline{d}_0^{(1)} + \underline{0} + (\underline{K}_{12}^{(1)}\underline{T}_{21})^T\underline{d}_2^{(2)} + \underline{K}_{11}^{(1)}\underline{d}_3^{(3)} + (\underline{K}_{12}^{(1)}\underline{T}_{21})\,\underline{d}_4^{(4)} \\
\underline{P}_4^{(4)} &= (\underline{K}_{04}^{(1)}\underline{T}_{41})^T\underline{d}_0^{(1)} + (\underline{K}_{12}^{(1)}\underline{T}_{21})\,\underline{d}_1^{(1)} + \underline{0} + (\underline{K}_{12}^{(1)}\underline{T}_{21})^T\underline{d}_3^{(3)} + \underline{K}_{11}^{(1)}\underline{d}_4^{(4)}
\end{aligned}
\right\} \qquad (3.4.4)
$$

This can be more clearly written in supermatrix form as:

$$
\left.
\begin{bmatrix} \underline{P}_0^{(1)} \\ \underline{P}_1^{(1)} \\ \underline{P}_2^{(2)} \\ \underline{P}_3^{(3)} \\ \underline{P}_4^{(4)} \end{bmatrix} =
\begin{bmatrix}
\underline{K}_{00} & \underline{K}_{01} & \underline{K}_{02} & \underline{K}_{03} & \underline{K}_{04} \\
\underline{K}_{01}^T & \underline{K}_{11} & \underline{K}_{12} & \underline{0} & \underline{K}_{12}^T \\
\underline{K}_{02}^T & \underline{K}_{12}^T & \underline{K}_{11} & \underline{K}_{12} & \underline{0} \\
\underline{K}_{03}^T & \underline{0} & \underline{K}_{12}^T & \underline{K}_{11} & \underline{K}_{12} \\
\underline{K}_{04}^T & \underline{K}_{12} & \underline{0} & \underline{K}_{12}^T & \underline{K}_{11}
\end{bmatrix}
\begin{bmatrix} \underline{d}_0^{(1)} \\ \underline{d}_1^{(1)} \\ \underline{d}_2^{(2)} \\ \underline{d}_3^{(3)} \\ \underline{d}_4^{(4)} \end{bmatrix}
\right\} \qquad (3.4.5)
$$

where $\underline{K}_{00} = \underline{K}_{00}^{(1)}$, $\underline{K}_{01} = \underline{K}_{01}^{(1)}$, $\underline{K}_{02} = \underline{K}_{02}^{(1)}\underline{T}_{21}$, $\underline{K}_{03} = \underline{K}_{03}^{(1)}\underline{T}_{31}$,

$\underline{K}_{04} = \underline{K}_{04}^{(1)}\underline{T}_{41}$, $\underline{K}_{11} = \underline{K}_{11}^{(1)}$ and $\underline{K}_{12} = \underline{K}_{12}^{(1)}\underline{T}_{21}$.

Equation (3.4.5) will be more generally referred to as

$$\underline{\underline{P}} = \underline{\underline{K}}\,\underline{\underline{d}} \qquad (3.4.5a)$$

Now, applying the symmetric co-ordinate transformation to the load and displacement vectors $\underline{\underline{P}}$ and $\underline{\underline{d}}$ as defined by equations (3.3.6) gives:

$$\underline{\underline{P}}_T = \underline{\underline{S}}\,\underline{\underline{P}} \qquad (3.4.6)$$

$$\underline{\underline{d}}_T = \underline{\underline{S}}\,\underline{\underline{d}} \qquad (3.4.7)$$

where $\underline{\underline{P}}_T$ and $\underline{\underline{d}}_T$ are the transformed load and displacement vectors respectively, and the transformation matrix $\underline{\underline{S}}$ is defined by:

$$\underline{\underline{S}} = \frac{1}{4}\begin{bmatrix} \underline{I} & \underline{0} & \underline{0} & \underline{0} & \underline{0} \\ \underline{0} & \underline{I} & \underline{I} & \underline{I} & \underline{I} \\ \underline{0} & \underline{I} & a\underline{I} & a^2\underline{I} & a^3\underline{I} \\ \underline{0} & \underline{I} & a^2\underline{I} & a^4\underline{I} & a^6\underline{I} \\ \underline{0} & \underline{I} & a^3\underline{I} & a^6\underline{I} & a^9\underline{I} \end{bmatrix} \qquad (3.4.8)$$

where $\underline{I}$ is the unit matrix, $\underline{0}$ the null matrix and $a^k = e^{i2\pi k/4}$

Multiplying both sides of equation (3.4.5a) by $\underline{\underline{S}}$ gives:

$$\underline{\underline{SP}} = \underline{\underline{SKd}}$$

which can be written as:

$$\underline{P}_T = \underline{\underline{S}}\ \underline{\underline{K}}\ \underline{d} \qquad (3.4.9)$$

From equation (3.4.7) $\underline{d} = \underline{\underline{S}}^{-1}\underline{d}_T$, where $\underline{\underline{S}}^{-1}$ is the inverse of $\underline{\underline{S}}$ and is defined by:

$$\underline{\underline{S}}^{-1} = \begin{bmatrix} 4\underline{I} & \underline{0} & \underline{0} & \underline{0} & \underline{0} \\ \underline{0} & \underline{I} & \underline{I} & \underline{I} & \underline{I} \\ \underline{0} & \underline{I} & \bar{a}\underline{I} & \bar{a}^2\underline{I} & \bar{a}^3\underline{I} \\ \underline{0} & \underline{I} & \bar{a}^2\underline{I} & \bar{a}^4\underline{I} & \bar{a}^6\underline{I} \\ \underline{0} & \underline{I} & \bar{a}^3\underline{I} & \bar{a}^6\underline{I} & \bar{a}^9\underline{I} \end{bmatrix} \qquad (3.4.10)$$

where $\bar{a}^k = e^{-i2\pi k/4}$. Thus substituting for $\underline{d}$ in equation (3.4.9) gives:

$$\underline{P}_T = \underline{\underline{S}}\ \underline{\underline{K}}\ \underline{\underline{S}}^{-1}\underline{d}_T \qquad (3.4.11)$$

Equation (3.4.11) represents the transformed stiffness relationship between the applied loads and resulting displacements in the complex Fourier space. The supermatrix obtained from the product $\underline{\underline{S}}\underline{\underline{K}}\underline{\underline{S}}^{-1}$ is thus the transformed structure stiffness supermatrix, which will be referred to as $\underline{\underline{K}}_T$, and because of the predominantly circulant nature of $\underline{\underline{S}}$, has the form* :

$$\underline{\underline{K}}_T = \begin{bmatrix} \underline{K}_{T00} & \frac{1}{4}\underline{K}_{T01} & \frac{1}{4}\underline{K}_{T02} & \frac{1}{4}\underline{K}_{T03} & \frac{1}{4}\underline{K}_{T04} \\ \underline{K}_{T01}^T & \underline{K}_{T11} & \underline{0} & \underline{0} & \underline{0} \\ \underline{K}_{T02}^T & \underline{0} & \underline{K}_{T22} & \underline{0} & \underline{0} \\ \underline{K}_{T03}^T & \underline{0} & \underline{0} & \underline{K}_{T33} & \underline{0} \\ \underline{K}_{T04}^T & \underline{0} & \underline{0} & \underline{0} & \underline{K}_{T44} \end{bmatrix} \qquad (3.4.12)$$

where $\underline{K}_{T00} = \underline{K}_{00}$,

$\underline{K}_{T11} = (\underline{K}_{11} + \underline{K}_{12} + \underline{K}_{12}^T)$, $\underline{K}_{T01} = (\underline{K}_{01} + \underline{K}_{02} + \underline{K}_{03} + \underline{K}_{04})$,

$\underline{K}_{T22} = (\underline{K}_{11} + a\,\underline{K}_{12} + \bar{a}\,\underline{K}_{12}^T)$, $\underline{K}_{T02} = (\underline{K}_{01} + \bar{a}\,\underline{K}_{02} + \bar{a}^2\underline{K}_{03} + \bar{a}^3\underline{K}_{04})$,

$\underline{K}_{T33} = (\underline{K}_{11} + a^2\underline{K}_{12} + \bar{a}^2\underline{K}_{12}^T)$, $\underline{K}_{T03} = (\underline{K}_{01} + \bar{a}^2\underline{K}_{02} + \bar{a}^4\underline{K}_{03} + \bar{a}^6\underline{K}_{04})$,

$\underline{K}_{T44} = (\underline{K}_{11} + a^3\underline{K}_{12} + \bar{a}^3\underline{K}_{12}^T)$ and $\underline{K}_{T04} = (\underline{K}_{01} + \bar{a}^3\underline{K}_{02} + \bar{a}^6\underline{K}_{03} + \bar{a}^9\underline{K}_{04})$.

Similarly from equations (3.4.6) and (3.4.7) $\underline{\underline{P}}_T$ and $\underline{\underline{d}}$ are defined by:

$$\underline{\underline{P}}_T = \begin{bmatrix} \underline{P}_{T0} \\ \underline{P}_{T1} \\ \underline{P}_{T2} \\ \underline{P}_{T3} \\ \underline{P}_{T4} \end{bmatrix}, \qquad \underline{\underline{d}} = \begin{bmatrix} \underline{d}_0 \\ \underline{d}_1 \\ \underline{d}_2 \\ \underline{d}_3 \\ \underline{d}_4 \end{bmatrix} \qquad (3.4.13)$$

where $\underline{P}_{T0} = \frac{1}{4}\underline{P}_0^{(1)}$, $\underline{d}_0 = 4\underline{d}_{T0}$

$\underline{P}_{T1} = \frac{1}{4}(\underline{P}_1^{(1)} + \underline{P}_2^{(2)} + \underline{P}_3^{(3)} + \underline{P}_4^{(4)})$, $\underline{d}_1 = (\underline{d}_{T1} + \underline{d}_{T2} + \underline{d}_{T3} + \underline{d}_{T4})$,

$\underline{P}_{T2} = \frac{1}{4}(\underline{P}_1^{(1)} + a\,\underline{P}_2^{(2)} + a^2\underline{P}_3^{(3)} + a^3\underline{P}_4^{(4)})$, $\underline{d}_2 = (\underline{d}_{T1} + \bar{a}\,\underline{d}_{T2} + \bar{a}^2\underline{d}_{T3} + \bar{a}^3\underline{d}_{T4})$,

$\underline{P}_{T3} = \frac{1}{4}(\underline{P}_1^{(1)} + a^2\underline{P}_2^{(2)} + a^4\underline{P}_3^{(3)} + a^6\underline{P}_4^{(4)})$, $\underline{d}_3 = (\underline{d}_{T1} + \bar{a}^2\underline{d}_{T2} + \bar{a}^4\underline{d}_{T3} + \bar{a}^6\underline{d}_{T4})$,

$\underline{P}_{T4} = \frac{1}{4}(\underline{P}_1^{(1)} + a^3\underline{P}_2^{(2)} + a^6\underline{P}_3^{(3)} + a^9\underline{P}_4^{(4)})$ and $\underline{d}_4 = (\underline{d}_{T1} + \bar{a}^3\underline{d}_{T2} + \bar{a}^6\underline{d}_{T3} + \bar{a}^9\underline{d}_{T4})$.

---

* see section 3.6

By considering the nature of the element matrices of $\underline{\underline{K}}_T$ (equation 3.4.12), it can be shown that:

$$\underline{K}_{T44} = \bar{\underline{K}}_{T22} \quad \text{(the complex conjugate of } \underline{K}_{T22}\text{)}$$

$$\text{and} \quad \underline{K}_{T04} = \bar{\underline{K}}_{T02} \quad \text{hence} \quad \bar{\underline{K}}^T_{T04} = \underline{K}^T_{T02}$$

A similar simplification can be made in the transformed load and displacement vectors. The transformed stiffness relationship between the applied load and resulting displacement may thus be written as:

$$\begin{bmatrix} \underline{P}_{T0} \\ \underline{P}_{T1} \\ \underline{P}_{T2} \\ \underline{P}_{T3} \\ \underline{P}_{T4} \end{bmatrix} = \begin{bmatrix} \underline{K}_{T00} & \frac{1}{4}\underline{K}_{T01} & \frac{1}{4}\underline{K}_{T2} & \frac{1}{4}\underline{K}_{T03} & \frac{1}{4}\bar{\underline{K}}_{T02} \\ \underline{K}^T_{T01} & \underline{K}_{T11} & & & \\ \underline{K}^T_{T02} & & \underline{K}_{T22} & & \\ \underline{K}^T_{T03} & & & \underline{K}_{T33} & \\ \bar{\underline{K}}^T_{T02} & & & & \bar{\underline{K}}_{T22} \end{bmatrix} \begin{bmatrix} \underline{d}_{T0} \\ \underline{d}_{T1} \\ \underline{d}_{T2} \\ \underline{d}_{T3} \\ \bar{\underline{d}}_{T2} \end{bmatrix} \qquad (3.4.14)$$

$$\begin{aligned} \underline{P}_{T0} &= \underline{K}_{T00}\underline{d}_{T0} + \tfrac{1}{4}\underline{K}_{T01}\underline{d}_{T1} + \tfrac{1}{4}\underline{K}_{T02}\underline{d}_{T2} + \tfrac{1}{4}\underline{K}_{T03}\underline{d}_{T3} + \tfrac{1}{4}\bar{\underline{K}}_{T02}\bar{\underline{d}}_{T2} \\ \underline{P}_{T1} &= \underline{K}^T_{T01}\underline{d}_{T0} + \underline{K}_{T11}\underline{d}_{T1} \\ \underline{P}_{T2} &= \bar{\underline{K}}^T_{T02}\underline{d}_{T0} + \underline{K}_{T22}\underline{d}_{T2} \\ \underline{P}_{T3} &= \bar{\underline{K}}^T_{T03}\underline{d}_{T0} + \underline{K}_{T33}\underline{d}_{T3} \\ \underline{P}_{T4} &= \underline{K}^T_{T02}\underline{d}_{T0} + \bar{\underline{K}}_{T22}\bar{\underline{d}}_{T2} \end{aligned} \qquad (3.4.15)$$

By rearranging equations (3.4.15), explicit expressions for the element vectors of the transformed displacement vector may be obtained, thus:

$$\begin{aligned} \underline{d}_{T0} &= [\underline{K}_{T00} - \tfrac{1}{4}\underline{K}_{T01}\underline{K}^{-1}_{T11}\underline{K}^T_{T01} - \tfrac{1}{4}(\underline{K}_{T02}\underline{K}^{-1}_{T22}\bar{\underline{K}}^T_{T02} + \bar{\underline{K}}_{T02}\bar{\underline{K}}^{-1}_{T22}\underline{K}^T_{T02}) - \tfrac{1}{4}\underline{K}_{T03}\underline{K}^{-1}_{T33}\bar{\underline{K}}^T_{T03}]^{-1} \\ &\quad [\underline{P}_{T0} - \tfrac{1}{4}\underline{K}_{T01}\underline{K}^{-1}_{T11}\underline{P}_{T1} - \tfrac{1}{4}(\underline{K}_{T02}\underline{K}^{-1}_{T22}\underline{P}_{T2} + \bar{\underline{K}}_{T02}\bar{\underline{K}}^{-1}_{T22}\bar{\underline{P}}_{T2}) - \tfrac{1}{4}\underline{K}_{T03}\underline{K}^{-1}_{T33}\underline{P}_{T3}] \\ \underline{d}_{T1} &= \underline{K}^{-1}_{T11}(\underline{P}_{T1} - \bar{\underline{K}}^T_{T01}\underline{d}_{T0}) \\ \underline{d}_{T2} &= \underline{K}^{-1}_{T22}(\underline{P}_{T2} - \bar{\underline{K}}^T_{T02}\underline{d}_{T0}) \\ \underline{d}_{T3} &= \underline{K}^{-1}_{T33}(\underline{P}_{T3} - \bar{\underline{K}}^T_{T03}\underline{d}_{T0}) \\ \underline{d}_{T4} &= \bar{\underline{d}}_{T2} \end{aligned} \qquad (3.4.16)$$

From the above expansion and rearrangement it can be seen that only the transformed displacement vectors $\underline{d}_{T_0}$, $\underline{d}_{T_1}$, $\underline{d}_{T_2}$ and $\underline{d}_{T_3}$ need to be calculated (not $\underline{d}_{T_4}$). The real structure displacement

vector $\underline{\underline{d}}$ is then found by transforming back into real space using the supermatrix $\underline{\underline{S}}^{-1}$.

Having developed the analytical theory for a four-fold cyclically symmetric structure, it will now be expanded to deal with an n-fold cyclically symmetric one.

3.5 - The Analysis of an n-fold Cyclically Symmetric Structure

The expansion of the theory developed in the previous section, to deal with structures having any degree of cyclic symmetry, is, again, based on expressing the structure load-displacement stiffness relationship in terms of segment co-ordinate systems, rather than an overall global system. As for the four-fold cyclically symmetric structure, an n-fold cyclically symmetric structure may be represented by its segment boundaries (see figure 3.5.1)

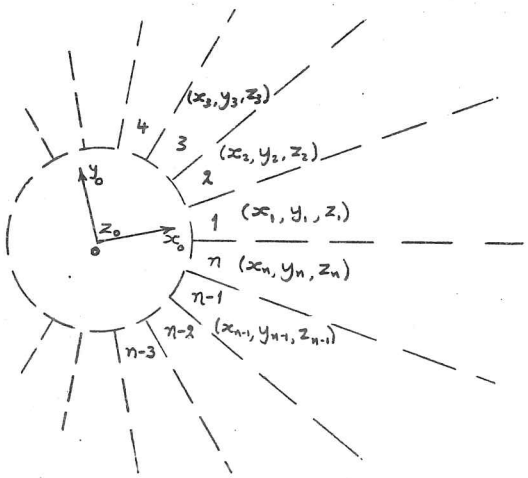

Fig.3.5.1 - An n-fold cyclically symmetric structure represented by its segment boundaries.

The $z_0, z_1, z_2, \ldots, z_n$ axes all coincide with the axis of cyclic symmetry which is directed out of the page. Also, the x_0, y_0, z_0 and x_1, y_1, z_1 co-ordinate systems are assumed to coincide.

Let $\underline{d}_0, \underline{d}_1, \underline{d}_2, \ldots, \underline{d}_n$ be the displacement vectors for each segment relative to their respective co-ordinate systems. Similarly, let $\underline{P}_0, \underline{P}_1, \underline{P}_2, \ldots, \underline{P}_n$ be the load vectors for each segment, again, relative to their respective co-ordinate systems.

For any segment 'q', let the number of other segments directly connected to it by structural members in either direction be $2m$ - in other words, moving in an anti-clockwise direction from segment q, $(q+m)$ is the number of the furthest segment to which it is connected.

The structural stiffness relationship for an n-fold cyclically symmetric structure, in terms of its segment co-ordinates, is thus given by:

$$\left.\begin{bmatrix} \underline{P}_0 \\ \underline{P}_1 \\ \underline{P}_2 \\ \vdots \\ \underline{P}_{n-1} \\ \underline{P}_n \end{bmatrix} = \begin{bmatrix} \underline{K}_{00} & \underline{K}_{01} & \underline{K}_{02} & \cdots & \underline{K}_{0n} \\ \underline{K}_{01}^T & \underline{K}_{11} & \underline{K}_{12} & \cdots & \underline{K}_{1n} \\ \underline{K}_{02}^T & \underline{K}_{1n} & \underline{K}_{11} & \cdots & \underline{K}_{1n-1} \\ \vdots & \vdots & \underline{K}_{1n} & \ddots & \vdots \\ & \underline{K}_{1p} & \vdots & & \\ & \underline{0} & \underline{K}_{1p} & & \\ & \vdots & \underline{0} & & \\ & \underline{0} & \vdots & & \\ & \underline{K}_{1m} & \underline{0} & & \\ & \vdots & \underline{K}_{1m} & & \\ & \vdots & \vdots & \underline{K}_{11} & \underline{K}_{12} \\ \underline{K}_{0n}^T & \underline{K}_{12} & \underline{K}_{13} & \underline{K}_{1n} & \underline{K}_{11} \end{bmatrix} \begin{bmatrix} \underline{d}_0 \\ \underline{d}_1 \\ \underline{d}_2 \\ \vdots \\ \underline{d}_{n-1} \\ \underline{d}_n \end{bmatrix} \right\} \quad (3.5.1)$$

where $\underline{K}_{00} = \underline{K}_{00}^{(1)}$, $\underline{K}_{11} = \underline{K}_{11}^{(1)}$, $\underline{K}_{01} = (\underline{K}_{01}^{(1)} \underline{T}_{11})$

and $\underline{K}_{1l} = (\underline{K}_{1l}^{(1)} \underline{T}_{11})$. $(p=n-m+1)$.

The transformation matrix $\underline{\underline{S}}$ and its inverse $\underline{\underline{S}}^{-1}$ for an n-fold cyclically symmetric structure are then defined as:

$$\underline{\underline{S}} = \frac{1}{n}\begin{bmatrix} \underline{I} & \underline{0} & \underline{0} & \underline{0} & \cdots & \underline{0} & \underline{0} \\ \underline{0} & \underline{I} & \underline{I} & \underline{I} & \cdots & \underline{I} & \underline{I} \\ \underline{0} & \underline{I} & a\underline{I} & a^2\underline{I} & \cdots & a^{n-2}\underline{I} & a^{n-1}\underline{I} \\ \underline{0} & \underline{I} & a^2\underline{I} & a^{2\times 2}\underline{I} & \cdots & a^{(n-2)2}\underline{I} & a^{(n-1)2}\underline{I} \\ \vdots & \vdots & \vdots & \vdots & & \vdots & \vdots \\ \underline{0} & \underline{I} & a^{n-2}\underline{I} & a^{2(n-2)}\underline{I} & \cdots & a^{(n-2)(n-2)}\underline{I} & a^{(n-1)(n-2)}\underline{I} \\ \underline{0} & \underline{I} & a^{n-1}\underline{I} & a^{2(n-1)}\underline{I} & \cdots & a^{(n-2)(n-1)}\underline{I} & a^{(n-1)(n-1)}\underline{I} \end{bmatrix} \qquad (3.5.2)$$

$$\underline{\underline{S}}^{-1} = \begin{bmatrix} n\underline{I} & \underline{0} & \underline{0} & \underline{0} & \cdots & \underline{0} & \underline{0} \\ \underline{0} & \underline{I} & \underline{I} & \underline{I} & \cdots & \underline{I} & \underline{I} \\ \underline{0} & \underline{I} & \bar{a}\underline{I} & \bar{a}^2\underline{I} & \cdots & \bar{a}^{n-2}\underline{I} & \bar{a}^{n-1}\underline{I} \\ \underline{0} & \underline{I} & \bar{a}^2\underline{I} & \bar{a}^{2\times 2}\underline{I} & \cdots & \bar{a}^{(n-2)2}\underline{I} & \bar{a}^{(n-1)2}\underline{I} \\ \vdots & \vdots & \vdots & \vdots & & \vdots & \vdots \\ \underline{0} & \underline{I} & \bar{a}^{n-2}\underline{I} & \bar{a}^{2(n-2)}\underline{I} & \cdots & \bar{a}^{(n-2)(n-2)}\underline{I} & \bar{a}^{(n-1)(n-2)}\underline{I} \\ \underline{0} & \underline{I} & \bar{a}^{n-1}\underline{I} & \bar{a}^{2(n-1)}\underline{I} & \cdots & \bar{a}^{(n-2)(n-1)}\underline{I} & \bar{a}^{(n-1)(n-1)}\underline{I} \end{bmatrix} \qquad (3.5.3)$$

The transformed structural stiffness relationship then takes the form:

$$\begin{bmatrix} \underline{P}_{T_0} \\ \underline{P}_{T_1} \\ \underline{P}_{T_2} \\ \underline{P}_{T_3} \\ \vdots \\ \underline{P}_{T_{n-1}} \\ \underline{P}_{T_n} \end{bmatrix} = \begin{bmatrix} \underline{K}_{T_{00}} & \frac{1}{n}\underline{K}_{T_{01}} & \frac{1}{n}\underline{K}_{T_{02}} & \frac{1}{n}\underline{K}_{T_{03}} & \cdots & \frac{1}{n}\underline{K}_{T_{0n-1}} & \frac{1}{n}\underline{K}_{T_{0n}} \\ \underline{K}^T_{T_{00}} & \underline{K}_{T_{11}} & & & & & \\ \underline{K}^T_{T_{02}} & & \underline{K}_{T_{22}} & & & & \\ \underline{K}^T_{T_{03}} & & & \underline{K}_{T_{33}} & & & \\ \vdots & \vdots & & & & & \\ \underline{K}^T_{T_{0n-1}} & & & & & \underline{K}_{T_{n-1n-1}} & \\ \underline{K}^T_{T_{0n}} & & & & & & \underline{K}_{T_{nn}} \end{bmatrix} \begin{bmatrix} \underline{d}_{T_0} \\ \underline{d}_{T_1} \\ \underline{d}_{T_2} \\ \underline{d}_{T_3} \\ \vdots \\ \underline{d}_{T_{n-1}} \\ \underline{d}_{T_n} \end{bmatrix} \qquad (3.5.4)$$

Now, as for the four-fold example it can be shown that :-

$$\underline{P}_{T_n} = \bar{\underline{P}}_{T_2} \ , \quad \underline{P}_{T_{n-1}} = \bar{\underline{P}}_{T_3} \ , \ . \ . \ .$$

$$\underline{K}_{T_{0n}} = \bar{\underline{K}}_{T_{02}} \ , \quad \underline{K}_{T_{0n-1}} = \bar{\underline{K}}_{T_{03}} \ , \ . \ . \ .$$

$$\bar{\underline{K}}^{T}_{T_{0n}} = \underline{K}_{T_{20}} \ , \quad \bar{\underline{K}}^{T}_{T_{0n-1}} = \underline{K}_{T_{30}} \ , \ . \ . \ .$$

$$\underline{K}_{T_{nn}} = \bar{\underline{K}}_{T_{22}} \ , \quad \underline{K}_{T_{n-1n-1}} = \bar{\underline{K}}_{T_{33}} \ , \ . \ . \ .$$

Therefore $\underline{d}_{T_n} = \bar{\underline{d}}_{T_2} \ , \quad \underline{d}_{T_{n-1}} = \bar{\underline{d}}_{T_3} \ , \ . \ . \ .$

Thus, as a result of this simplification, only the transformed displacement vectors $\underline{d}_{T_0}$ to $\underline{d}_{T_{n'}}$ need to be calculated for a complete solution to be obtained

where $n' = (\frac{n+2}{2})$ for n even

or $n' = (\frac{n+1}{2})$ for n odd.

This represents a reduction of nearly a half in the number of degrees of freedom which need to be considered in order to obtain the displacement solution for the whole structure.

Appendix 3.1 contains expressions for the elements of the transformed load and displacement vectors $\underline{\underline{P}}_T$ and $\underline{\underline{d}}_T$ and for the elements of the transformed stiffness matrix, in terms of the real load and displacement vectors and stiffness matrix.

Having found the transformed displacement solution, it can be used to calculate the real displacement solution, by applying the reverse transformation defined by $\underline{\underline{S}}^{-1}$. Expressions for the elements of the complete real displacement vector, in terms of the transformed displacement vector elements, can also be found in Appendix 3.1.

A further transformation of $\underline{\underline{d}}$ is required to obtain the structural displacement solution in terms of a global co-ordinate system - rather than segment co-ordinate systems. This transformation is defined by:-

$$\underline{\underline{d}}_{\circ} = \underline{\underline{T}}_{\circ}\,\underline{\underline{d}} \qquad (3.5.5)$$

where $\underline{\underline{T}}_{\circ} = \begin{bmatrix} \underline{I} & & & \\ & \underline{I} & & \\ & & \underline{T}_{21} & \\ & & & \underline{T}_{n1} \end{bmatrix}$.

So that the global co-ordinate system coincides with the central region and first cyclic segment co-ordinate systems, the element transformation matrix T_{ml} transforms the m^{th} segment displacement vector from its own segment co-ordinate system to the first segment co-ordinate system.

3.6 - Discussion

During the development of the theory presented here, and while writing the computer program which implements it, many underlying simplifications and relationships have been found. Advantage has been taken of many of these in the computer program to reduce to a more easily coded form the rather involved algebra of the theory.

The relationship which is perhaps the most interesting is that between the transformation supermatrix $\underline{\underline{S}}$ and the structural stiffness supermatrix $\underline{\underline{K}}$ defined with respect to the segment co-ordinate systems. As can be seen in equations (3.4.12) and (3.5.4) the transformed stiffness supermatrix $\underline{\underline{K}}_{T}$ is significantly diagonalized. In fact, if there were no central region to be considered, the first row and column of $\underline{\underline{K}}_{T}$ would consist of zero element matrices, leaving $\underline{\underline{K}}_{T}$ a fully diagonalized supermatrix. So, for example, if the four-fold cyclically symmetric structure considered earlier had no central

$$\underline{\underline{d}}_{\theta} = \underline{\underline{T}}_{\theta}\,\underline{\underline{d}} \qquad (3.5.5)$$

where $\underline{\underline{T}}_{\theta} = \begin{bmatrix} \underline{I} & & & \\ & \underline{I} & & \\ & & \underline{T}_{21} & \\ & & & \underline{T}_{n1} \end{bmatrix}$.

So that the global co-ordinate system coincides with the central region and first cyclic segment co-ordinate systems, the element transformation matrix T_{ml} transforms the m^{th} segment displacement vector from its own segment co-ordinate system to the first segment co-ordinate system.

3.6 - Discussion

During the development of the theory presented here, and while writing the computer program which implements it, many underlying simplifications and relationships have been found. Advantage has been taken of many of these in the computer program to reduce to a more easily coded form the rather involved algebra of the theory.

The relationship which is perhaps the most interesting is that between the transformation supermatrix $\underline{\underline{S}}$ and the structural stiffness supermatrix $\underline{\underline{K}}$ defined with respect to the segment co-ordinate systems. As can be seen in equations (3.4.12) and (3.5.4) the transformed stiffness supermatrix $\underline{\underline{K}}_T$ is significantly diagonalized. In fact, if there were no central region to be considered, the first row and column of $\underline{\underline{K}}_T$ would consist of zero element matrices, leaving $\underline{\underline{K}}_T$ a fully diagonalized supermatrix. So, for example, if the four-fold cyclically symmetric structure considered earlier had no central

region, its transformed stiffness supermatrix would be defined by:

$$\underline{\underline{K}}_T = \frac{1}{4}\begin{bmatrix} \underline{I} & \underline{I} & \underline{I} & \underline{I} \\ \underline{I} & a\underline{I} & a^2\underline{I} & a^3\underline{I} \\ \underline{I} & a^2\underline{I} & a^4\underline{I} & a^6\underline{I} \\ \underline{I} & a^3\underline{I} & a^6\underline{I} & a^9\underline{I} \end{bmatrix} \begin{bmatrix} \underline{K}_{11} & \underline{K}_{12} & \underline{0} & \underline{K}_{12}^T \\ \underline{K}_{12}^T & \underline{K}_{11} & \underline{K}_{12} & \underline{0} \\ \underline{0} & \underline{K}_{12}^T & \underline{K}_{11} & \underline{K}_{12} \\ \underline{K}_{12} & \underline{0} & \underline{K}_{12}^T & \underline{K}_{11} \end{bmatrix} \begin{bmatrix} \underline{I} & \underline{I} & \underline{I} & \underline{I} \\ \underline{I} & \bar{a}\underline{I} & \bar{a}^2\underline{I} & \bar{a}^3\underline{I} \\ \underline{I} & \bar{a}^2\underline{I} & \bar{a}^4\underline{I} & \bar{a}^6\underline{I} \\ \underline{I} & \bar{a}^3\underline{I} & \bar{a}^6\underline{I} & \bar{a}^9\underline{I} \end{bmatrix} \qquad (3.6.1)$$

$$\underline{\underline{K}}_T = \begin{bmatrix} (\underline{K}_{11} + \underline{K}_{12} + \underline{K}_{12}^T) & & & \\ & (\underline{K}_{11} + a\underline{K}_{12} + \bar{a}\underline{K}_{12}^T) & & \\ & & (\underline{K}_{11} + a^2\underline{K}_{12} + \bar{a}^2\underline{K}_{12}^T) & \\ & & & (\underline{K}_{11} + a^3\underline{K}_{12} + \bar{a}^3\underline{K}_{12}^T) \end{bmatrix} \qquad (3.6.2)$$

Now there are two important and related aspects of equations (3.6.1) and (3.6.2) which are of interest. The first is that if all the element matrices of the supermatrix are replaced by scalar elements, the equations (3.6.1) and (3.6.2) become:

$$\underline{k}_T = \frac{1}{4}\begin{bmatrix} 1 & 1 & 1 & 1 \\ 1 & a\,1 & a^2 1 & a^3 1 \\ 1 & a^2 1 & a^4 1 & a^6 1 \\ 1 & a^3 1 & a^6 1 & a^9 1 \end{bmatrix} \begin{bmatrix} k_{11} & k_{12} & 0 & k_{12}^T \\ k_{12}^T & k_{11} & k_{12} & 0 \\ 0 & k_{12}^T & k_{11} & k_{12} \\ k_{12} & 0 & k_{12}^T & k_{11} \end{bmatrix} \begin{bmatrix} 1 & 1 & 1 & 1 \\ 1 & \bar{a}\,1 & \bar{a}^2 1 & \bar{a}^3 1 \\ 1 & \bar{a}^2 1 & \bar{a}^4 1 & \bar{a}^6 1 \\ 1 & \bar{a}^3 1 & \bar{a}^6 1 & \bar{a}^9 1 \end{bmatrix} \qquad (3.6.3)$$

$$\underline{k}_T = \begin{bmatrix} (k_{11} + k_{12} + k_{12}^T) & & & \\ & (k_{11} + a k_{12} + \bar{a} k_{12}^T) & & \\ & & (k_{11} + a^2 k_{12} + \bar{a}^2 k_{12}^T) & \\ & & & (k_{11} + a^3 k_{12} + \bar{a}^3 k_{12}^T) \end{bmatrix} \qquad (3.6.4)$$

which is more recognizable as the familiar eigenvector diagonalization, where $\underline{S}$ is a matrix formed from the eigenvectors of the matrix to be diagonalized, $\underline{k}$ [15]. Another important result of this transformation is that the elements of the diagonalized matrix are the eigenvalues of the original matrix $\underline{k}$. The second and related point, is that the structural stiffness supermatrix (and thus the matrix $\underline{k}$) is a

Circulant matrix. That is, the element matrices of each row are formed from successive cyclic permutations of the elements in the first row. Now the eigenvalues of an $n \times n$ circulant matrix ($\underline{k}$ is a 4×4 circulant matrix) are given by [16]:

$$\lambda_k = 1,\ a_k,\ a_k^2,\ \ldots,\ a_k^{n-1} \qquad \text{for } k = 1, 2, 3, \ldots, n \qquad \text{where } a_k = \exp\{i2\pi k/n\} \tag{3.6.5}$$

which, as expected, is the form of the columns of the transformation matrix $\underline{S}$ and supermatrix $\underline{\underline{S}}$.

From the properties of a circulant matrix pointed out above, it will be seen that the eigenvalues of such a matrix are very simply found. Now if a real system is being modelled, the eigenvalues often have a physical interpretation - as in structural vibration analysis, for example. Since we are concerned here with the modelling of real structures, a physical interpretation of the eigenvalues of $\underline{\underline{K}}_T$, or, more correctly, eigenmatrices of $\underline{\underline{K}}_T$, since they are, in fact, the diagonal element matrices of $\underline{\underline{K}}_T$ (see equation 3.6.2), can reasonably be sought.

Such a physical interpretation may be developed from recognising that the elements of the eigenvectors, which form the transformation supermatrix $\underline{\underline{S}}$ (and also the matrix $\underline{S}$), are equivalent to the terms of the Complex Fourier series. The transformation of the structural stiffness relationship $\underline{\underline{P}} = \underline{\underline{K}}\underline{\underline{d}}$ into $\underline{\underline{P}}_T = \underline{\underline{K}}_T\underline{\underline{d}}_T$ can thus be thought of as a transformation from real space into complex Fourier space. What follows from this interpretation is that the eigenmatrices (the diagonal element matrices of $\underline{\underline{K}}_T$) can be thought of as representing the components of the cyclic segment stiffness matrix corresponding to each term of the complex Fourier series. In other words, the component matrices of the complex Fourier series represent the cyclic

segment stiffness matrices which are the diagonal element matrices of $\underline{\underline{K}}_T$. Thus the first eigenmatrix is the cyclically symmetric stiffness component; the second is the $\cos\alpha$ $(\alpha=0\rightarrow 2\pi)$ varying stiffness component; the third, the $\cos 2\alpha$ varying stiffness component, and so on.

Continuing this Fourier analysis interpretation, the element vectors of $\underline{\underline{P}}_T$ will then represent the coefficients of the finite Fourier series of the applied loading. So, by examining the relative magnitudes of these coefficient vectors, the dominant terms of the Fourier series may be found. This would then indicate which of the stiffness terms would most effectively be adjusted, to produce a change in the structural displacement response, to a particular applied load.

The introduction of a non-cyclically symmetric central region, which requires one more row and column (of element matrices) to be added to $\underline{\underline{K}}_T$, is unlikely to have any significant effect on the above interpretation of the physical significance of the $\underline{\underline{K}}_T$ diagonal element matrices. This is because the off-diagonal element matrices in the first row and column of $\underline{\underline{K}}_T$, which result from the structural connections between the cyclic segments and the central region, will normally be very sparsely populated compared to the diagonal element matrices, and so the actual eigenmatrices of $\underline{\underline{K}}$ will differ only slightly from the diagonal element matrices of $\underline{\underline{K}}_T$.

3.7 - References

1. Southwell, R.V. - On the Calculation of Stresses in Braced Frameworks. Proc.Roy.Soc., vol.139-A, pp.475, 1944.

2. Newell, J.S. - The use of Symmetric and Anti-Symmetric Loadings. J. of Aeronautical Science, Jan. 1939, pp.235.

3. Andree, W.L. - Das B = U Verfahren: R. Oldenbourg, Munchen and Berlin, 1919.

4. Renton, J.D. - On the Stability Analysis of Symmetrical Frameworks. Quart.Jours. Mech. and Applied Maths., V17, pt.2, 1964, pp.175.

5. Nooshin, M. & Butterworth, J.W. - Techniques for the Analysis of Cyclically Symmetric Structures. Int.Assoc. for Shell & Spat. Struct.Symp. on Ind.Spat. & Shell Struct.Lect., Kielce, Pd. June 18-23, 1973, pp.337-349. Pub. by Int.Assoc. for Shell & Spat. Struct., Kielce Pol., 1973.

6. MSC/NASTRAN Application Manual, 2.2-1 (1974). MacNeal-Schwendler Corporation.

7. Fortescue, C.L. - Method of Symmetrical Co-ordinates applied to the Solution of Polyphase Networks. Trans. AIEE, V37, prt.2, 1918, p.1027.

8. Smoot Katow, M. - Techniques used to Evaluate the Performance of the NASA/JPL 210-ft. Reflector Structure under environmental loads. Structures Technology for Large Radio & Radar Telescope Systems, pp.185, MIT Press, 1969.

9. Vold, H., Knapp, H. & Hermann, P. - ASKA-CS Cyclic Symmetry user's guide. Institut fur Statik und dynamik der luft-und Kaumfahrtkonstruktionen, University of Stuttgart, 1977.

10. Colyer, B. - Axi-symmetric Structures. Rutherford Engineering Laboratory Internal Report, 1978.

11. Kron, G. - A Set of Principles to Interconnect the Solutions of Physical Systems. J.App.Phys., vol.24, No.8, 1953, pp.965.

12. Kron, G. - The Application of Tensors to Electrical Engineering Problems. Gen.Elect.Rev., vol.38, 1935, pp.242.

13. Kron, G. - Solving Highly Complex Elastic Structures in Easy Stages. J.App.Mechn., vol.22, No.2, 1955, pp.235.

14. Wagner, C.F. & Evans, R.D. - Symmetric Components, 1st Ed. McGraw-Hill Book Company Inc., 1933.

15. Strang, G. - Linear Algebra and its Applications. Academic Press, 1970, pp.187.

16. Hall, G.G. - The International Encyclopedia of Physical Chemistry and Chemical Physics. Topic 1, Mathematical Techniques, vol.4, Matrices and Tensors. Pergamon Press, 1963.

Chapter Four - Programming the Cyclic Symmetry Analysis Theory

4.0 - Introduction

The theoretical analysis method presented in the previous chapter is formulated according to the matrix Displacement Method of structural analysis [1,2]. It is therefore based on the usual assumptions of linear-elastic material behaviour, small structure geometry deformations and that real structure joint behaviour can be adequately modelled using a number of degrees of freedom at a point. Thus, before it can sensibly be used, it must be implemented in the form of a computer program.

This chapter describes the decisions made concerning the general form of such a program, and its detailed structure and application, concluding with a discussion of various aspects of the program and its use, together with some recommendations for its improvement.

4.1 - Program Versatility

How specialised, or how general, a program is designed to be, not only affects its overall structure but it also governs to a large extent its detailed form. A balance has to be found between writing a completely general program, which can cope with every conceivable formulation of the type of problem being considered, and a very specialised code that is only able to deal with one such formulation.

Since it is a development program that has been written, to implement and test a new analytical method, rather than a 'commercial' one, based on previously established theory, the decisions made concerning its versatility were influenced by the need to analyse a set of problems which would provide a complete and rigorous test of both program and theory - thus demonstrating the advantages of the new analytical method. Also, because its development was to provide a

fast accurate analysis stage in the complete millimetre wave telescope design procedure, it obviously needed to be capable of dealing with this type of structure. On this basis, the Cyclic Symmetry Analysis program has been written simply to analyse three-dimensional, cyclically symmetric, tubular framework structures, which may possess a region of structural non-cyclic symmetry, and are subjected to non-cyclically symmetric loadings.

The limits governing the size of the structures which the program can handle were also influenced by the size of the telescope structure to be analysed, and are defined in Appendix 4.1.

4.2 - Choice of Framework Joint Model

There are two, now standard, types of joint model which can be used in the analysis of framework structures [1]; the pin-joint or the rigid-joint. The pin-joint model assumes that there is no bending or torsional stiffness at the joints, whereas the rigid-point does include such terms. This means that a structure modelled using rigid-joints has twice as many variables as that when modelled using pin-joints (in the case of a three-dimensional structure). Since the initial aim of the program was to demonstrate the new cyclic symmetry analysis method, which could quite adequately be done using the simpler pin-joint model, it was decided to use this joint model.

This question of what type of joint model to use was raised again when it came to using the program for the displacement analysis of telescope structures (see chapter 6, section 6.3).

4.3 - Problem Description and Data Generation

The way in which structural analysis problems are described to a computer program, via the input data, has an important influence on

both the program organization and how easy it is to use as an analysis tool. It is therefore an aspect which must be carefully considered and defined before starting to write the computer code.

The problem is how a structure's geometry, topology and loading can be described to the program simply and unambiguously, without requiring large amounts of data. As a result of the repeated segments of a cyclically symmetric structure, the amount of data required to describe its geometry and topology can be considerably reduced, compared to the amount required by a more conventional analysis program - which does not take advantage of the cyclic symmetry. However, care must be taken when describing the connections between cyclic segments and also between the central region and cyclic segments. It was with this situation in mind that the data input requirements of the cyclic symmetry analysis program were formulated. They are designed to encourage a user to appreciate the implications of dividing a structure into cyclic segments - also, to facilitate easy checking and enable alterations to be made simply and quickly.

The other main influence on the data input requirements was the more specific load conditions to which millimetre wave telescope structures are subjected. These are self-weight loading and point mass loads - produced by the reflecting panels at their support points. By incorporating the ability to consider two load conditions at a time, the two important load cases of zenith pointing and horizon pointing may be analysed in one run - although any other two pointing angles may be considered. A detailed description of the data input format for the cyclic symmetry analysis program is given in Appendix 4.1, and an example data file, for the structure considered in section 3.5, can be seen in table 4.2.6 of Appendix 4.2.

4.4 - Program Structure and Organisation

In common with modern 'Structured Programming' methods, and to break up the task of writing the program into a number of smaller ones, as well as to ease the problem of checking and debugging the code, five sequential stages were defined, each corresponding to a section of the theory. These five stages were then coded as five separate Fortran programs which run consecutively and communicate with each other by reading from, and writing to, a common pool of binary files (see figure 4.4.1).

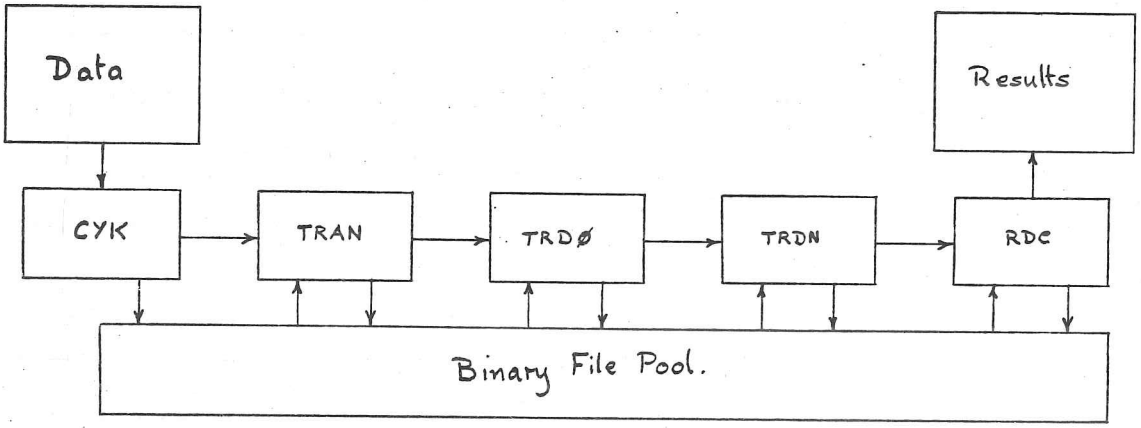

Fig.4.4.1 - The Cyclic Symmetry Analysis Program Structure.

The first program, CYK , can be described as a setting up procedure; it reads all the data required by the complete program (that is all five sub-programs) forming all the stiffness matrices and load vectors as it does so. It also constructs various control parameter arrays used later by other sub-programs.

The second sub-program, TRAN , as its name implies, carries out the transformation of the problem into Complex Fourier Space by implementing equations (A3.1.1), (A3.1.2) and (A3.1.3) of Appendix 3.1. Since the mini-computer on which the program was first developed could only support Fortran II, which does not have complex variables, all the complex arithmetic has been coded explicitly - the program was

later transferred to a larger computer when more core store was required. At first it seemed that having to carry out the complex arithmetic explicitly would considerably increase the coding task; however, it quickly became clear that, although some of the coding would be more complicated, there are some important simplifications in the complex albegra which could be taken advantage of.

The sub-program which follows, TRDØ , has the job of calculating the transformed central region displacement vector which, as can be seen from equation (A3.1.4) (of Appendix 3.1), represents a large part of the total calculations needed to find the complete transformed displacement solution. The remaining terms of equation (A3.1.4) are then calculated by the fourth sub-program, TRDN , to find the transformed cyclic segment displacement vectors. All that is then required is for this complete solution to be transformed back into real space, which is carried out by the last sub-program, RDC . A further transformation is performed by RDC on the real displacement solution to obtain the whole displacement solution in terms of one global co-ordinate system - rather than with respect to the cyclic segment co-ordinate axis sets. The complete joint displacement solution is then written out to a results file as well as a binary pool file for use by results processing programs.

4.5 - Program Performance

In order to measure the performance of the cyclic symmetry analysis program, and compare it with that of a conventional Finite Element Analysis program (which takes no advantage of any structural cyclic symmetry to reduce the size of the analysis task), a structure possessing some cyclic symmetry, as well as a general non-cyclically symmetric region, has been analysed. This analysis is of a proposed

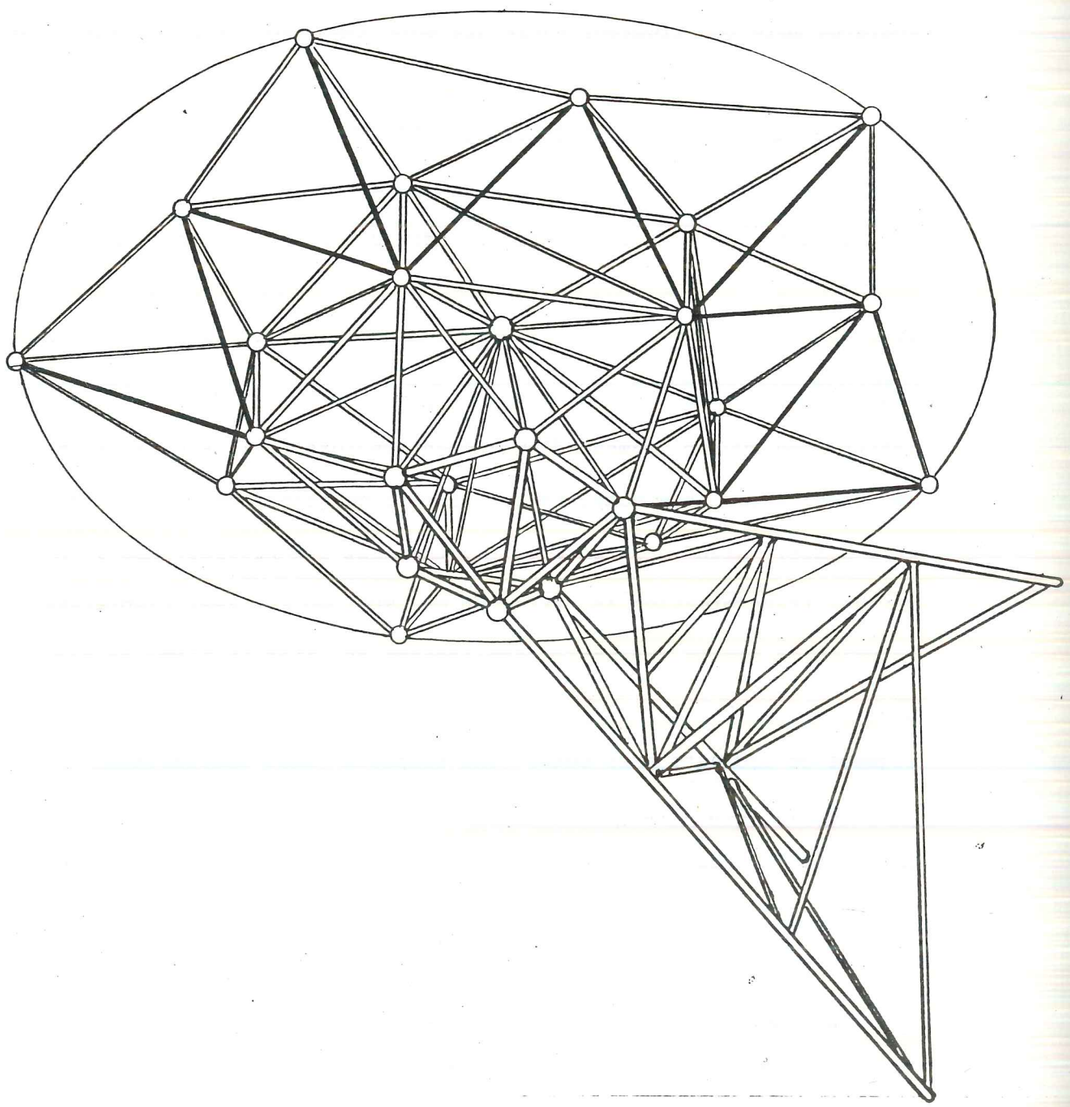

Fig.4.5.1 - Proposed primary structure design of an off-shore drilling rig helicopter landing pad.

design for the primary framework structure of a helicopter landing pad to be built on the side of an off-shore drilling rig (see figure 4.5.1).

A detailed description of this helipad structure is given in Appendix 4.2, together with a listing of the data file generated for its analysis using the cyclic symmetry program. The nodal displacement solutions produced by both the cyclic symmetry analysis program, and a conventional Finite Element Analysis program, are also presented in Appendix 4.2. The loading applied to the structure for the analysis simulates a helicopter landing towards the edge of the pad, out of line of the supporting arm, which therefore produces a non-cyclically symmetric loading (see Appendix 4.2 for details).

As can be seen from figure 4.5.1, the complete platform structure consists of a cantilevered support arm (which forms the non-cyclically symmetric central region) to carry the cyclically symmetric deck supporting structure. This is formed from five identical, equally spaced, radial ribs, each connected to the neighbouring ribs both directly and via an intermediate joint. All the radial ribs are connected to the cantilever support arm via a pentagonal pyramid type structure situated on the end of the support arm.

For the analysis using the cyclic symmetry program, only the cantilever arm structure, one rib and its connection to its neighbouring ribs need to be defined by the input data, as opposed to the whole structure geometry for the conventional analysis. In the example structure considered here, the size of the cyclic symmetry analysis data file only represents a reduction of the order of 35% on the size of the conventional data file. However, for structures having high orders of cyclic symmetry, the savings in the amount of data which must be generated are very much greater, and can be as much as 85-90% .

To sensibly compare the results produced by the cyclic symmetry

analysis program, with those produced by a conventional Finite Element analysis program, they have to be seen in the context of the expected rounding errors which accumulate during the numerical calculations. In other words, before the two solutions can be said to compare well, it has to be established that the differences which do exist are within the expected rounding error range. Since a detailed study of the numerical calculations carried out by both types of program would be required to accurately define their respective rounding error ranges (a difficult and time-consuming procedure), a less rigorous but more practical scheme for estimating the rounding error ranges was used.

This scheme involved preparing two sets of data for the conventional* analysis program, each describing the same (helipad) structure and loading, but using a different joint node numbering scheme in the cyclically symmetric deck supporting structure. The results for each of these data sets (presented in tables 4.2.2 and 4.2.3 of Appendix 4.2) generally differ in the fourth decimal place. The data files were then analysed again with the same program, but this time using double precision arithmetic. These results (see tables 4.2.4 and 4.2.5 of Appendix 4.2) showed there to be hardly any difference between the two solutions. This therefore confirms that the differences occurring in the single precision results are due to rounding errors - the accumulation being slightly different for each case. It also means that the double precision solution can be treated as a true solution, thus enabling the difference between both the single precision conventional analysis and cyclic symmetry analysis solutions, and the true solution to be estimated. This was done by

---

*This was a program written to implement the standard pin-joint finite element analysis, of a complete structure, which used the same matrix inversion and multiplication routines as the cyclic symmetry program.

calculating the root mean square values of the difference between the mantissa values of true (double precision) and single precision values, thus indicating how many decimal places the solution are accurate to. For the conventional analysis, the error estimate is 0.0003 , that is, it is accurate to four decimal places, and for the cyclic symmetry analysis the error estimate is 0.003 - an accuracy to three decimal places. Now the difference between these two error estimates can be shown to be due to a greater accumulation of rounding errors in the calculations carried out by the cyclic symmetry analysis program (see Appendix 4.2). It can therefore be said that both the cyclic symmetry and conventional analysis solutions compare well: thus confirming the accuracy of the cyclic symmetry analysis program.

A comparison of the amount of central processor time used by each program for the helipad analysis, shows the cyclic symmetry program to have taken 75% of the time used by the conventional program. Like the reduction in data required, this saving of central processor time will increase as the number of cyclic segments and overall size of the structure increases. A point is then reached where the only practical method of analysis is one in which advantage is taken of the cyclic symmetry properties to reduce the size of the analysis task - a facility up to now only available for purely cyclically symmetric structures which have no central, on axis, structure.

4.6 - Discussion

Writing a piece of computer code to implement a new analytical method is a very good way of achieving complete understanding of the method. It has also proved to be a useful way of ironing out all the algebraic errors which occurred in the formal development and presentation of the method - something which otherwise would have

been difficult to do.

Although the program structure of five separate sub-programs was largely governed by the core store limitations of the mini-computer it was first developed on, it proved to be a useful way of organising the program even when it was transferred to a larger computer. It not only allowed bugs to be isolated from other bugs as well as already correct code, but also enabled intermediate results, of the calculations performed by each sub-program, to be obtained very easily - by reading the files in the binary file pool using an auxiliary program. The multi-program structure also provides a useful degree of flexibility. This aspect has proved particularly advantageous in the telescope structure design procedure, where the program is used many times - once for each time round the design loop, Since to improve the homological deformation performance of a particular structure, changes are usually only made to the cyclically symmetric surface supporting structure, and not the central region structure, re-analysis of the central region structure is often unnecessary - at least for small structure changes. The time taken for the complete re-analysis can thus be significantly reduced by using the old transformed central region displacement vector and missing out sub-program TRDØ - which normally takes a large proportion of the complete analysis time.

The results of the error analysis (see section 4.5 and Appendix 4.2) show that, although the cyclic symmetry analysis results are accurate to one decimal place less than those of the conventional analysis program, they are still good enough not to require the use of double precision arithmetic. As the size of the problem considered increases the accuracy of the results can be expected to fall. However, the rate at which the deterioration takes place will in general be less than that of a conventional analysis program.

Apart from some small improvements which could usefully be made to the data input format and some of the computational methods used to carry out the various matrix operations, one facility which it would be very useful to include in a new program is a selection of different types of structural elements. The addition of a rigid-joint beam element and a thin panel element, would considerably improve the general application of the program.

As with any computer program, it is very difficult to feel that it is finished or that it cannot be improved. However, even with its several apparent deficiencies, the present cyclic symmetry analysis code clearly demonstrates the effectiveness of the new method in dealing with structures having mixed cyclically symmetric and non-cyclically symmetric parts.

A more detailed list of recommendations and suggestions for the development of any new cyclic symmetry analysis program is given in Appendix 4.3.

4.7 - References

1. Livesley, R.K. - Matrix Methods of Structural Analysis, 2nd Ed. Pergamon Press Ltd., 1975.

2. Przemieniecki, J.S. - Theory of Matrix Structural Analysis. McGraw-Hill Book Company, 1968.

Chapter Five - Homological Aspects of the Design Procedure

5.0 - Introduction

We return now to the remaining stages of the proposed design procedure outlined in chapter two (see figure 2.3.1). These remaining stages can be divided into two pairs: stages one and five, and stages three and four. The first pair of stages is concerned with the detailed design of a potentially homologically deforming structure (within the overall cyclically symmetric form already decided upon), and how it is best altered to improve its homological deformation performance. The second pair of stages, three and four, is concerned with establishing how close to perfect homological deformation the actual structure deformation behaviour needs to be for a given observable wavelength, and how its deviation from perfect homological deformation can be measured.

The components of the first pair of stages will now be considered in detail, starting with a review of the design variables which could be used to make the required adjustments to a structure whose homological behaviour is not yet good enough. The second pair of stages will then be considered in some detail.

5.1 - Homology Design Variables

In his paper [1] on the design of homologically deforming Radio Telescope Dishes, von Hoerner defines four sets of design variables (he uses the term 'degrees of freedom') which a homologically deforming structure will have: (1) the geometric shape - for example the joint co-ordinates of a framework structure; (2) its topology - joint connections; (3) the member cross-sectional areas; and (4) the homology parameters - the paraboloid origin shifts, focal length change and

axis tilt. Having established that at least mathematical (theoretical) homologically deforming structure solutions exist, he goes on to outline a method for finding the nearest solution to a given (initial) structure which involves varying all the member cross-sectional areas - the nearest solution being defined as the one requiring the set of smallest area changes. The reason for choosing the member cross-sections as the design variables, is that the problem of finding the set of smallest area changes, which will give perfect homological deformation, can be formulated as a fairly straightforward minimization problem (see ref. [1]).

The result of this approach to finding a homologically deforming structure, is a design which requires a large number of different member cross-sectional areas which do not necessarily correspond to any which are actually available from manufacturers. So in order to build such a design, the nearest available section must be used, thus introducing errors into the structure which will produce some degree of non-homological deformation. A sensitivity analysis was carried out by von Hoerner (with numerical work by Jennings and Biswar of the Department of Civil Engineering, University of Virginia, Charlottesvile, Va.) in which he established that the use of available sections would not produce unacceptable deviations from the desired homological deformation. From this work, he quotes a figure of 5% as being an acceptable variation of the available sections used from the computed (ideal) values. However, in a later paper [2], he gives a figure of 12% which, since it is based on the results obtained from an improved computer program, capable of modelling more realistic structures, is considered to be the more accurate of the two.

This cross-sectional area tolerance limit was obtained for large radio telescope structures of 300-400 ft. diameter, designed for

observations at centimetre wavelengths. Scaling this figure for a 15 m (50 ft.) diameter dish, capable of observing at wavelengths as short as 0.35 mm , gives a cross-sectional area tolerance ($\Delta A/A$) of 5.3% * - a larger diameter would require an even tighter tolerance for the same wavelength. Now this limit of 5.3% on the variation of the cross-sections used, from the computed value, cannot be met using currently available structural steel sections. For this reason, at least, finding homologically deforming telescope structure designs, suitable for use at millimetre and sub-millimetre wavelengths, by simply varying the member cross-sectional areas, is not practical.

Another problem which results from this method of design, is that it is possible for joints to occur where members of widely different sizes have to be joined, which is not easy to do in practice. Also, because the number of members in a structure of 15 metres diameter will be much smaller than in one of 100 m (300 ft.) diameter, the effects of any area differences will be much more significant and less likely to be cancelled out by other members.

The impracticality of the exclusive use of member cross-sectional areas as the design variables, does not mean that they cannot be used at all in seeking a homological design, but that they can only be used as a secondary design variable. This means that another set of design variables must be used as the primary set. Looking again at von Hoerner's list of design variables, it is clear that the only other set which can provide enough variables in practice, is that of the joint positions (structure geometry). The structure topology can only

---

* Using the relationship $(\Delta A/A) \propto \lambda/D^2$, where λ is the shortest wavelength to be observed and D is the telescope dish diameter (see table 4 of ref. [2]), and demanding a greater surface accuracy of $\lambda/27$ mm r.m.s., compared to the $\lambda/16$ mm r.m.s. used by von Hoerner.

be used as a secondary variable as a result of its rather limited variability - two joints are either connected or they are not.

The advantage of using the structural geometry as the primary design variable set, over member cross-sections, is that its construction (assuming a homologically deforming design can be found by this method) would only suffer from the inaccuracies of manufacture. Thus, within these limitations, and those of the theory used in the numerical analysis, a perfect homologically deforming structure may actually be built. This fact becomes more important when designing telescope structures which are to be used at millimetre and sub-millimetre wavelengths, because inaccuracies introduced by other components of the telescope become more significant, leaving less room for homology errors. These other errors are produced by reflecting surface panel and secondary reflector errors, tracking errors, the effect of members differing from their nominal (manufactured) size and the differences between the real structure behaviour and that predicted by the theory used in the numerical analysis.

Having decided to adjust the position of the joints in the surface supporting structure, in order to try and improve its homological deformation behaviour (stage five in the design loop), the minimum number of joints which an initial design must have, for at least theoretical homology solutions to exist, will now be established.

5.2 - Theoretical Homological Structure Conditions

The parabolic reflecting surface of a radio telescope consists of a large number of individual panels, each supported at points around their edges by the surface supporting structure. The number of support points, and thus panels, is made large enough for the gravitational deformation of the panels, between neighbouring support points, to be

within the specified (acceptable) surface error tolerance. Since the deformations of the structure at any angle of elevation can be defined as a linear combination of the zenith and horizon pointing deformations (see section 2.1), the structural homology conditions will be developed by considering these two cases separately.

A free paraboloid, defined with respect to three mutually perpendicular axes (x, y and z), has seven degrees of freedom: three translational movements of the origin along each axis, a rotation of the paraboloid about each axis, and a focal length variation. In the zenith pointing case, which for a cyclically symmetric supporting structure produces a cyclically symmetric deformation, it can be seen that if the support points of one cyclic segment lie on a paraboloid, whose axis points to the zenith (i.e. z-direction, see figure 2.8.1), then all the surface support points in the remaining cyclic segments will lie on the same paraboloid. Now the only degrees of freedom which need to be used for the initial paraboloid (having its axis along the z-coordinate axis and origin at the co-ordinate origin) to be transformed into the deformed paraboloid, are a vertical shift of the origin along the z-axis and a focal length change (see section 2.2). Thus the number of conditions which must be satisfied for the support points of one cyclic segment to lie on a parabolic surface, of the required form (and thus defined by two points), is given by:

$$C_z = (n_{sy} - 2) \,, \qquad (5.2.1)$$

where n_{sy} is the number of surface support points per cyclic segment.

For the horizon pointing case the gravitational deformation will be anti-symmetric, and it has been shown (see section 2.2) that a paraboloid whose axis is tilted about the y-axis and whose origin is shifted along the x-axis, can be fitted to this form of deformation.

Thus, again only two degrees of freedom of the initial paraboloid need to be varied: the x position of the origin and the angle between the paraboloid axis and the z-axis, in the x-z plane (see figure 2.2.2). So the number of conditions which must be satisfied for the support points of one cyclic segment to lie on the new paraboloid (which is also defined by two points) is given by:

$$C_h = (n_{sy} - 2). \qquad (5.2.2)$$

Now the number of design variables available to satisfy these two conditions, assuming only the positions of the joints other than those at panel support points, may be varied, and that the member cross-sections are fixed (initially at least), is given by:

$$D_f = 2(P_y - n_{sy}) , \qquad (5.2.3)$$

where P_y is the number of joints per cyclic segment, each having two degrees of freedom. Only the degrees of freedom of joints in one segment can be used because once the positions of these joints is defined, the positions of the joints in all the other segments are defined - by the cyclic symmetry. Also, only two degrees of freedom per joint is generally available, radially and axially, since any non-radial or non-axial movement would either be out of the plane of the radial ribs or tend to destroy the reflective symmetry usually possessed by each cyclic segment (which results from the way the surface panels are arranged).

Thus, for a supporting structure, whose panel support points cannot take arbitrary positions, to satisfy both the zenith and horizon pointing conditions

$$D_f \geq C_z + C_h , \qquad (5.2.4)$$

which, in terms of the number of joints (including support points) in a single cyclic segment, becomes:

$$P_y \geq (2n_{sy} - 2) \ . \qquad (5.2.5)$$

Equation (5.2.5) thus defines the minimum number of joints per cyclic segment which a structure, designed to support a given number of fixed (panel attachment) points, must have for a set of positions of its free joints to exist which represent a structure that will deform homologically in both the zenith and horizon pointing positions.

5.3 - Practical Homological Structure Conditions

The theoretical condition defined by equation (5.2.5) can only be regarded as a minimum condition, since even though there may be homological joint position solutions, they will not necessarily satisfy the practical conditions which exist. These practical conditions take the form of limitations on the distances between joints, to avoid buckling of longer members and leave room for joints at the ends of short members. Also, the position of free joints clearly cannot be in front of the supported reflecting surface. Furthermore, there are practical limits on the values of the four homology parameters (x_o, z_o, ϕ and Δf , see figures 2.2.1 and 2.2.2), in particular on the variation of focal length. This arises from the fact that if the reflecting panels are made for a paraboloid surface having the correct horizon pointing focal length, they will not have the correct focal length in the zenith pointing direction. In practice, then, for a 15 m dish of focal length 5.4 m , having five rings of reflecting panels, a maximum focal length variation of 3.2 mm is all that is allowable if observations are to be made at millimetre and sub-millimetre wavelengths (see Appendix 5.1).

To improve the possibility of finding a practical homological solution the initial structure needs to have as many free joints as possible - without unnecessarily complicating the structure's geometry. It should also be reasonably close to a homological solution to start with. The member cross-sectional areas may be used as secondary design variables, only taking the value of available sections, to improve undesirable or nearly impractical joint positions which may occur.

5.4 - Surface Accuracy and a Best Fit Paraboloid

The second pair of design loop stages, three and four, are concerned with establishing a design goal and how progress towards this goal is to be measured. This design goal is defined as the maximum allowable deviation of the actual structural deformation from the desired homological form. Any other structural requirements which arise from the overall telescope specifications, are treated as conditions under which the homological deformation goal must be found.

Although both optical reflecting telescopes and radio telescopes (of the reflecting antenna type) use the same type of reflecting surface - having a parabolic shape - which, on the face of it, is not unexpected, there is an important difference between the way in which they operate that is significant when considering the effect any deviation of the reflecting surface, from a perfect paraboloid, has on the performance of the two types of telescope. In the case of an optical telescope, where it is only the intensity of light collected (by a photographic plate, for instance) that is important, it would be possible to use a number of independent reflecting surfaces, all focusing light to the same point (see figure 5.4.1). This is because, as a result of irregularities in the atmosphere, the phase of the individually reflected signals (by each elemental reflector) is not

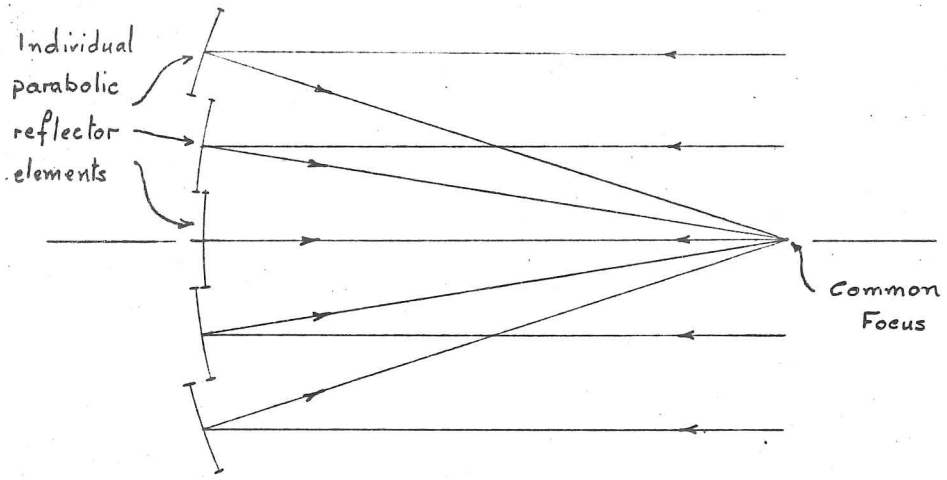

Fig.5.4.1 - A multi-element reflector, having a common focus.

itself coherent, so that the varying path lengths of the reflected signals, which also produce an incoherent signal at the focus, do not matter. This, however, is not the case for radio wavelength signals, which are not affected by atmospheric conditions to the same extent. The reason for using a single parabolic reflector is therefore not just that it focuses a wide parallel beam of radiation to a single point (which, as has just been pointed out, can be done by other means), but also that the focused beam is still coherent. This is because the path lengths of every part of the focused beam are the same, no matter which part of the parabolic surface reflects it (see figure 5.4.2).

The gain of a parabolic reflector, according to the theoretical work of Ruze [3], is a measure of the signal incoherence produced by surface errors, which is given by:

$$G = G_o \exp\{-(2\pi\varepsilon/\lambda)^2\} , \qquad (5.4.1)$$

where G_o is the no error gain, λ the operating wavelength and ε the r.m.s. signal path length variation produced by surface inaccuracies. Equation (5.4.1) assumes that the errors are small, that they are uniformly distributed across the surface, that the phase errors they produce are random and described by a Gaussian probability

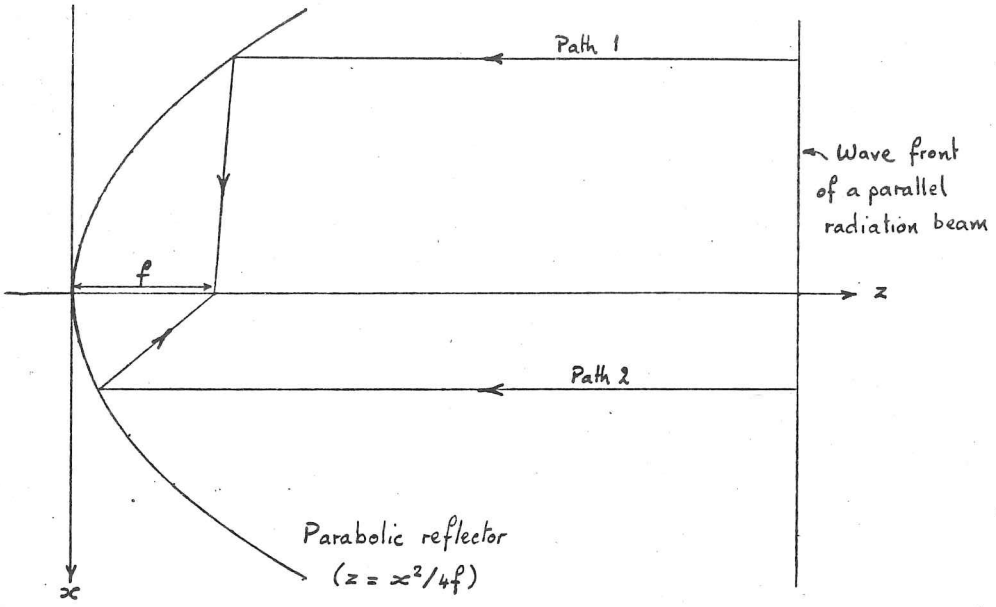

Fig.5.4.2 - The lengths of path 1 and path 2 are the same.

density function, and that the errors over a region defined as the correlation interval are independent of the errors in the other regions of the aperture (the correlation interval describes the average distance over which the surface errors are substantially constant). Defining the reflector surface efficiency as $\eta_s = G/G_o$, equation (5.4.1) may be rewritten as:

$$\eta_s = \exp\{-(2\pi\varepsilon/\lambda)^2\} . \qquad (5.4.2)$$

As was described in section 1.1, the performance of a radio telescope is affected by many different aspects; for the parabolic reflecting surface the major factors, which introduce errors, are:

(i) error resulting from the manufacturing inaccuracies of each reflecting surface panel,

(ii) deviations (from a parabolic shape) of each panel under its own weight,

(iii) panel adjustment errors, due, for instance, to inaccuracies in the measuring device,

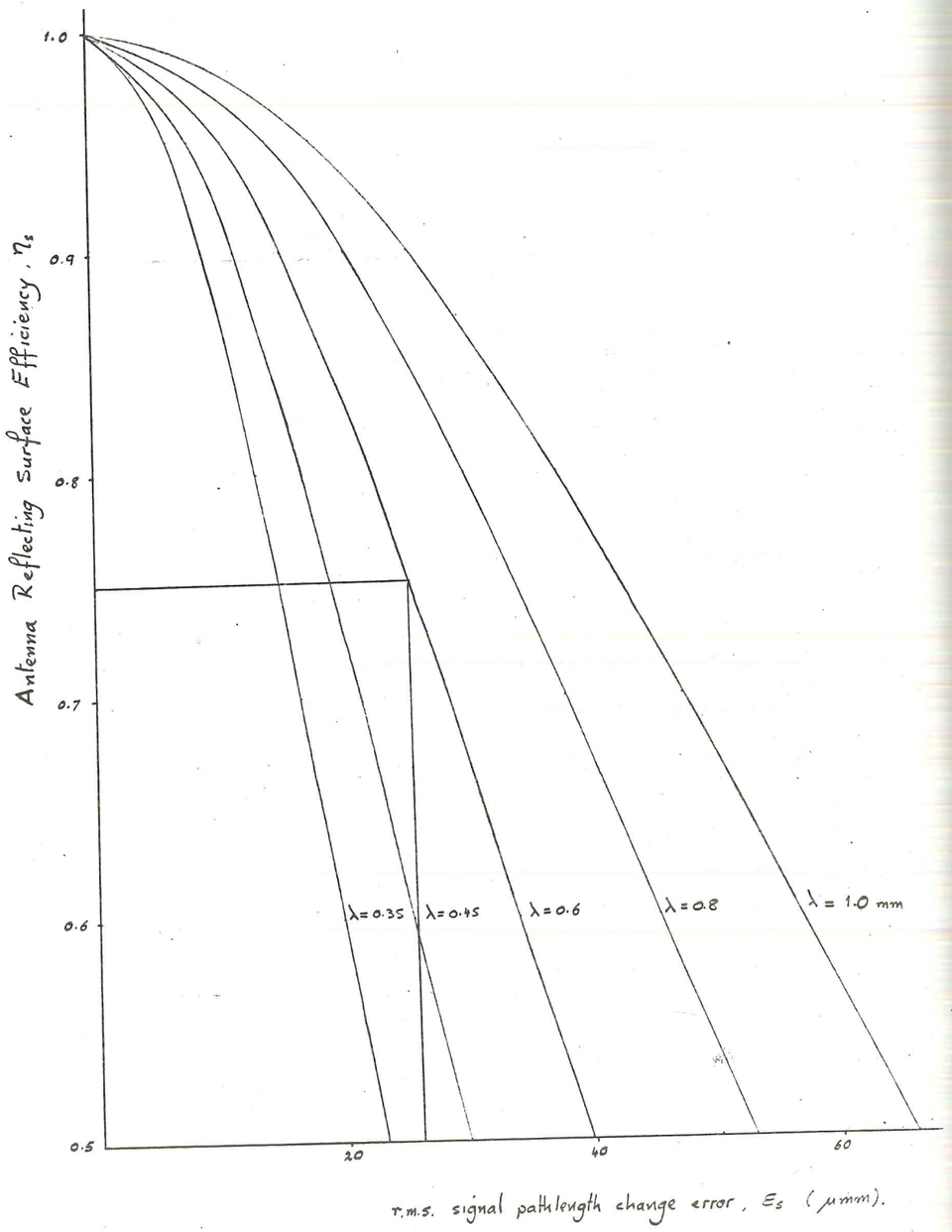

Fig.5.4.3 - Wavelength curves given by $\varepsilon_s = \frac{\lambda}{4\pi}\sqrt{-\text{Log}_e\,\eta_s}$.

(iv) deviations resulting from non-homological deformation behaviour of the surface supporting structure.

Now the errors produced by components (i) to (iii) are more or less independent of the size of the telescope and the observed wavelength, and are difficult to significantly reduce. Manufacturing techniques and technology, although considerably improved in recent years, still set the lowest practical limit on these error components. For telescopes designed to observe centimetre and longer wavelengths, the errors associated with components (i) to (iii) can be made small in comparison with the total allowable surface error. This therefore allows most of the total surface error budget to be taken by the supporting structure errors. When it comes to parabolic reflectors operating at millimetre and sub-millimetre wavelengths, however, the first three error components are no longer insignificant, so the allowable structural deformation errors can only be of the order of one quarter the total surface error budget.* Thus the allowable r.m.s. signal path length change error, produced by the surface supporting structure of a millimetre wave telescope, is given by:

$$\varepsilon_s \leq \frac{\lambda}{4\pi}\sqrt{-\text{Log}_e\,\eta_s}\,, \qquad (5.4.3)$$

on rearranging equation (5.4.2), where ε_s is the r.m.s. signal path length change error produced by the surface supporting structure alone. Plotting ε_s against η_s for values of λ from 1.0 mm to 0.35 mm gives a set of curves (see figure 5.4.3) from which the allowable supporting structure r.m.s. signal path length change error can be found for a telescope having a given reflecting surface efficiency and observing at

---

*Since the total r.m.s. surface error, ε_T , is the square root of the sum of the component r.m.s. errors squared, the supporting structure r.m.s. error is of the order $\sqrt{\varepsilon_T^2/4}$, i.e. $\varepsilon_T/2$.

a given wavelength. Thus, for example, at a wavelength of 0.6 mm and a surface efficiency of 0.75 , the allowable r.m.s. signal path length change error, produced by deviations of the supported reflecting surface from the desired parabolic shape, is 0.026 mm r.m.s.

Having established how accurately the surface supporting structure must conform to a parabolic shape, the next stage is to formulate a measure of how well a given structure manages to do this - in other words, how close to homological the structure deformation behaviour is.

It has already been shown that a sufficient condition for homological deformation of the supporting structure to occur at any angle of elevation, is that the structure deforms homologically at the two elevation positions of zenith and horizon pointing. Thus measuring how close to homological behaviour the zenith and horizon pointing deformations are, provides a sufficient measure of the structures over all homological performance. Since homological deformation does not demand any particular paraboloid to be maintained - just that one is - the way in which a structure's homological behaviour can be measured, is by calculating the r.m.s. signal path length change produced by the deviations of the surface support points from a best fit paraboloid surface, for each of the two pointing cases - the best fit paraboloid being found by minimizing the square of the signal path length changes. A least squares method for calculating the parameters of the zenith and horizon pointing best fit paraboloids, and the r.m.s. signal path length change error in each case, is given in Appendix 5.2.

Having found the r.m.s. errors for the zenith and horizon pointing cases, σ_z and σ_h respectively, the overall r.m.s. signal path length change error, or homology error, σ_o is given by:

$$\sigma_o = \sqrt{\frac{\sigma_z^2 + \sigma_h^2}{2}} \qquad (5.4.4)$$

which can then be compared with the allowable error found using equation (5.4.3) to see if the structure design is good enough.

5.5 - References

1. Von Hoerner, S. - Homologus Deformations of Tiltable Telescopes. J.Struct.Div., Proc. A.S.C.E., ST.5, Oct. 1967, pp.461.

2. Von Hoerner, S. - Homologus Deformation of Tiltable Telescopes. Structures Technology for Large Radio and Radar Telescope Systems. Ed. Mar, J.W. & Liebowitz, H. MIT Press, 1969, pp.311.

3. Ruze, J. - Antenna Tolerance Theory - A Review. Proc. IEEE, vol.54, no.4, April 1966, pp.633-640.

Chapter Six - Implementation of the Design Procedure

6.0 - Introduction

Having established the theoretical basis for all the stages of the proposed design procedure, and having written the cyclic symmetry analysis program, their implementation and organization within a computer supported design package will now be described. In order to present the important aspects of this implementation, including a number of modifications which were made to certain stages, the design of an actual millimetre wave telescope structure will be followed - various excursions from this main path will, however, be made to describe in detail these important aspects.

6.1 - Initial Structure Design, Data Generation and Checking

The set of specifications for the telescope design is based on those for the U.K. Millimetre Wave Telescope [1] (see Box 6.1.1). They are deliberately simplified to avoid unnecessarily complicating the

Reflector diameter	15 m
Central hole diameter (for cassegrain operation)	1 m
Focal length	5.4 m
Minimum observable wavelength	0.4 mm
Reflecting surface efficiency at 0.4 mm	80 %
Instrument to be housed in a Raydome	

Box 6.1.1 - Millimetre wave telescope specifications

content of this chapter. The initial structure design, produced from the specifications, is for a cyclically symmetric surface supporting structure which is mounted on a central yoke structure containing the

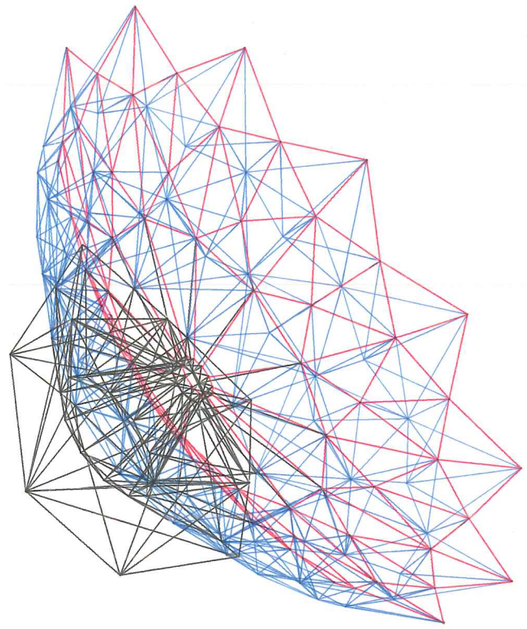

Fig.6.1.2 - Initial telescope structure design.

——— members connecting surface support points,

——— cyclically symmetric backing structure members,

——— members forming the central drum and elevation mounting structure.

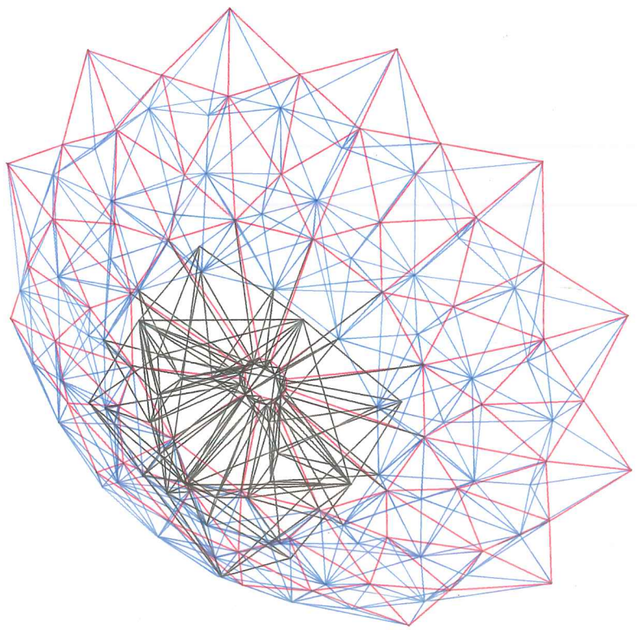

two elevation bearings and semi-circular elevation control track support (see figure 6.1.2). The cyclically symmetric surface supporting dish structure consists of twelve main cantilevered ribs connected to the central drum and twelve secondary ribs placed between them. It is designed to support three rings of reflecting panels - twelve in the inner ring and twenty-four in the outer two rings. Each panel is supported at three points on its edge. A detailed description of this design is given in Appendix 6.1.

The next step is to describe the initial structure design to the cyclic symmetry analysis program, according to the format described in Appendix 3.1. The major part of this task involves defining the positions of the joints in the central region and first cyclic segment, and the structural members connecting them. It is also the most difficult and error prone; the remaining data consists of relatively small amounts of load description and joint constraint definitions. Checking the data before it is presented to the analysis program is therefore an important part of data generation. In order to enable this data checking to be carried out quickly and accurately, a support program has been written and developed which reads the generated data file in the same way as the analysis program. It then uses the joint co-ordinates and member connections to produce a picture of the described structure. This picture can either be drawn on the screen of a graphics terminal, or, when hard copies are required, by a multi-pen digital plotter. Figure 6.1.2 is an example of this type of output - the two different views being obtained via an object rotation option provided by the Data Checking program. In the case of the graphics terminal output further 'interactive' options have been included to enable a specific region to be enlarged, and thus looked at in more detail. This process of rotating the picture to find the

most useful view, and then picking out and scaling up specific parts, can be continued for as long, and for as many times, as the designer wishes, correcting data errors as they are found.

The accuracy of the geometric and topological data can thus be established before it is presented to the cyclic symmetry analysis program. The remaining sections of the data file, defining the loading and constraints, are easily checked by 'hand', since they generally form only a small part of the whole data file.

6.2 - Stereoscopic Three-Dimensional Pictures

One of the most important aims in developing the design procedure presented here, has been to enable structures having non-cyclically symmetric central regions to be considered, without having to model the whole structure. This is so that the effect of the deformations of the central region, containing the elevation supports of a telescope structure, can be included in the homological deformation analysis. Now in order to maintain the high degrees of cyclic symmetry required by the surface supporting part of the structure, the central region structure must not interfere with it. In other words, structural members forming the central region must not obstruct the cyclic segment members.

For simple space-frame type structures, it is not too difficult to determine whether any members get in the way of each other, by examining various two-dimensional projections - such as those produced by the Data Checking program described in section 6.1. However, when it comes to the more complex structures proposed for homologically deforming telescopes, it is very difficult. As can be seen in figure 6.1.2, the central area becomes very confused. It was in an attempt to develop a quick and convenient way of carrying out a check

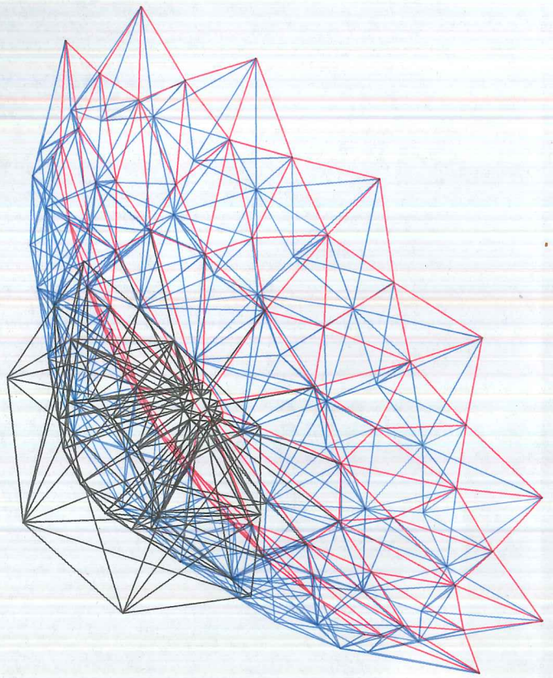

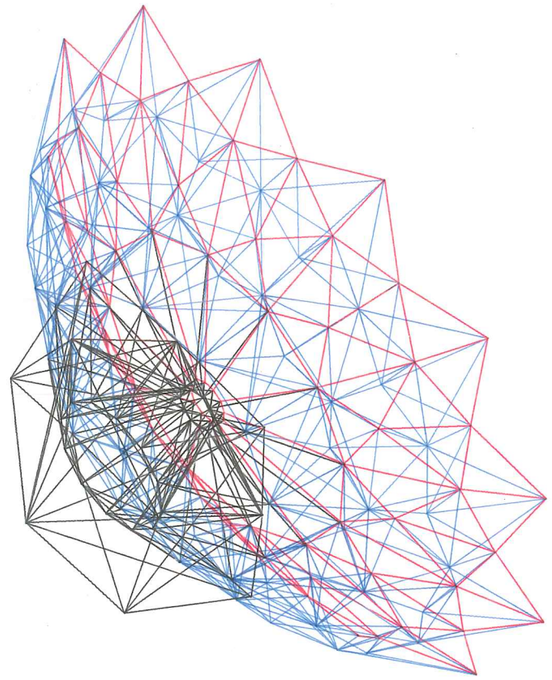

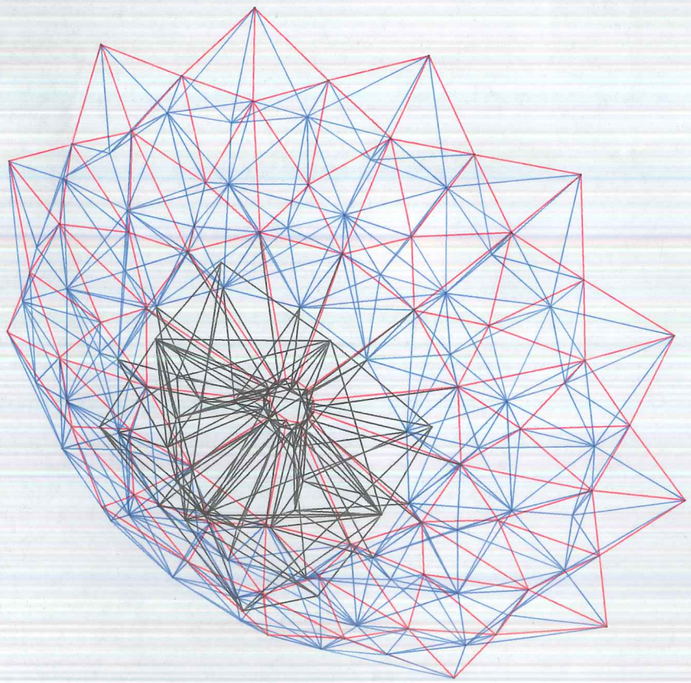

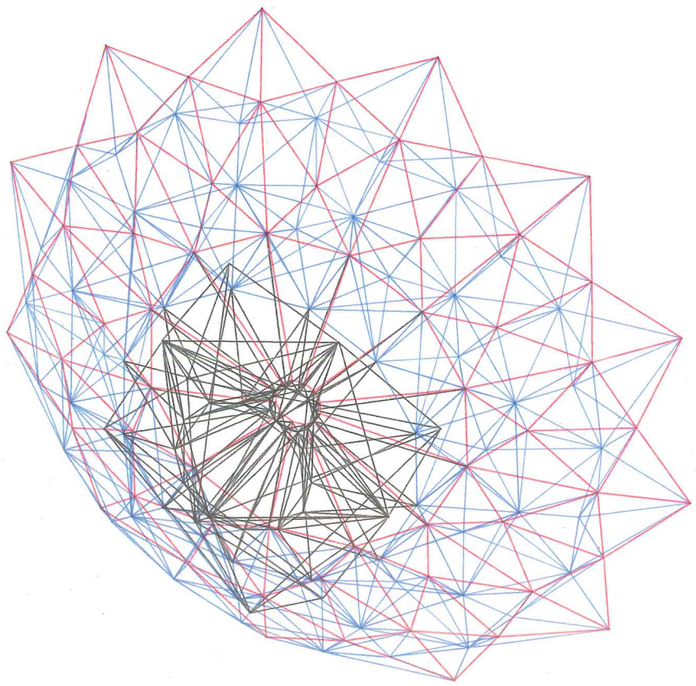

on central region interference, that a second support program was written to produce 'stereo pairs' of selected views of the structure (from the generated data file).. By using a suitable stereo viewer to look at these 'pairs' a three-dimensional image can be seen*, thus enabling the relationship between the central region and the cyclic segments to be studied very much more easily.

The basic proportions governing the viewing distances and position of the two viewpoints (the eyes), were determined in accordance with the recommendations made by Gossling [2] in his notes on computer generated pairs for a Gaf Viewmaster (which uses small transparencies). These, and the transformation algorithms used in the program are described in Appendix 6.2. As an example, the stereo pairs for the two views presented in figure 6.1.2 are shown in figure 6.2.1. When viewed using a stereoscope these pictures produce a three-dimensional image which clearly resolves the rather confused central region area.

Further examples of stereo pairs, including some of the helicopter landing pad structure used to check the analysis program, can be found in the pocket at the back of this volume.

This completes the initial design stage, so we can now move on to the displacement analysis stage. The theory and computer program used here have already been described in chapters three and four, but before going on to consider the results, the question of the joint model used will again be considered.

6.3 - A New Joint Model

When the computer program implementing the cyclic symmetry analysis

---

*It should be noted that not everyone can see these three-dimensional images, but most can after varying amounts of practice!

theory was first written, the primary aim was to demonstrate the validity of the theory. With this aim in mind a simple three-degree of freedom pin-joint model was used. Now, although this joint model was good enough for the purposes of demonstrating the advantages and accuracy of both the theory and computer code, it was not clear that it would be good enough for the displacement analysis of telescope structures.

It is generally accepted that for the stress analysis of medium to heavily loaded space frames (i.e. significantly more than self weight loading), the pin-joint can reasonably be used - as shown by Parkes [3], for instance. However, when it comes to the analysis of lightly loaded frameworks, where it is the displacements that are of primary interest, not the stresses, there is no clear reason for assuming that a pin-joint model is still suitable. This is especially the case in the central region where many of members are short, so the behaviour predicted by the pin-joint would be rather different from that of the more appropriate rigid-joint model, which uses six degrees of freedom - as opposed to the three used by the pin-joint model.

To introduce a rigid-joint model into the program would considerably increase the time taken to complete the displacement analysis stage, which, as already pointed out, is to be avoided if possible. For this reason a new joint model has been developed which still only uses three degrees of freedom, yet produces structure deformations of a form much closer to those produced using a full six degree of freedom rigid-joint model, for short structure members having low slenderness ratios. This was done by introducing a lateral stiffness term into the conventional pin-joint stiffness matrix - the size of the lateral stiffness term being chosen to give the closest match of deformation behaviour with that of the rigid-joint model.

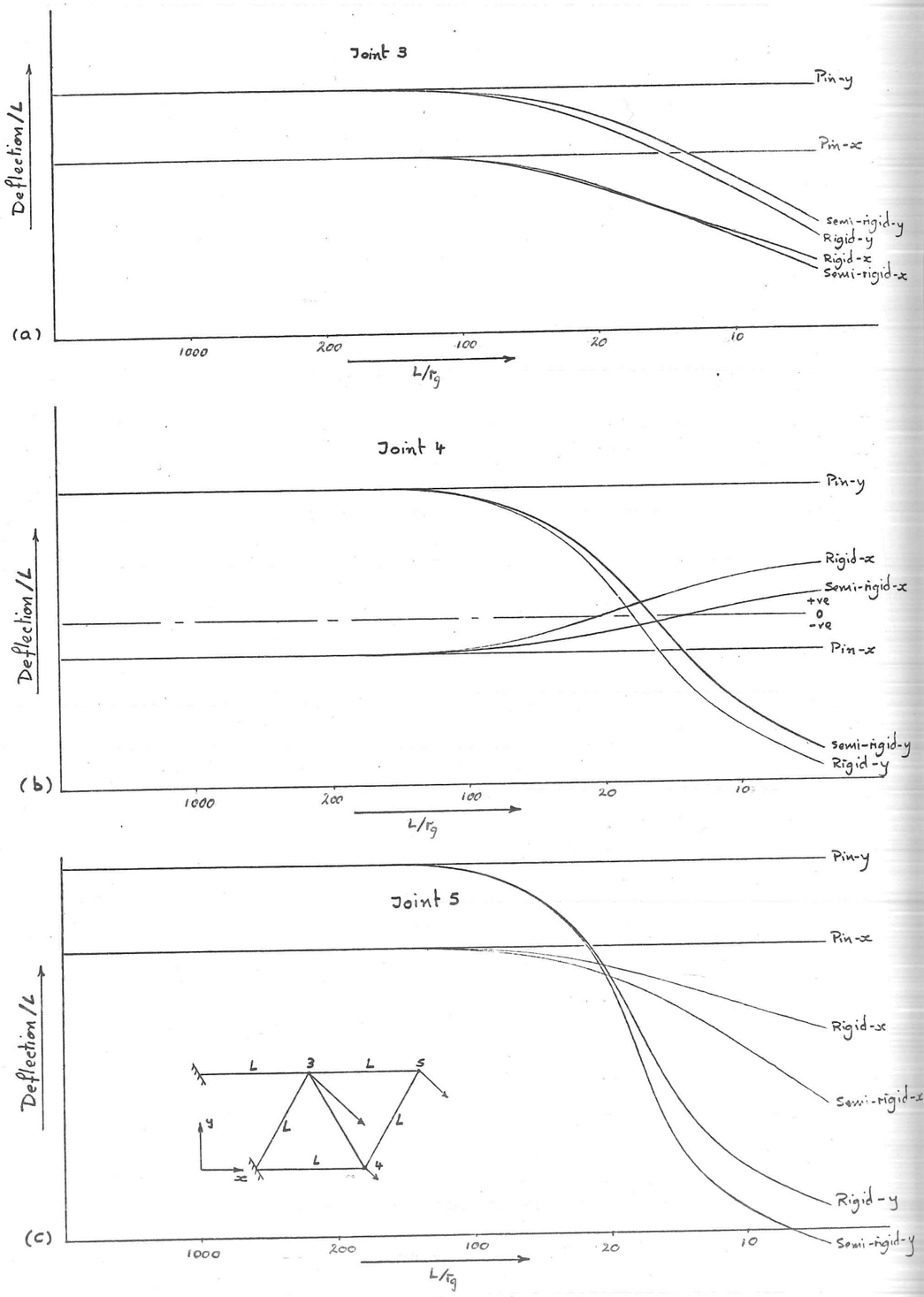

Fig.6.3.1 - Comparison of new semi-rigid joint displacement behaviour with that of a pin-joint and a convention rigid-joint, in a two-dimensional truss.

The details of this 'semi-rigid' joint model are given in Appendix 6.3, and a comparison of its deformation behaviour, with that of pin-joint and rigid-joint models when used in a simple cantilever truss, is presented in figure 6.3.1 (see Appendix 6.3 for details of the calculations involved in producing this comparison).

From figure 6.3.1, it can be seen that the displacement behaviour of the semi-rigid joint follows closely that of the rigid-joint over the whole range of slenderness ratios, rather than only over the high values, as is the case with the pin-joint. This new joint model is therefore shown to be more suitable for dealing with the wide range of slenderness ratios found in telescope structures, than the pin-joint model; yet not to significantly affect the time taken by the analysis stage - a fact borne out by comparisons made between the results produced using this semi-rigid joint model and those produced using a rigid-joint model (implemented in another program).

6.4 - Deformation Analysis Results

We now return to the main path to consider the displacement results produced by the cyclic symmetry analysis program.

One very common aspect of numerical structural analysis using digital computers, is the vast quantity of numbers that tends to be produced. Clearly, to attempt to evaluate these results just by looking at all the numbers is not practical - unless the structure is very small. For this reason it is usual to have some form of results processing which often produces graphical output.

By further developing the Data Checking program, an option for drawing deformation pictures has been provided. These are simply produced by adding the suitably scaled-up nodal displacements to the original nodal co-ordinates and them, using the same drawing routines

Fig.6.4.1 - Zenith pointing and horizon pointing deformation modes
(deformation magnification = 1200).

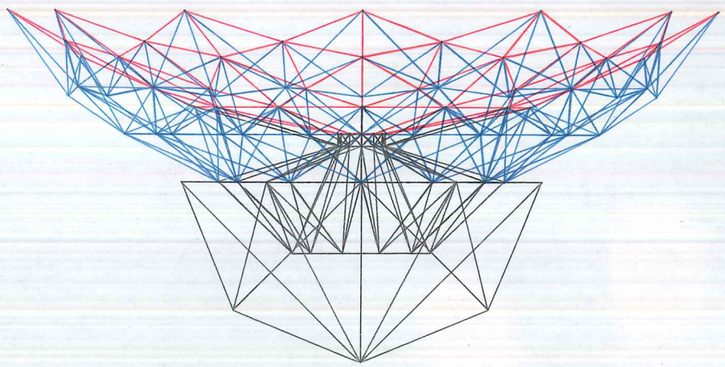

Zenith pointing

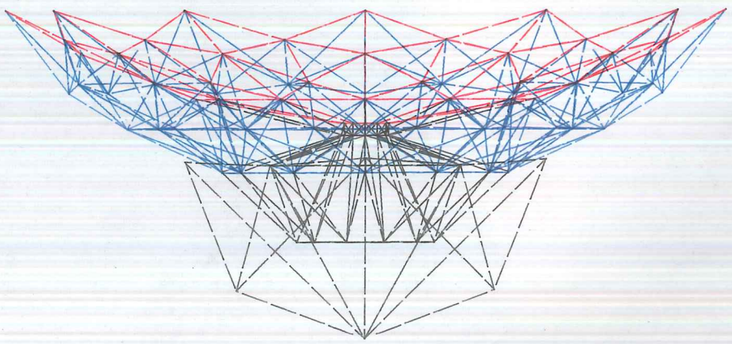

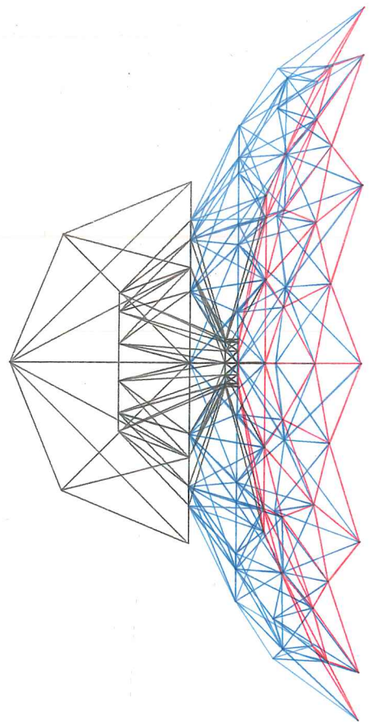

Horizon pointing

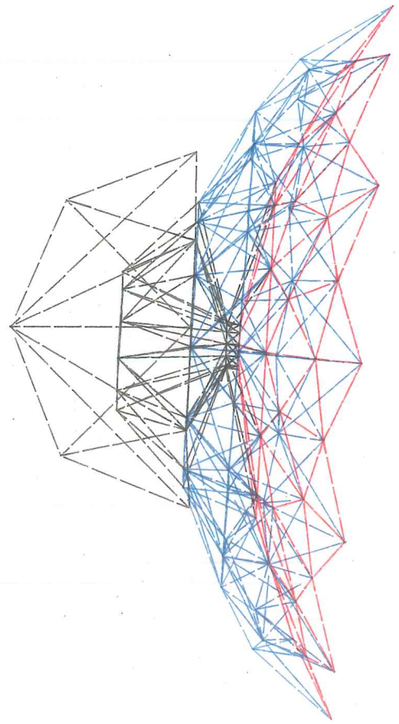

as before,
of the defo
initial str
figure 6.4.
indication
but an idea
does not pr
performance
type of ove
non-cyclic
non-reflect
deformation

The de
its effect
these pictu
usually sma
large magni
heavily dis

6.5 - The Be

As desc
particular
signal path
as a result
to find thi
Appendix 5.
error, a th
represents

Calcula

as before, to draw the deformed shape. Figure 6.4.1 presents examples of the deformation pictures produced from the numerical results of the initial structure displacement analysis. As can be seen from figure 6.4.1, these deformation pictures do not provide a very clear indication of the deformation behaviour of any one particular joint, but an idea of the overall behaviour can be gained. Although this does not provide enough information for assessing the homological performance of a structure, it does enable a check to be made on the type of overall deformation behaviour expected - in other words, on non-cyclic symmetry in the zenith pointing deformation solution and non-reflective symmetry (across the x-z plane) in the horizon pointing deformation solution.

The deformation behaviour of the central region structure, and its effect on the dish structure deformation, can also be studied using these pictures. The danger here is that the displacement values are usually small, compared with those of the dish structure, so that a large magnification is needed to 'see' their effects, which tends to heavily distort the deformations of the dish structure.

6.5 - The Best Fit Paraboloid and r.m.s. Error

As described in section 5.3, the homological performance of a particular structure is measured by calculating the r.m.s. value of the signal path length changes occurring at all the surface support points as a result of their deviation from a best fit paraboloid. In order to find this best fit paraboloid (according to the method set out in Appendix 5.2), and to calculate the r.m.s. signal path length change error, a third support program has been written. This program thus represents stage three of the design procedure.

Calculating the r.m.s. signal path length change errors for the

FIG. 6.5.1

Homology Deviation Surfaces

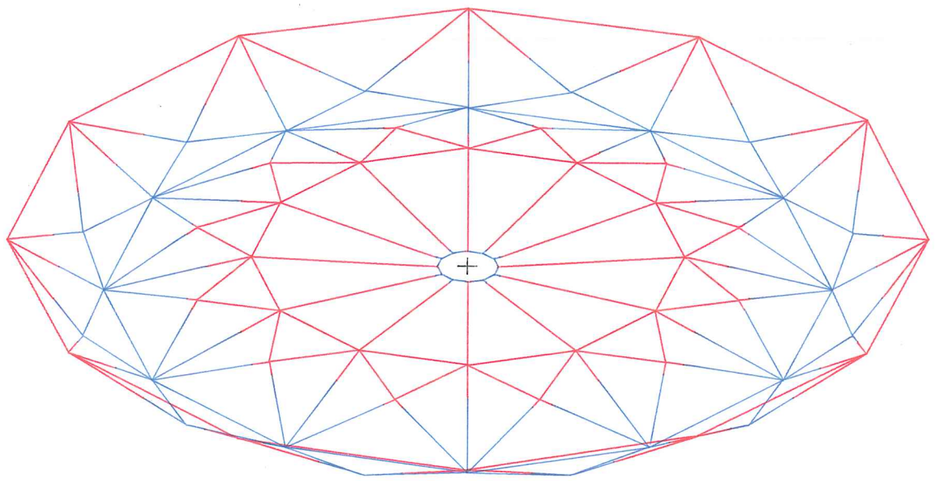

Zenith Pointing - RMS Error = .0278

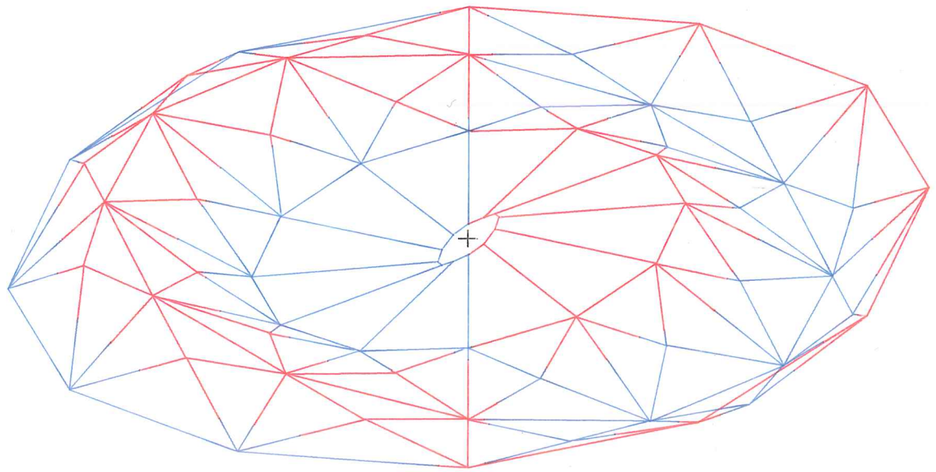

Horizon Pointing - RMS Error = .0395

two cases of zenith and horizon pointing, provides a measure of how close to the required homological performance a particular structure's deformation behaviour is, but it gives no indication of how its behaviour deviates from perfect homological deformation. Now before any design changes can reasonably be made, it is necessary to have some idea of the form of the deviation from homology. From such information, measures to improve the deformation behaviour of specific support points, or groups of support points, can be formulated.

In an attempt to present this homology deviation clearly and conveniently, another subroutine was added to the Best Fit program to draw 'homology deviation surfaces'. These surfaces are formed by plotting the deviation of each support point from the best fit paraboloid as a vertical height above or below a flat surface which represents perfect homological deformation. Examples of the zenith and horizon pointing error surfaces for the initial structure are presented in figure 6.5.1. The use of two colours helps to indicate whether a point is above or below the zero error surface. Points above this surface, joined by red lines, are said to be too 'hard', since they lie 'above' the best fit paraboloid; whereas points below it, joined by blue lines, are said to be too 'soft', since they lie below the best fit paraboloid.

The program was also extended to produce stereo pairs of these homology deviation surfaces. This was done to try to improve the information retrieval from these pictures - in other words, to try and make it easier for the designer to decide what is actually going on. (Examples of such stereo pairs can again be found in the pocket at the back of this volume.)

Results of the Best Fit Paraboloid Analysis of the Initial Structure Deformation

Zenith Pointing	Horizon Pointing
Δf = 1.289 mm	Δf^* = 0.0 mm
x_o^* = 0.0 mm	x_o = -5.619 mm
z_o = -0.127 mm	z_o^* = 0.0
ϕ^* = 0.0 mm	ϕ = 5.86×10^{-4} rad
σ_z = 0.0278 mm r.m.s.	σ_h = 0.0395 mm r.m.s.

*assumed to be zero

Box 6.6.1 - Details of the best fit paraboloids.

6.6 - Testing the Homological Performance

The next stage in the design procedure is to decide whether the desired level of homological performance has been reached. This is the easiest of the design stages and is achieved by simply comparing the overall r.m.s. surface error (see equation 5.4.4) with that required to meet the specified performance. Thus, using the performance specifications (see Box 6.1.1) and equation 5.4.3, the maximum allowable r.m.s. surface support point error is given by:

$$\varepsilon_s \leq 0.015 \text{ mm r.m.s.} \qquad (6.6.1)$$

Now for the initial structure design the overall r.m.s. error, σ_o, is given by:

$$\sigma_o = \sqrt{\frac{(0.0278)^2 + (0.0395)^2}{2}}$$

$$\sigma_o = 0.0341 \text{ mm r.m.s.} \qquad (6.6.2)$$

using the zenith and horizon pointing r.m.s. errors given in Box 6.6.1. As can be seen, σ_o is greater than ε_s, and so the structure's homological performance needs to be improved.

The other quantity which must be checked is the change in focal length (from the initial value) that occurs in the zenith pointing case. From the specifications the limit for this variation is calculated to be 1.3 mm (see Appendix 5.1) and the value obtained from the Best Fit analysis of the initial structure deformation is 1.29 mm - just within the limit.

6.7 - Formulating Design Modifications

The fifth and final stage of the design loop is perhaps the most difficult, since it does not involve any analytical processes which

can be given to the computer. The formulation of design modifications which will produce reductions in both the zenith and horizon pointing r.m.s. errors, and not in one at the expense of the other, is an art which is learnt by experience. It is here that the cycle time of the design loop (which depends on the time taken to complete the previous stages) becomes important - a short cycle time encourages designers to 'experiment' more freely and thus gain the necessary experience quickly. The gaining of this experience is largely a process of trial and error to begin with until a 'feel' is gained for the relationship between the structural geometry and its homological deformation performance.

For this reason it is difficult to formally define how design modifications are arrived at, but basically it involves trying to make the soft support points harder and the hard points softer, as indicated by the homology deviation surfaces (see figure 6.5.1). This is generally easier to do for the zenith pointing case than for the horizon pointing case. The reason for this is that it is easier to imagine how the vertical (z-direction) stiffness of any particular point might be varied, compared with deciding how the stiffness opposing horizontal forces may best be altered.

6.8 - The Effect of the Design Modifications

To demonstrate the formulation of design modifications and the effect they have on the homological performance of the structure, the changes made to the initial structure, based on its homology deviation surfaces (see figure 6.5.1), will be described.

It has been found useful to consider the improvement of an initial structure's homological deformation performance in two stages. In the first stage, member cross-sections are altered - the values used being

can be given to the computer. The formulation of design modifications which will produce reductions in both the zenith and horizon pointing r.m.s. errors, and not in one at the expense of the other, is an art which is learnt by experience. It is here that the cycle time of the design loop (which depends on the time taken to complete the previous stages) becomes important - a short cycle time encourages designers to 'experiment' more freely and thus gain the necessary experience quickly. The gaining of this experience is largely a process of trial and error to begin with until a 'feel' is gained for the relationship between the structural geometry and its homological deformation performance.

For this reason it is difficult to formally define how design modifications are arrived at, but basically it involves trying to make the soft support points harder and the hard points softer, as indicated by the homology deviation surfaces (see figure 6.5.1). This is generally easier to do for the zenith pointing case than for the horizon pointing case. The reason for this is that it is easier to imagine how the vertical (z-direction) stiffness of any particular point might be varied, compared with deciding how the stiffness opposing horizontal forces may best be altered.

6.8 - The Effect of the Design Modifications

To demonstrate the formulation of design modifications and the effect they have on the homological performance of the structure, the changes made to the initial structure, based on its homology deviation surfaces (see figure 6.5.1), will be described.

It has been found useful to consider the improvement of an initial structure's homological deformation performance in two stages. In the first stage, member cross-sections are altered - the values used being

FIG. 6.8.1

Homology Deviation Surfaces

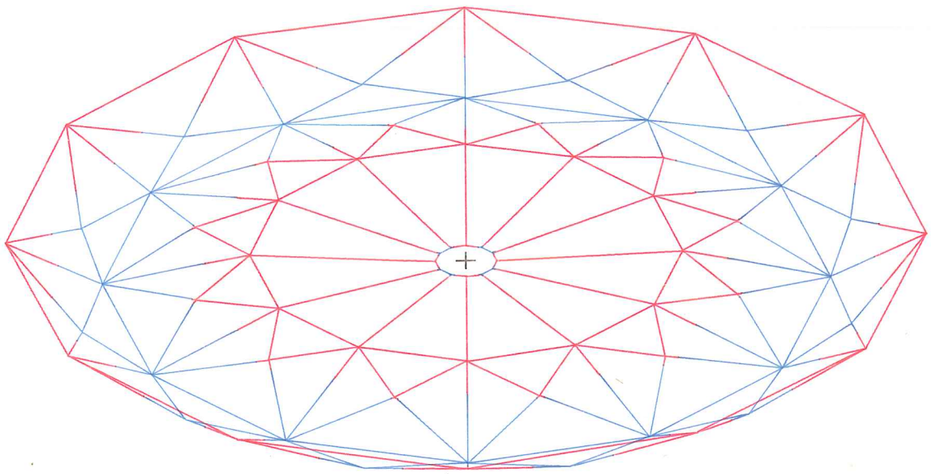

Zenith Pointing - RMS Error = .0191

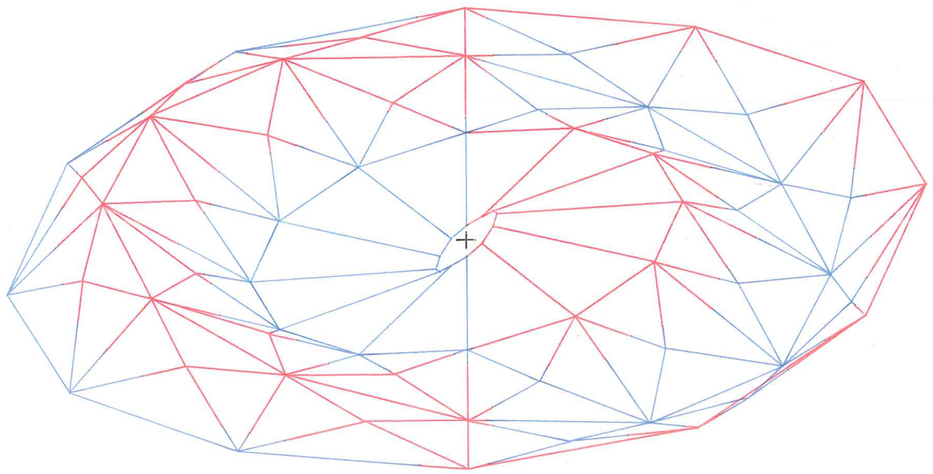

Horizon Pointing - RMS Error = .0331

restricted to those available - in an attempt to remove large scale, non-homological aspects of the structure's deformation. The second stage can be thought of as the removing of small scale, non-homologies using only the joint positions as variables. This two stage approach is only a guide, so the varying of joint positions in the first stage, or cross-sections in the second, is not ruled out. Another point which must be made clear is that not all initial structures go through this two stage improvement procedure - in fact many initial structure designs of an inexperienced user will not. This is because for any further improvement to be made in the homological deformation behaviour of such structures, the change in deformation form required is so large that it is not possible to obtain it by just changing cross-sections or joint positions. In these cases a dead end is reached and no amount of 'tunning' using joint position variations, will significantly improve the homological behaviour - a new initial structure therefore has to be designed, which, hopefully, does not suffer the same problem.

The modifications made to the initial structure considered here were therefore changes in member cross-sections. They were aimed at reducing the stiffness of the rim of the dish structure, which, as can be seen from figure 6.5.1, is too hard in both the zenith and horizon pointing cases. The homology deviation surfaces produced from the deformation analysis results of the modified structure, are presented in figure 6.8.1. As can be seen an improvement was obtained in both the zenith and horizon cases, which gives a new σ_o value of 0.0270 mm r.m.s. - a 21% improvement. By making further cross-section changes - the values used being only those available from manufacturers - and a change in one joint position, a further improvement was obtained which gave an overall r.m.s. error of σ_o = 0.0209 mm r.m.s.

FIG. 6.9.1

Homology Deviation Surfaces

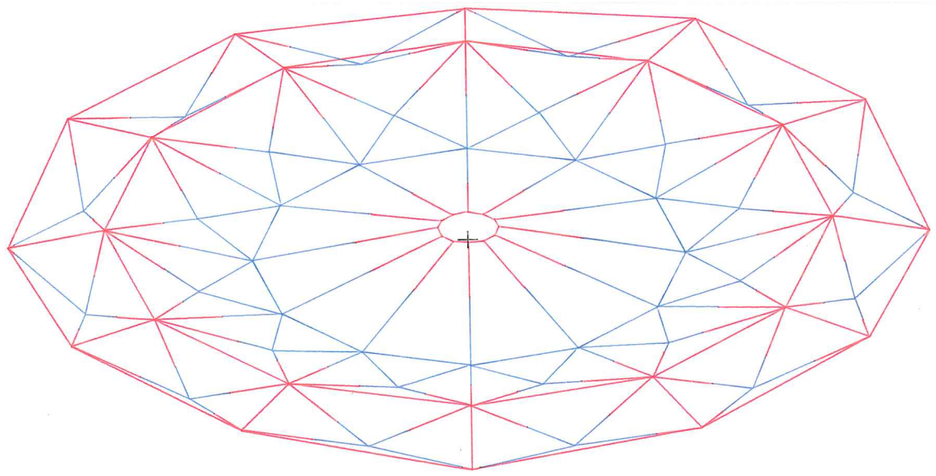

Zenith Pointing - RMS Error = .0096

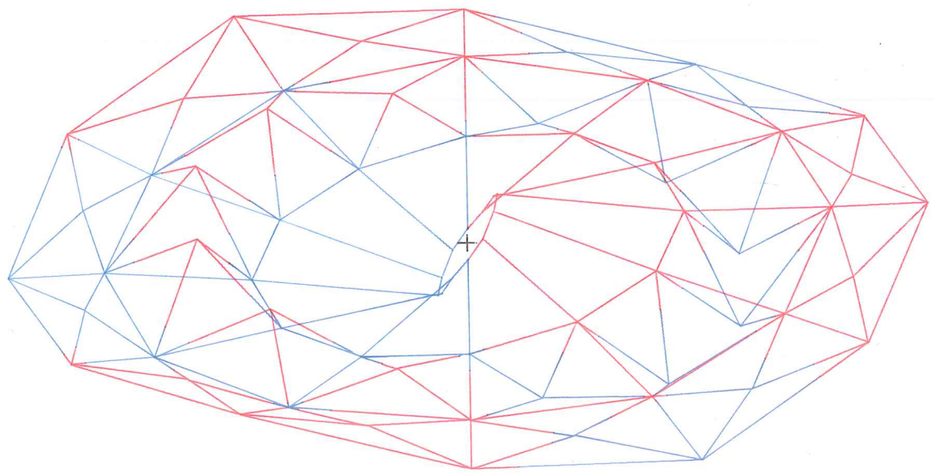

Horizon Pointing - RMS Error = .0185

6.9 - The Final Design

After going round the design loop (stages two to five) ten times, and making a series of modifications to both joint positions and member cross-sections, a design having an overall r.m.s. error of $\sigma_o = 0.0147$ mm was obtained. The required homological performance had therefore been achieved. The homology deviation surfaces for this tenth modification of the initial design is given in figure 6.9.1.

Having reached the specified level of homological performance does not necessarily mean that further improvement is not possible, but for the particular design considered here, it did prove to be the limit - certainly as far as the horizon pointing performance is concerned.

Table 6.9.2 presents the values of the homology parameters Δf, z_o, x_o and ϕ for each modification, together with the zenith pointing, horizon pointing and overall r.m.s. errors. To indicate some of the differences between the initial structure and the final one, the geometries of a primary radial rib (containing support points 1, 2, 4 and 6), are presented for comparison in figure 6.9.3.

	Zenith Pointing			Horizon Pointing			
Modification No.	Δf (mm)	z_o (mm)	σ_z (mm rms)	x_o (mm)	ϕ (rad)	σ_h (mm rms)	σ_o (mm rms)
0	1.29	-0.127	0.0278	-5.62	5.85×10^{-4}	0.0395	0.0341
1	1.27	-0.127	0.0191	-5.36	5.61×10^{-4}	0.0331	0.0270
2	1.34	-0.122	0.0103	-5.75	5.99×10^{-4}	0.0277	0.0209
3	1.34	-0.125	0.0057	-5.74	6.01×10^{-4}	0.0291	0.0210
4	1.09	-0.149	0.0278	-5.05	5.35×10^{-4}	0.0187	0.0237
5	1.10	-0.146	0.0236	-5.08	5.39×10^{-4}	0.0180	0.0210
6	1.13	-0.141	0.0190	-4.97	5.39×10^{-4}	0.0205	0.0198
7	1.14	-0.133	0.0113	-5.0	5.28×10^{-4}	0.0199	0.0162
8	1.15	-0.133	0.0124	-5.06	5.32×10^{-4}	0.0196	0.0164
9	1.13	-0.133	0.0125	-5.22	5.45×10^{-4}	0.0192	0.0162
10	1.15	-0.134	0.0096	-5.24	5.42×10^{-4}	0.0185	0.0147

Table 6.9.2 - Structure homological performance after each modification

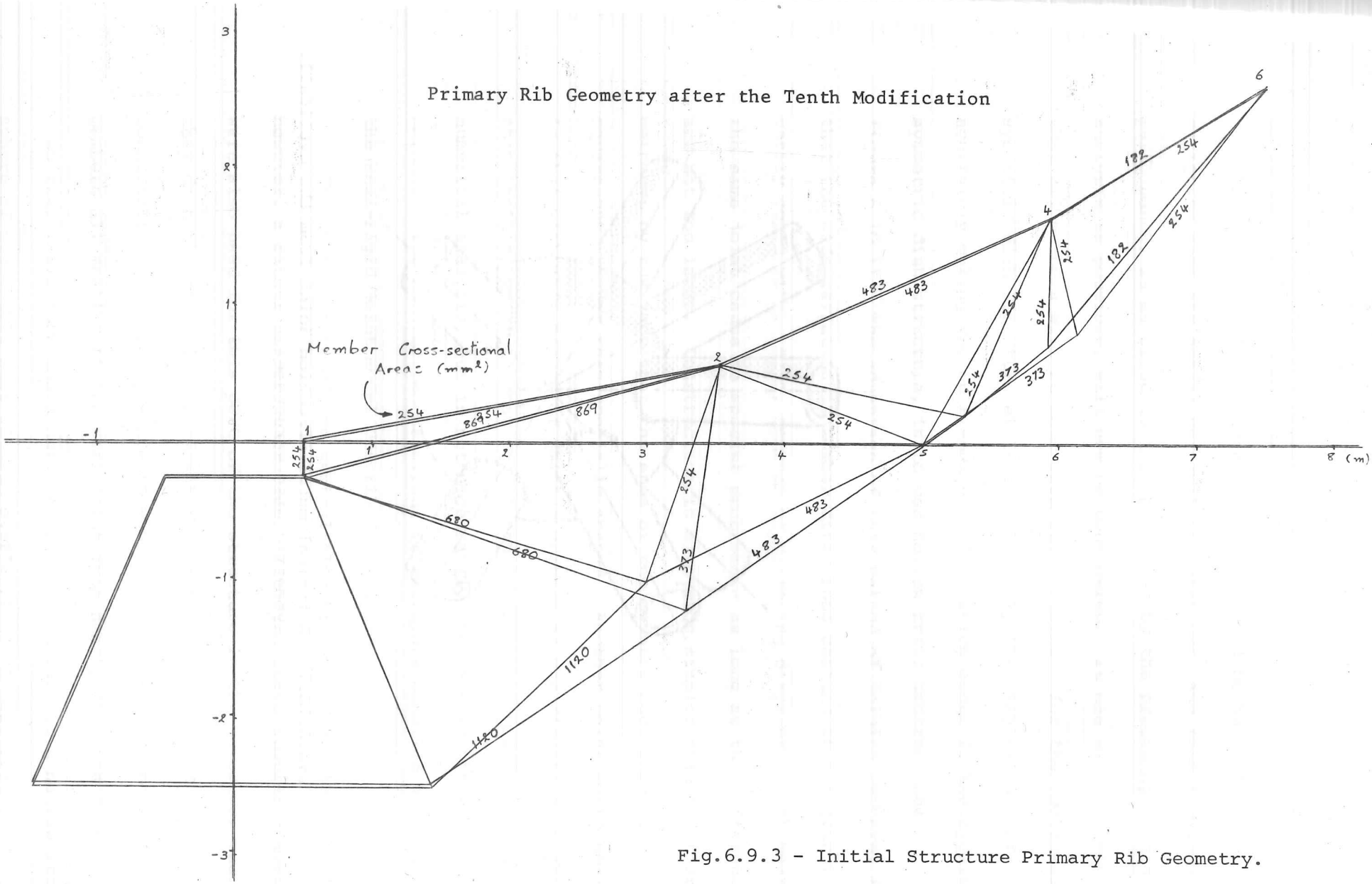

Fig.6.9.3 - Initial Structure Primary Rib Geometry.

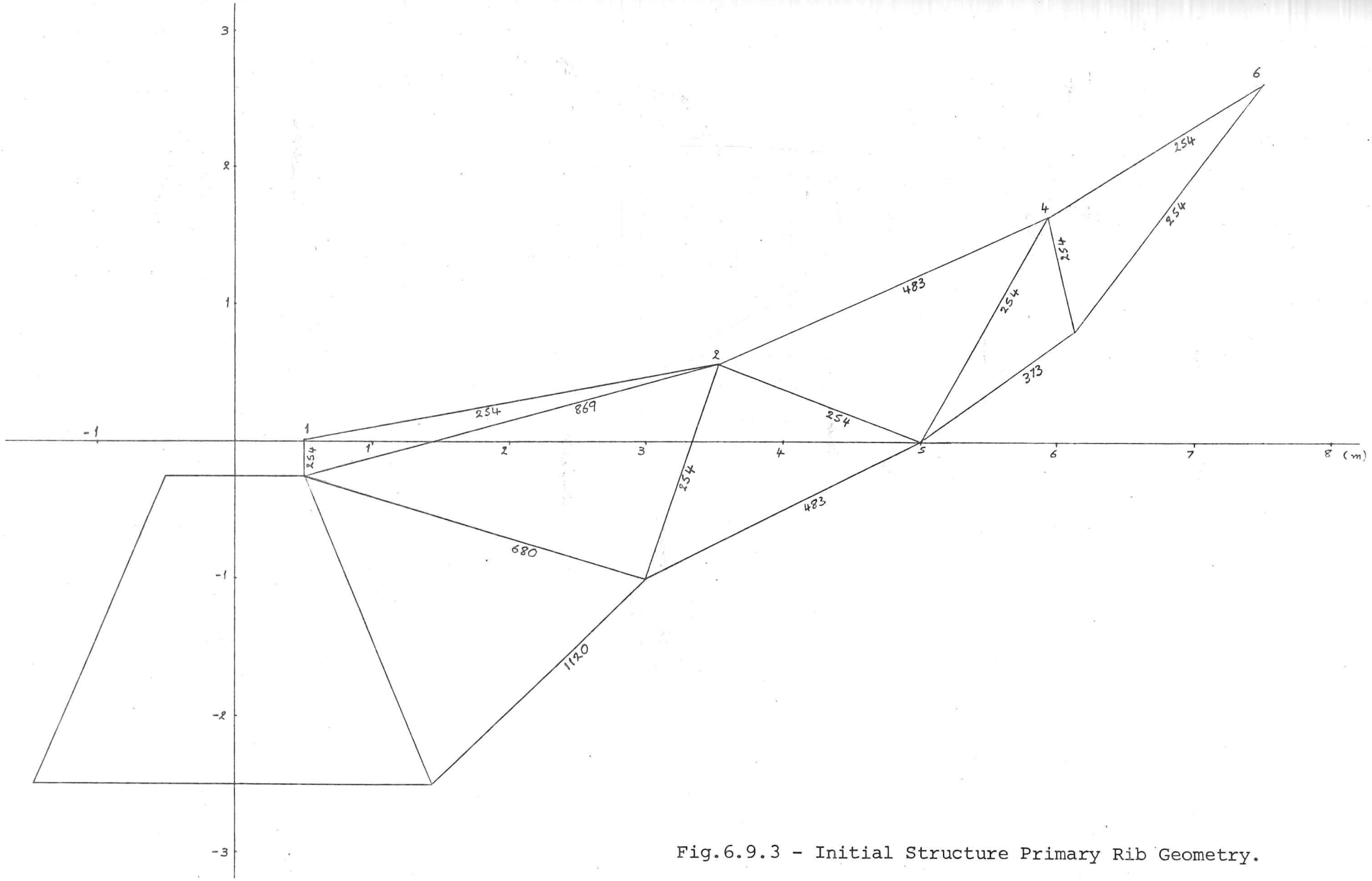

Fig.6.9.3 - Initial Structure Primary Rib Geometry.

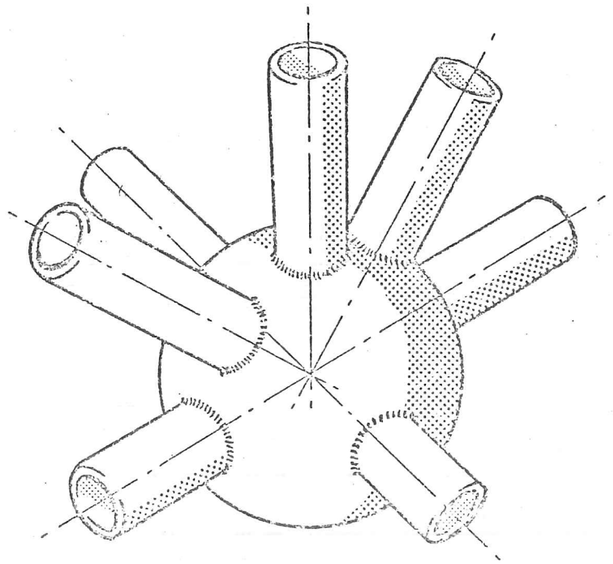

Fig.6.10.1 - A typical multi-direction joint from the cyclically symmetric dish structure.

6.10 - The Question of its Construction

The question of how a real structure could be built to this final design so that its actual deformation behaviour, and thus homological performance, is as close to that predicted by the preceding theoretical analysis as possible, will now be considered. It has already been said that all members will be made from steel tubing - for the cyclically symmetric dish structure at least. Probably the simplest way of accurately making the multi-member joints which occur in the cyclically symmetric dish structure, is to use hollow steel spheres (see figure 6.10.1). The advantage of this method of joining members, is that the wide variation in member directions meeting at one joint, is easily coped with. Also, members of differing diameters which meet at the same joint cause no special problems - as long as the differences are not too large. Construction is also made simpler than in other methods, by the fact that the ends of the members need only to be square-cut, rather than specially shaped. Another point worth noting is that with this method of joining members no one direction is stiffer than another, which is what is assumed in the joint model used in the numerical analysis, but is not necessarily the case in other joining methods. Its deformation behaviour is therefore modelled well using the semi-rigid joint model described in section 6.3.

The construction of the central elevation mounting structure is, however, a rather different problem. Although steel tubular members were also used for this part of the structure in the numerical analysis, they do not necessarily represent the most suitable method of construction, especially since it would involve large numbers of members all meeting at the same joint from nearly the same direction - so that their ends would not fit onto the surface of a hollow steel sphere of reasonable size without overlapping. A more practical method

of building the central barrel and its four point support structure (see Appendix 6.1 for details) might be to use shaped steel panels - a weight reduction of this otherwise rather heavy construction could be made by introducing holes at suitable places in the panels.

The remaining parts of the structure, that is the elevation circle and axis mounting structure, is more like a traditional heavy steel framework type structure and so does not present any particularly major construction problems.

The use of a radial rib type structure in the surface supporting dish - rather than a lattice type structure - also provides for easier construction, since all the ribs can be made on a two dimensional jig in a work shop, and then the interconnecting members added on site. By using one jig the high accuracy required at the manufacturing stage of a millimetre wave telescope structure is more easily attained.

6.11 - References

1. Report of the Panel to Review the Future of Radio Astronomy in the U.K., Science Research Council, Space and Radio Board, February 1977, Table 3.1, pp.59,60.

2. Gossling, T.H. - Computer-Generated Stereo-pairs for the gaf Viewmaster (9.12.75), Cambridge Engineering Department Library, Pam. File 188.

3. Parkes, E.W. - Braced Frameworks, 2nd Ed., Pergamon Press, 1974, sections 4.1, pp.129, and 4.3, pp.134.

Chapter Seven - Discussion and Conclusions

7.0 - Introduction

In this final chapter a discussion is presented of certain points raised at the various stages of the design procedure, followed by an overall view of the complete procedure. A set of conclusions is then drawn concerning, not only the primary aim of this work, but also a number of other aspects which have arisen during the development and use of the proposed design procedure.

7.1.1 - The Initial Structural Design

The constraints usually associated with the deformation of large structures are ones concerning only their size - the deformations either having to be a minimum, or within a given range. Less frequently, a structure may be required to assume specific deformations for a given load. Thus, the designer of a structure required to maintain a given form as it deforms under a varying load, has few examples from which to draw inspiration. As a result, there is a strong tendency, when designing a homological deforming telescope structure, to follow the designs of the traditional 'stiff' radio telescope structures. Now these stiff structures almost invariably use some kind of interconnected radial rib type design which, apart from the elevation mounting, can generally be described as cyclically symmetric - the Jodrell Bank 250 ft. dish, Cambridge one-mile and five-kilometre dishes, Parkes 210 ft. dish, N.R.A.O. 140 ft. and Lebedev 22 m dishes, being examples. Thus, following the previous designs does in fact lead to the type of structure described in section 2.2 (and Appendix 2.1) as being potentially homologically deforming: a fact borne out by the results obtained for these types of structure - those presented here being a typical example.

The stiff structure designs cannot, however, be followed much further. The positions of the 'free' joints (those which are allowed to be adjusted) in a 'stiffest' structure design are not necessarily the best for a homologically deforming design. For a homologically deforming design the free joints are best positioned such that the stiffness of the dish structure varies smoothly in the radial direction. It also needs to have constant stiffness circumferentially, but this follows automatically from the cyclic symmetry. The position of each free node and its connection with other nodes, should also be such that the adjustment of any one particular free node does not affect the deformation behaviour of too large a part of the structure. In general, a good policy has been found to be one which provides each surface support node with at least one associated free node. This also ensures that the segment joint number condition (defined by equation 5.2.5) is satisfied. Another useful aim to ease the construction problem, as well as to avoid free joint position changes affecting too large a part of the structure's deformation behaviour, is to use as few structural members as possible (but still satisfy stability requirements). In practice this means avoiding cross-bracing by using triangular forms rather than rectangular ones.

One other aspect of the initial design stage worth noting, is the successful use of the three-dimensional stereoscopic pictures as a means of checking for unwanted member intersections - as well as providing a general idea of what the design would actually look like in three-dimensions. The use of stereoscopic pictures does take some practice, and it helps to know about what you are looking at; but since this will be the case with anyone designing these structures, it is not in practice a major problem. Perhaps their only disadvantage is that their effectiveness cannot be adequately demonstrated in these two

dimensional pages - the use of a stereoscopic viewer to look at the examples provided in the pocket at the back of this volume is therefore recommended.

7.1.2 - The Deformation Analysis

The discussion sections presented at the end of chapters three and four, dealing with the theory of the cyclic symmetry analysis and its implementation, cover most of the points raised in the deformation analysis stage. An aspect not dealt with there, however, and which has caused some problems, concerns the presentation of the large amounts of matrix algebra used in the theoretical development of the analysis method - see chapter three. In cases where it has not been possible to type equations, authors have usually resorted to writing them in by hand. Now there is clearly nothing wrong with this, except that it is a notoriously error prone method - especially where many terms have sub- and super-scripts. It was for this reason then, that a means of using a multi-style character set, available on the digital plotter (used to produce many of the diagrams here) to write these equations, was developed. The much stricter geometrical layout which can be achieved by this means has enabled typographic errors to be more easily detected. It is, however, not a very fast way of producing these equations - it takes considerably longer than writing them by hand.

7.1.3 - Measurement of Homological Performance

In order to achieve a sufficiently accurate implementation of the least squares fit and r.m.s. homology deviation error analysis (see Appendix 5.2), it proved necessary to use double precision arithmetic throughout the computer program. The numerical error in the r.m.s. error values calculated by this program can be shown to be less than

0.0001 mm r.m.s., compared to typical r.m.s. error values of 0.08 to 0.005 mm r.m.s.

There is one important difference between the method for finding the best fit paraboloid presented and used here, and that used by others concerned with measuring the homological performance of telescope structures, and it concerns which quantity (squared) is actually minimised. In the methods used by von Hoerner, Zarghame, Kowaleski and Zeibrath, and Hills and Colyer, it is the distance squared along the best fit surface normal to a deformed surface supporting point, which is minimised; whereas in the method used here it is the square of the resulting signal path length change, produced by the deformation of a surface supporting point, which is minimised. The effect of this difference is for the signal path length change minimisation method to produce r.m.s. homology deviation errors about 20% larger than those predicted by the normal distance minimisation method. For example, the overall r.m.s. homology deviation error, σ_o , for the final design is 0.0146 mm r.m.s. (see figure 6.9.1), whereas it would be 0.0115 mm r.m.s. if the normal distance minimisation method was used. In other words, the method used here to measure the homological performance of a telescope structure is a harsher one than that used by other people. It is also considered to be a better way of measuring homological performance, especially when designing telescopes to operate at very short wave lengths.

7.1.4 - Homological Performance Test

Strictly speaking, the effect of the reflecting panels being supported on a paraboloid having a slightly different focal length to the one whose surface the reflecting panels are actually a part of, should be included in the zenith pointing homological performance

assessment. This will in general increase the zenith pointing, and thus overall, r.m.s. homology deviation error. So, in the case of the final design whose zenith pointing focal length change is 1.15 mm (see table 6.9.2), the zenith pointing r.m.s. homology deviation error should really be given as 0.0177 mm r.m.s. (rather than 0.0096 mm r.m.s.) - using the analysis described in Appendix 5.1. This produces a new overall r.m.s. homology deviation error of 0.0180 mm r.m.s., which is, in fact, now above that specified in table 6.1.1.

The reason for this focal length change error being so large, compared to the structural r.m.s. error, is mainly because only three rings of reflecting panels are used to form the parabolic surface. If more were used, and in practice this would have to be the case because those required by a design having three rings of panels would be too large to make successfully, the effect of each panel not being mounted on its actual paraboloid on the zenith pointing error would be reduced.

7.1.5 - Improving the Homological Performance

As was said when considering the formulation of design modifications (see section 6.7), it is difficult to formally define what constitutes a potentially good homologically deforming structure. What can be said, though, is that there are certain structures which are easier to evolve into a high homological performance structure than others. These can be recognised by the ease with which beneficial modifications can be formulated - in other words, how easy it is to decide correctly what effect any particular modification will have on the structure's performance.

A point which has come out of the experience gained in using the design procedure to look at the homological performance possibilities of a number of types of structures - some having a lattice type frame-

work rather than interconnected ribs - is that the distinction between free joint position changes and cross-sectional area changes, as primary and secondary design variables, is not as clear as was first suggested. This is not to say that they should not be considered as primary and secondary design variables, but rather that the effectiveness of each type varies from design to design. In other words, there are some designs where it proves easier to obtain improvements in the homological performance by making changes mostly to member cross-sections (but only using those available), rather than free joint position changes and vice versa.

7.2 - An Overall View of the Design Procedure

In order to put into context an overall view of the design procedure presented here, the work and methods of other millimetre wave telescope projects will briefly be described. At present there are five projects which involve the design and construction of a millimetre wave telescope using the principle of homological deformation. All have slightly different performance aims - reflecting the differing interests of the astronomers for whom the telescopes are being built.

The group which has been working on the design of millimetre wave telescopes the longest (yet is perhaps the furthest from actually building one) is at the National Radio Astronomy Observatory (N.R.A.O.), West Virginia, U.S.A. This group, led by von Hoerner, now have a final design for a 25 m (82 ft.) dish which will be built in a radome, and has a minimum observable wave length specification of 0.8 mm. In their homological design, this group used von Hoerner's automatic design program (see section 1.5) to produce a highly optimised structural design, having very good homological behaviour, in theory at least. However, as has already been pointed out (section 5.1), the problem with von Hoerner's

method of systematically changing all the cross-section of the structural members, is that a final design requires many different cross-sections which are not necessarily available from manufacturers. Worse still, is the fact that the design contains joints at which members of widely different cross-sections meet. These two aspects of von Hoerner's design method therefore make the accurate construction of a millimetre wave telescope structure rather difficult. Another point about von Hoerner's work worth noting here, is that the first program written to implement his method took no advantage of any symmetry that the structures being analysed possessed (cyclic or otherwise) and it could only deal with designs having fewer than 20 surface support points, and 130 members. A second 'improved' program was subsequently written, which takes advantage of structural symmetry to the extent that only one quadrant of the complete structure is considered. Using this new program structures having up to 90 surface support points and 600 members have been optimised, which still does not compare well with the 360 surface support point limit (and 2500 members) of the cyclic symmetry analysis program used in the work presented here.

The next group to start work on the design of a 30 m (98 ft.) millimetre wave telescope from part of an organisation, combining French and German efforts, called the International Radio Astronomy Millimetric (I.R.A.M.). This telescope is in fact being designed and built by the same people who were involved in the 100 m Bonn dish. In this case the design is for an open air telescope (i.e. no protective housing), that can operate down to about 2 mm , which is to be built in Southern Spain on top of one of the mountains in the Sierra Nevada range. An interesting aspect of this project is that the cyclically symmetric surface supporting structure and its elevation mounting structure have been designed quite separately - in the sense that both parts have not

been included in one complete numerical analysis. This was done by designing the dish structure so that the large supporting ring, to which the elevation structure is connected, always remains circular. The elevation mounting structure was then also designed so that this 'common' ring remains circular. In theory there seems to be nothing against this method of design, but quite how successful it is in practice is difficult to judge. However, being able to include both the dish and elevation mounting components of the telescope structure would clearly avoid this situation and would also enable a much more integrated design to be analysed.

The most advanced millimetre wave telescope project is for a Japanese 45 m (150 ft.) dish. This telescope is very near completion and forms part of a synthesis array - the other elements being smaller (10 m) dishes. A much less ambitious performance has been aimed at for this instrument, compared to the N.R.A.O. and I.R.A.M. designs. However, very little detail has been made available concerning this project and virtually nothing on the method used to design the homologically deforming structure, but since it is not a very highly optimized design it seems unlikely that it involved an automatic procedure.

The next project, in order of starting, is the U.K. millimetre wave telescope project, which as already mentioned (section 1.6) is for a 15 m dish to be built on Las Palma (in the Canary Islands). Although the design method used by this group takes full advantage of the structural cyclic symmetry, it is not able to include any non-cyclically symmetric elevation mounting structure - so again the two, (dish and elevation mounting) structure components have to be analysed separately.

The fifth, and most recent, project is again an I.R.A.M. project,

this time for a three dish millimetre wave synthesis telescope all of 15 m diameter. The published performance specifications for these instruments are very similar to those of the U.K. millimetre wave telescope so the design method used by this group is going to have to be more refined than that used for the I.R.A.M. 30 m dish.

The natural tendency when considering the design procedure presented here, is to be more aware of its short-comings than its successes. However, despite the fact that there are improvements which could be made, it is clear from the preceding discussion of the methods used by other millimetre wave telescope projects, that it does provide a more effective means of designing a complete homologically deforming telescope structure. This is because, although it is quite possible to achieve good homologically deforming telescope structure designs by just considering the cyclically symmetric dish part of the structure (as the U.K. 15 m and I.R.A.M. 30 m designs show), when they are supported on an elevation mounting structure this homological behaviour will be altered, even if the design procedure has involved ensuring deformation compatibility between the dish structure and elevation mounting structure components, and so the homological performance of the complete telescope structure will not be known before it is built. This problem becomes increasingly serious as the surface accuracy requirement of a telescope increases and there is bound to be a point at which it can only be solved by including the elevation mounting structure in the design of a homologically deforming telescope structure.

7.3 - Computer Supported Design

The term 'Computer Supported Design' is used to describe the role played by the computer in the design procedure presented here, rather

than the term 'Computer Aided Design' which, as a result of its very wide usage, has become somewhat ambiguous. It is also to contrast it with design methods which only require someone to start them off, and then look at the results - the rest being done by a programmed computer, as is the case in von Hoerner's method. There undoubtedly are occasions when the use of a computer to carry out an automatic search or optimization is the only practical means of solving a particular problem. However, to relegate the designer to the status of a machine minder is to totally deny the essential part that the human mind plays in the process of design. Design, or more specifically, what is usually called 'Engineering Design', is a very disciplined art, but it is still an art, and computers are not artists - not yet anyway! The use of a computer in any design procedure should therefore be such that it enables the human designer to extend his abilities, not replace them.

The design procedure presented here is thus in stark contrast to the fully automatic procedure developed by von Hoerner and others - where the direction of design is out of reach of the human designer once the program has been given an initial design. By the introduction of a high degree of user interaction and control, the designer is placed in a much better position to guide the design direction, so that only useful paths are followed, and also to understand the reasoning behind the final design and its deformation behaviour. Perhaps more important though, is the fact that this interactive flexibility allows the whole subject of homologically deforming structures to be studied and therefore the necessary experience and 'feel' for the problem gained. The vastly more powerful problem solving and inspirational capacity of the human mind, both conscious and subconscious, can thus be set to work, instead of the inevitably narrow and limited powers with which a computer can be programmed.

7.4 - Conclusions

Although there is room for further development and improvement to be made in some of the techniques and methods used in a few of the stages of the design procedure, they have provided a means of clearly demonstrating the effectiveness of the proposed procedure. The following conclusions can therefore be drawn concerning, not only the primary aim of this work, but also some of the more important aspects arising from individual stages of the design procedure.

I. A design procedure has been developed, and its effectiveness demonstrated, for use in the study and design of the homologically deforming surface supporting structure of telescopes for use at millimetre and sub-millimetre wavelength observations. The design procedure has the considerable advantage over other methods used, of being able to deal with a complete telescope structure without this resulting in a long time-consuming computer analysis, or having to ignore parts of the elevation mounting structure.

II. The theoretical development of an analytical method has been achieved, which takes advantage of any cyclic symmetry a structure might have, to greatly reduce the otherwise large analysis task it creates in terms of traditional methods, but which still allows a non-cyclically symmetric region of the structure to be included in the analysis, and is able to deal with any form of cyclically symmetric or general, non-cyclically symmetric, loading.

III. A computer program implementing the theoretical cyclic symmetry analysis, has been written and developed, which successfully demonstrates the advances made by the theory in being able to include a non-cyclically symmetric region in an otherwise cyclically symmetric structure subjected to non-cyclically symmetric loadings, and thus form an effective deformation analysis stage in an interactive computer

supported design procedure.

IV. The theoretical basis for, and computational implementation of, a criterion for measuring the homological deformation performance of a telescope surface supporting structure has been developed and used, which is superior to that used by previous workers in this area.

V. It has been demonstrated that the use of a mixture of design variables, in the form of structure geometry variations and member cross-sectional area changes (which are only allowed to take the values of those sections available from manufacturers) provides an efficient means of modifying an initial structure design to improve its homological deformation performance sufficiently for it to meet the low reflecting surface errors demanded of the structures for telescopes designed to observe at millimetre wavelengths, in a small number of design modification cycles - and in such a way that the resulting modified structure remains a realistic and practical design.

VI. A successful balance has been achieved between the roles played by the computer and human designer in the computer supported design procedure that has been developed, and is presented here. As a result, the considerable capacity of modern digital computers to carry out large amounts of numerical calculations, and to manipulate data structures very quickly, is used to enhance and extend the also considerable capacity of the human mind, both conscious and subconscious, to provide the essential inspiration, comprehension and problem-solving abilities required to practice the art of Engineering Design.

7.5 - Postscript

As with any research project many ideas and concepts are found and developed, paths followed and areas looked into which cannot be included in a single volume such as this. They remain however, some of the most

valuable experiences gained while working as a research student. It can therefore only be regarded as a privilege to have had the opportunity to gain such experiences; to discover the ideas and work of so many other people, both dead and alive. Indeed, the work presented here reflects this to some extent by the fact that it has its roots in both the work of Joseph Fourier (1768-1830), and that of von Hoerner, which was started less than twenty years ago. Between these two many others have contributed, wittingly and unwittingly, such as Fortescue, with his symmetric components for the analysis of polyphase electrical circuits, to the solution of the problems which occurred in the development of the various stages of the complete design procedure. In doing so they have helped bring together the two previously unlinked areas of symmetric components and Fourier's transformation method, and the design of millimetre wave telescope structures.

APPENDICES

Appendix 2.1 - Horizon pointing gravitational deformation for of a cyclically symmetric structure*

Suppose, for the purpose of clarity, that the structure has a sufficient degree of cyclic symmetry for it to have reflective symmetry in both the x-y plane and x-z plane, see figure A2.1.1. In other words,

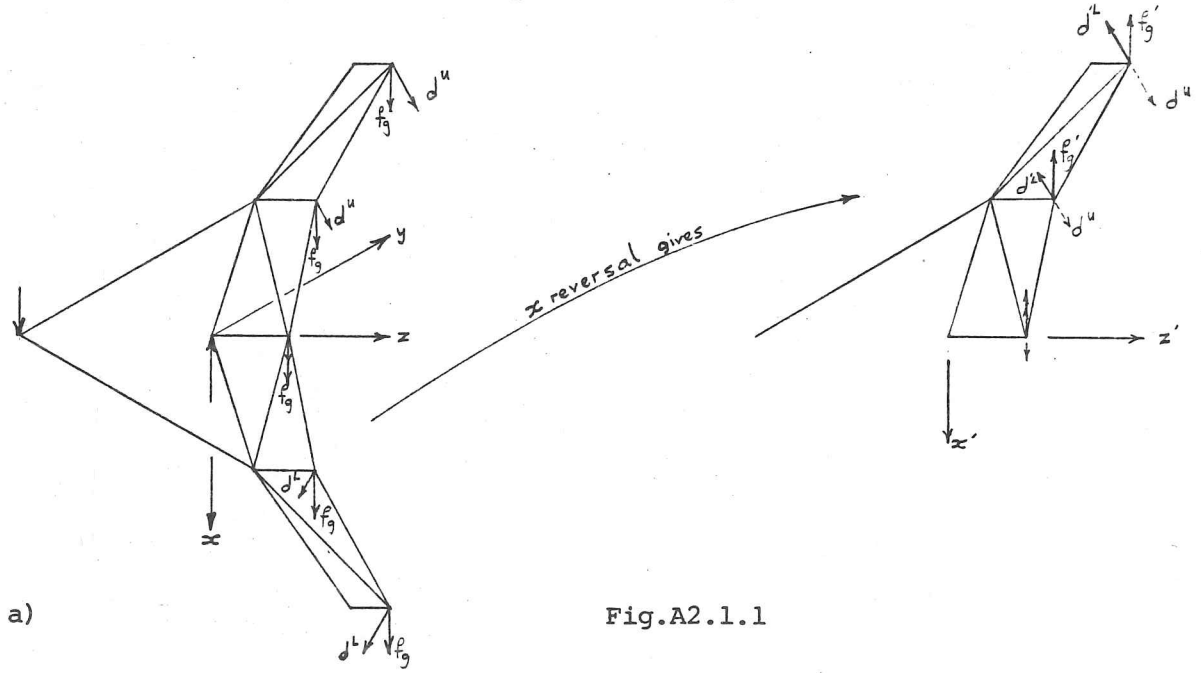

a)

Fig.A2.1.1

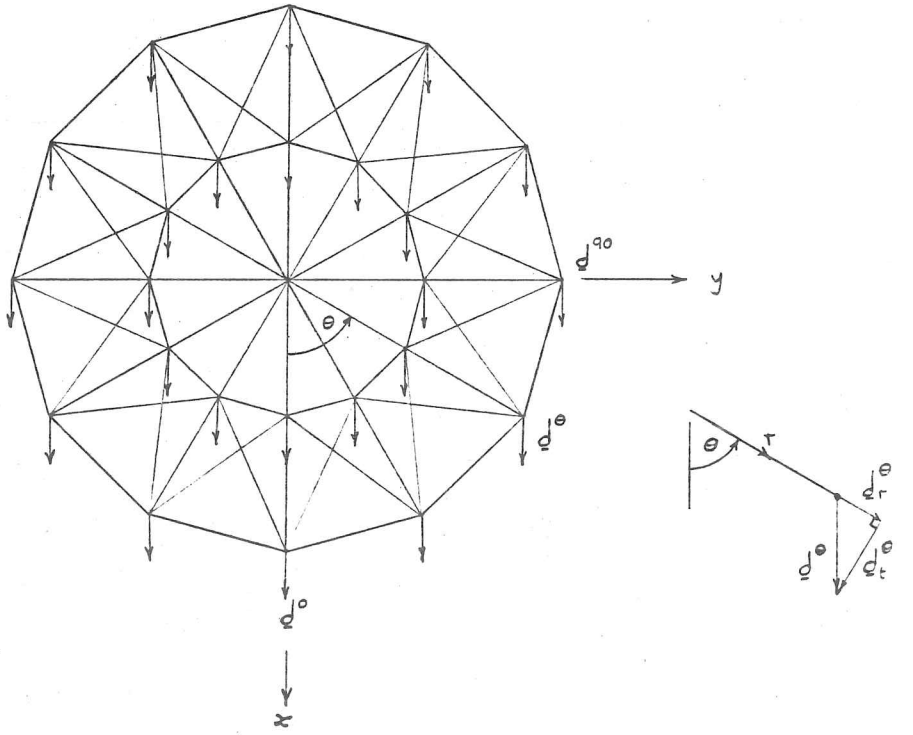

b)

*Based on a similar argument given by Hills in ref. 3 of chapter two.

it has an integer number of symmetric segments in each quadrant.

By reversing the direction of the x-coordinate in the lower half of the structure, but keeping the y-direction the same, so that $(x',y',z') = (-x,y,z)$, it can be seen that it is identical with the upper half. However, if the loading acts in the x-direction, the sign must be changed, thus $\underline{f}'_g = -\underline{f}_g$. It therefore follows that the displacements in the lower half will have the opposite sign to those in the upper half, $\underline{d}^L = -\underline{d}^U$ (see figure 2.11a). In terms of the original co-ordinates the displacements in the lower half can be related to those of the corresponding point in the upper half by:

$$(d_x^L, d_y^L, d_z^L) = (d_x^U, -d_y^U, -d_z^U) \ . \qquad \text{(A2.1.1)}$$

Since there can be no discontinuity in the form of the displacements across the y-z plane, points in this plane will only move in the x-direction

$$\underline{d}_{x=0} = (d_x, 0, 0) \ . \qquad \text{(A2.1.2)}$$

Also, points which lie in the x-z plane will only move in the x and z directions and not the y-direction.

Thus, in terms of radial, tangential and axial deflections (instead of the x, y and z components), the deflections of structural points lying in the vertical plane will only have radial and axial components:

$$\underline{d}^0 = (d_r^0, 0, d_a^0) \ , \qquad \text{(A2.1.3)}$$

while the deflections of points in the horizontal plane will be purely tangential:

$$\underline{d}^{90} = (0, d_t^{90}, 0) \ , \qquad \text{(A2.1.4)}$$

see figure A2.1.1b.

Consider now a cyclically symmetric segment at an angle θ to the vertical. As a result of the cyclic symmetry the description of the structure relative to this segment will be the same as it is relative to any other segment. Thus by resolving the vertical loading into radial and tangential components, $f_g \cos\theta$ and $f_g \sin\theta$ respectively, we transform the displacement solution of the segment into the two types just considered. It follows then that the deflections in response to this combination of loads will have the form:

$$\begin{aligned} \underline{d}^{\theta} &= \underline{d}^{o} \cos\theta + \underline{d}^{90^o} \sin\theta \\ \underline{d}^{\theta} &= (\underline{d}^{o}_{r} \cos\theta, \underline{d}^{90^o}_{t} \sin\theta, \underline{d}^{o}_{a} \cos\theta) \ . \end{aligned} \tag{A2.1.5}$$

Now tangential deflections do not contribute to the surface error since they simply move the points parallel to the surface. The deformations normal to the surface are thus given by:

$$d^{\theta}_{n} = d^{\theta}_{r} \sin\psi + d^{\theta}_{a} \cos\psi \ , \tag{A2.1.6}$$

where ψ is the angle of the surface normal to the z-axis, see figure A2.1.2.

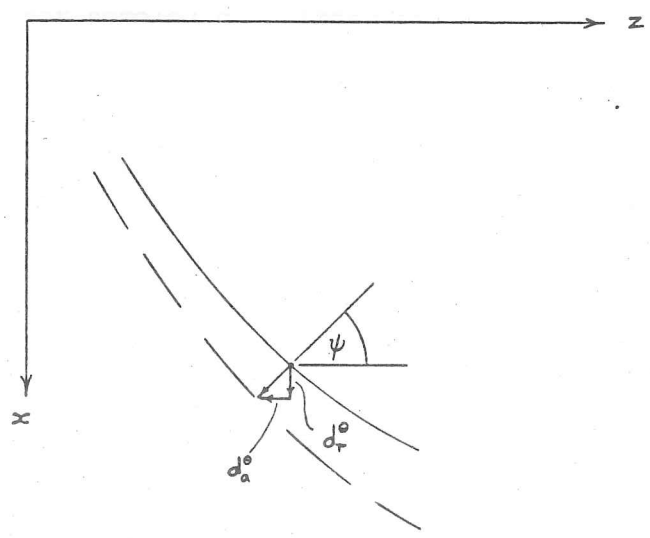

Fig.A2.1.6.

Now the surface normal deformations in a vertical segment have a similar form:

$$d_n^o = d_r^o \sin\psi + d_a^o \cos\psi \ , \qquad \text{(A2.1.7)}$$

so that those of a segment at an angle θ to this vertical segment may be expressed in terms of d_n^o as:

$$d_n^\theta = d_n^o \cos\theta \ . \qquad \text{(A2.1.8)}$$

Considering now the form of the horizon pointing homological deformation, which is a combination of a tilting of the initial parabolic surface and a shifting of its origin along the x-axis (see figure 2.2.2), the form of the displacements in the vertical plane will be given by:

$$d(r) = ax + bxr^2 \ , \qquad \text{(A2.1.9)}$$

where a and b are constants whose values depend on the amount of tilting and origin shifting which occurs. In terms of cylindrical co-ordinates this becomes:

$$d(r) = (ar + br^3)\cos\theta \ . \qquad \text{(A2.1.10)}$$

From this expression it can be seen that the desired form of the displacements for homological deformation to occur in the horizon pointing case, is such that the deflections in a segment at an angle θ to the vertical must be the same as those of the vertical segment but scaled by an amount $\cos\theta$. In other words:

$$d^\theta(r) = d^o(r) \cos\theta \ , \qquad \text{(A2.1.11)}$$

which is the same form as equation (A2.1.8), thus showing that a cyclically symmetric structure has the required form of deformation in the horizon pointing case for homological deformation to be theoretically possible.

Appendix 3.1 - Algebraic expressions for the element matrices of $\underline{\underline{P}}_T$, $\underline{\underline{K}}_T$, $\underline{\underline{d}}_T$ and $\underline{\underline{d}}$

3.1.1 - The transformed load vector $\underline{\underline{P}}_T$:-

$$\underline{P}_{T_0} = \frac{1}{n}\underline{P}_0^{(1)}$$

$$\underline{P}_{T_1} = \frac{1}{n}\left(\sum_{i=1}^{n}\underline{P}_i^{(i)}\right)$$

$$\underline{P}_{T_2} = \frac{1}{n}\left(\sum_{i=1}^{n}a^{(i-1)}\underline{P}_i^{(i)}\right)$$

. . . (A3.1.1)

$$\underline{P}_{T_r} = \frac{1}{n}\left(\sum_{i=1}^{n}a^{(r-1)(i-1)}\underline{P}_i^{(i)}\right)$$

. . .

$$\underline{P}_{T_{n'}} = \frac{1}{n}\left(\sum_{i=1}^{n}a^{(n'-1)(i-1)}\underline{P}_i^{(i)}\right)$$

3.1.2 - The transformed stiffness supermatrix $\underline{\underline{K}}_T$:-

$$\underline{K}_{T_{00}} = \underline{K}_{00}^{(1)}$$

$$\underline{K}_{T_{11}} = \left\{\underline{K}_{11}^{(1)} + \sum_{i=2}^{m+1}\left[(\underline{K}_{11}^{(1)}\underline{T}_{i1}) + (\underline{K}_{11}^{(1)}\underline{T}_{i1})^T\right]\right\}$$

$$\underline{K}_{T_{22}} = \left\{\underline{K}_{11}^{(1)} + \sum_{i=2}^{m+1}\left[a^{(i-1)}(\underline{K}_{11}^{(1)}\underline{T}_{i1}) + a^{(i-1)}(\underline{K}_{11}^{(1)}\underline{T}_{i1})^T\right]\right\}$$

. . . (A3.1.2)

$$\underline{K}_{T_{rr}} = \left\{\underline{K}_{11}^{(1)} + \sum_{i=2}^{m+1}\left[a^{(r-1)(i-1)}(\underline{K}_{11}^{(1)}\underline{T}_{i1}) + a^{(r-1)(i-1)}(\underline{K}_{11}^{(1)}\underline{T}_{i1})^T\right]\right\}$$

. . .

$$\underline{K}_{T_{n'n'}} = \left\{\underline{K}_{11}^{(1)} + \sum_{i=2}^{m+1}\left[a^{(n'-1)(i-1)}(\underline{K}_{11}^{(1)}\underline{T}_{i1}) + a^{(n'-1)(i-1)}(\underline{K}_{11}^{(1)}\underline{T}_{i1})^T\right]\right\}$$

$$\underline{K}_{T01} = (\underline{K}_{01}^{(1)} + \{\sum_{i=2}^{n} \underline{K}_{0i}^{(1)} \underline{T}_{i1}\})$$

$$\underline{K}_{T02} = (\underline{K}_{01}^{(1)} + \{\sum_{i=2}^{n} \bar{a}^{(i-1)} \underline{K}_{0i}^{(1)} \underline{T}_{i1}\})$$

. . . (A3.1.3)

$$\underline{K}_{T0r} = (\underline{K}_{01}^{(1)} + \{\sum_{i=2}^{n} \bar{a}^{(r-1)(i-1)} \underline{K}_{0i}^{(1)} \underline{T}_{i1}\})$$

. . .

$$\underline{K}_{T0n'} = (\underline{K}_{01}^{(1)} + \{\sum_{i=2}^{n} \bar{a}^{(n'-1)(i-1)} \underline{K}_{0i}^{(1)} \underline{T}_{i1}\})$$

3.1.3 - The transformed displacement vector $\underline{d}_T$:-

$$\underline{d}_{T0} = \{\underline{K}_{T00} - \tfrac{1}{n}(\underline{K}_{T01}\underline{K}_{T11}^{-1}\underline{K}_{T01}^{T}) - \tfrac{1}{n}[\sum_{i=2}^{t}(\underline{K}_{T0i}\underline{K}_{Tii}^{-1}\bar{\underline{K}}_{T0i}^{T} + \bar{\underline{K}}_{T0i}\bar{\underline{K}}_{Tii}^{-1}\underline{K}_{T0i}^{T})] - \tfrac{\delta}{n}(\underline{K}_{T0n'}\underline{K}_{Tn'n'}^{-1}\bar{\underline{K}}_{T0n'}^{T})\}^{-1}$$
$$\{\underline{P}_{T0} - \tfrac{1}{n}(\underline{K}_{T01}\underline{K}_{T11}^{-1}\underline{P}_{T1}) - \tfrac{1}{n}[\sum_{i=2}^{t}(\underline{K}_{T0i}\underline{K}_{Tii}^{-1}\underline{P}_{Ti} + \bar{\underline{K}}_{T0i}\bar{\underline{K}}_{Tii}^{-1}\bar{\underline{P}}_{Ti})] - \tfrac{\delta}{n}(\underline{K}_{T0n'}\underline{K}_{Tn'n'}^{-1}\underline{P}_{Tn'})\}$$

where $\delta = 1$, $t = n'-1$ and $n' = (\frac{n+2}{2})$ for n even

or $\delta = 0$, $t = n'$ and $n' = (\frac{n+1}{2})$ for n odd

$$\underline{d}_{T1} = \underline{K}_{T11}^{-1}(\underline{P}_{T1} - \underline{K}_{T01}^{T}\underline{d}_{T0})$$

$$\underline{d}_{T2} = \underline{K}_{T22}^{-1}(\underline{P}_{T2} - \bar{\underline{K}}_{T02}^{T}\underline{d}_{T0}) \qquad \text{(A3.1.4)}$$

. . .

$$\underline{d}_{Tr} = \underline{K}_{Trr}^{-1}(\underline{P}_{Tr} - \bar{\underline{K}}_{T0r}^{T}\underline{d}_{T0})$$

. . .

$$\underline{d}_{Tn'} = \underline{K}_{Tn'n'}^{-1}(\underline{P}_{Tn'} - \bar{\underline{K}}_{T0n'}^{T}\underline{d}_{T0})$$

3.1.4 - The real segment displacement vector $\underline{\underline{d}}$:-

$$\underline{d}_0^{(1)} = n\underline{d}_{\tau_0}$$

$$\underline{d}_1^{(1)} = \{\underline{d}_{\tau_1} + \sum_{i=2}^{t} (\underline{d}_{\tau_i} + \bar{\underline{d}}_{\tau_i}) + \delta \underline{d}_{\tau_{n'}}\}$$

$$\underline{d}_2^{(2)} = \{\underline{d}_{\tau_1} + \sum_{i=2}^{t} (\bar{a}^{(i-1)} \underline{d}_{\tau_i} + a^{(i-1)} \bar{\underline{d}}_{\tau_i}) + \delta a^{(n'-1)} \underline{d}_{\tau_{n'}}\}$$

.

.

. (A3.1.5)

$$\underline{d}_r^{(r)} = \{\underline{d}_{\tau_1} + \sum_{i=2}^{t} (\bar{a}^{(r-1)(i-1)} \underline{d}_{\tau_i} + a^{(r-1)(i-1)} \bar{\underline{d}}_{\tau_i}) + \delta a^{(r-1)(n'-1)} \underline{d}_{\tau_{n'}}\}$$

.

.

.

$$\underline{d}_n^{(n)} = \{\underline{d}_{\tau_1} + \sum_{i=2}^{t} (\bar{a}^{(n-1)(i-1)} \underline{d}_{\tau_i} + a^{(n-1)(i-1)} \bar{\underline{d}}_{\tau_i}) + \delta a^{(n-1)(n'-1)} \underline{d}_{\tau_{n'}}\}$$

where $\delta = 1$, $t = n'-1$ and $n' = (\frac{n+2}{2})$ for n even

or $\delta = 0$, $t = n'$ and $n' = (\frac{n+1}{2})$ for n odd.

Appendix 4.1 - Cyclic Symmetry Analysis Program Data Input Format

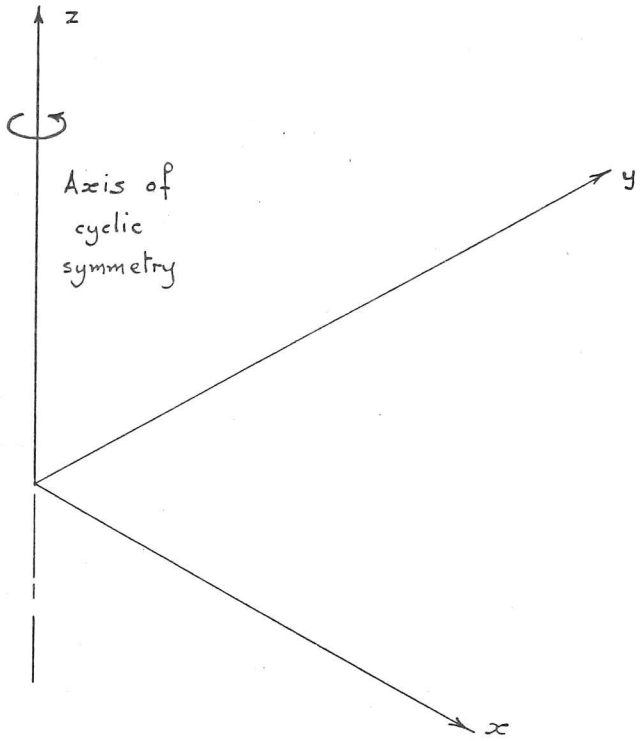

Fig.A4.1.1 - Definition of co-ordinate axes used to define central region and first cyclic segment node positions.

4.1.1 - Geometric limits

Maximum number of cyclic segments	=	30
Maximum number of central region nodes	=	40
Maximum number of nodes per cyclic segment	=	25
Maximum number of elements connecting central region to a cyclic segment	=	10
Maximum number of elements connecting two cyclic segments	=	40

4.1.2 - Segment boundary and node numbering conditions

The following conditions must be satisfied before a cyclically symmetric structure and its loading may be described, via the input data, to the cyclic symmetry analysis program.

Appendix 4.1 - Cyclic Symmetry Analysis Program Data Input Format

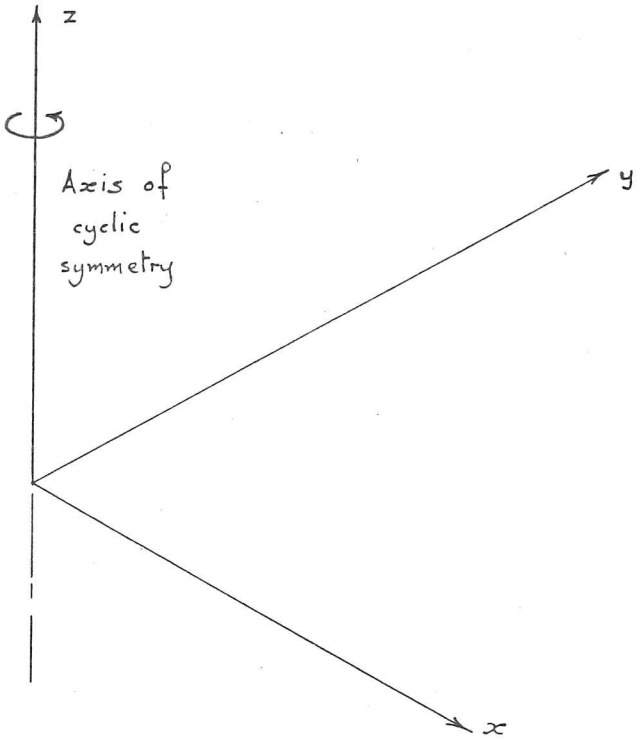

Fig.A4.1.1 - Definition of co-ordinate axes used to define central region and first cyclic segment node positions.

4.1.1 - Geometric limits

Maximum number of cyclic segments	= 30
Maximum number of central region nodes	= 40
Maximum number of nodes per cyclic segment	= 25
Maximum number of elements connecting central region to a cyclic segment	= 10
Maximum number of elements connecting two cyclic segments	= 40

4.1.2 - Segment boundary and node numbering conditions

The following conditions must be satisfied before a cyclically symmetric structure and its loading may be described, via the input data, to the cyclic symmetry analysis program.

i. The number of any node in the central region must be less than that of any node in the first cyclic segment. In other words, the node numbering must start with the central region nodes and not move on to the first cyclic segment nodes until all the central region nodes are numbered.

ii. The number of any node in the cyclic segment S_j must be less than that of any node in the cyclic segment S_{j+1} - i.e., each cyclic segment should be fully numbered before moving on to the next cyclic segment. In practice only the first two cyclic segments need to be numbered.

iii. The difference between the number of a node in cyclic segment S_j and that of the corresponding node in segment S_{j+1} must be the same for all other nodes in segments S_j and S_{j+1}. This condition requires the cyclic segment nodes to be numbered in the same way for each segment.

iv. The segment boundaries may <u>not</u> pass through any node so that the segment to which a particular node belongs is uniquely defined.

v. The structural connections between the central region and the cyclic segments must themselves by cyclically symmetric. This means that the boundary between non-cyclically symmetric structure and purely cyclically symmetric structure must be contained within the central region.

4.1.3 - Data file format

Having satisfied these conditions, the structure and its loadings are then described in the following order:

1. Title - Up to 80 alpha numeric characters including spaces used to form an identification title.

2. $N_1, N_2, N_3, \ldots, N_{10}$ - Data Control parameters, defined as follows:

   N_1 = number of cyclic segments,

   N_2 = number of nodes in central region,

   N_3 = number of nodes in central region connected to nodes in first cyclic segment,

   N_4 = number of nodes in a cyclic segment,

   N_5 = number of nodes in first cyclic segment connected to nodes in second cyclic segment,

   N_6 = number of elements in central region,

   N_7 = number of elements connecting central region to first cyclic segment,

   N_8 = number of elements in a cyclic segment,

   N_9 = number of elements connecting first and second cyclic segments,

   N_{10} = 0 for simple pin-jointed element or
   = 1 for hybrid element.

3. $x_i \; y_i \; z_i \quad i = 1, (N_2+N_4)$ - Nodal coordinates for central and first cyclic segment nodes - these must be continuously numbered, starting with 1 in the central region.

4. $N_{mat} \; g \; \alpha_1 \; \alpha_2$ - N_{mat} is the number of different element cross-sections and/or materials used

   g = acceleration due to gravity, for the two directions defined by α_1 and α_2, where:

   α_i = 0 for g in +ve x direction,

   α_i = 90 for g in -ve z direction.

5. $E_i \; \rho_i \; D_i \; t_i \quad i = 1, N_{mat}$ - E_i = Youngs modulus, ρ_i = density, D_i = tube diameter and t_i = wall thickness.

6. $n_1 \; n_2 \; m$ - N_6 central region element + N_8 cyclic segment elements, where n_1 & n_2 = node numbers ($n_1 < n_2$) and m is the material number as defined in (5).

7. $n_1 \; n_2 \; m$

   $n_{c_1} \; n_{c_2} \; n_{c_3} \; \ldots \; n_{c_{N_1-1}}$

   - N_7 elements connecting central region and first cyclic segment, $n_{c_1} \; n_{c_2} \ldots n_{c_{N_1-1}}$ are the central region nodes similarly connected to the other (N_1-1) cyclic segments.

8. n_1 n_2 m - N_9 elements connecting the first and second cyclic segments.

9. NFC1 NFC2 NYF1 NYF2 - NFC1 and NFC2 are the number of central region nodes subjected to point loads for each of the two loading cases respectively. NYF1 and NYF2 are the total number of cyclic segment nodes point loaded for each of the two loading cases respectively.

10. n f_x f_y f_z - NCF1 loaded central region nodes, where n = node number.

11. n f_x f_y f_z - NFC2 loaded central region nodes - second load case.

12. n_{cy} n_n f_x f_y f_z - NYF1 loaded cyclic segment nodes, where
n_{cy} = cyclic segment number
n_n = number of corresponding node in the first cyclic segment.

13. n_{cy} n_n f_x f_y f_z - NYF2 loaded cyclic segment nodes - second load case.

14. NMFY - Number of nodes per cyclic segment having point masses attached. Note these are assumed to be cyclically symmetric in distribution.

15. n mass - NMFY point mass loaded nodes; n = node number, mass = point mass.

8. n_1 n_2 m - N_9 elements connecting the first and second cyclic segments.

9. NFC1 NFC2 NYF1 NYF2 - NFC1 and NFC2 are the number of central region nodes subjected to point loads for each of the two loading cases respectively. NYF1 and NYF2 are the total number of cyclic segment nodes point loaded for each of the two loading cases respectively.

10. n f_x f_y f_z - NCF1 loaded central region nodes, where n = node number.

11. n f_x f_y f_z - NFC2 loaded central region nodes - second load case.

12. n_{cy} n_n f_x f_y f_z - NYF1 loaded cyclic segment nodes, where
n_{cy} = cyclic segment number
n_n = number of corresponding node in the first cyclic segment.

13. n_{cy} n_n f_x f_y f_z - NYF2 loaded cyclic segment nodes - second load case.

14. NMFY - Number of nodes per cyclic segment having point masses attached. Note these are assumed to be cyclically symmetric in distribution.

15. n mass - NMFY point mass loaded nodes; n = node number, mass = point mass.

16. NCC NYC - Number of central region and first cyclic segment nodes having one or more degrees of freedom constrained to zero displacement, respectively.

17. n k_x k_y k_z - NCC constrained central region nodes
$k_{x,y,z}$ = 1 for zero displacement constraint in the x, y or z direction (= 0 for no constraint)

18. n k_x k_y k_z - NYC constrained nodes in the first cyclic segment.

Appendix 4.2 - Helicopter Landing Pad Analysis Results and Error Estimation

Details of the structure's geometry and node numbering are given in figures A4.2.1 to A4.2.3 together with listings of the data files used in tables A4.2.6 and A4.2.7, and analysis results in tables A4.2.1 to A4.2.5.

Error Estimation

If we assume that the difference between the true (double precision) results and single precision Finite Element analysis of 0.0003 is due to rounding errors accumulating during the inversion of the structure stiffness matrix, an estimate of the error produced per degree of freedom is given by:

$$\varepsilon_{df} \approx \frac{0.0003}{(\frac{n+1}{2})^2} \qquad \text{(A4.2.1)}$$

where n is the order of the stiffness matrix, and 0.0003 is the r.m.s. difference between the mantissa values of the double precision and single precision solutions. Thus for $n = 99$, ε_{df} $1.2\ 10^{-7}$.

Using this value of ε_{df}, an estimate of the rounding error, which could be expected in the Cyclic Symmetry Analysis solution, can be made. In this case two matrix inversions are carried out in the calculation of the cyclic segment nodal displacements - both using the same method as used in the Finite Element analysis.

Thus

$$\varepsilon_{cy} \approx (\frac{48+1}{2})^2 (\frac{12+1}{2})^2 \times 1.2\times10^{-7} \qquad \text{(A4.2.2)}$$

$$\therefore \varepsilon_{cy} \approx 3.0\times10^{-3},$$

which agrees well with the estimated r.m.s. value of 2.9×10^{-3} calculated from the results. This therefore establishes that the difference between the conventional Finite Element analysis results and the Cyclic Symmetry

analysis results is due to the different accumulation of rounding errors.

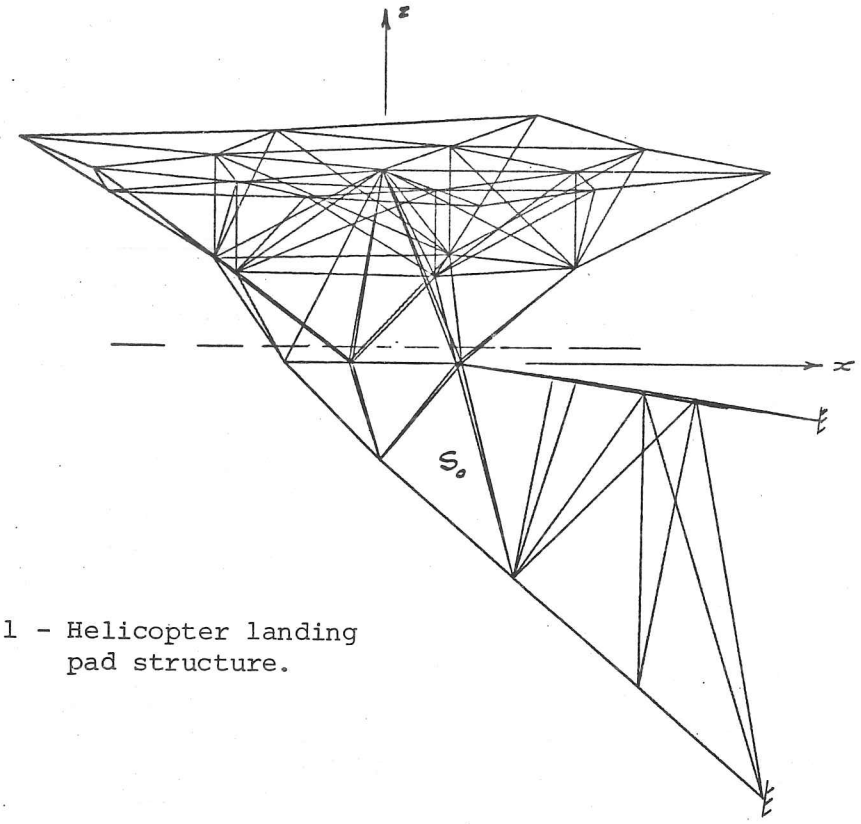

Fig.A4.2.1 - Helicopter landing pad structure.

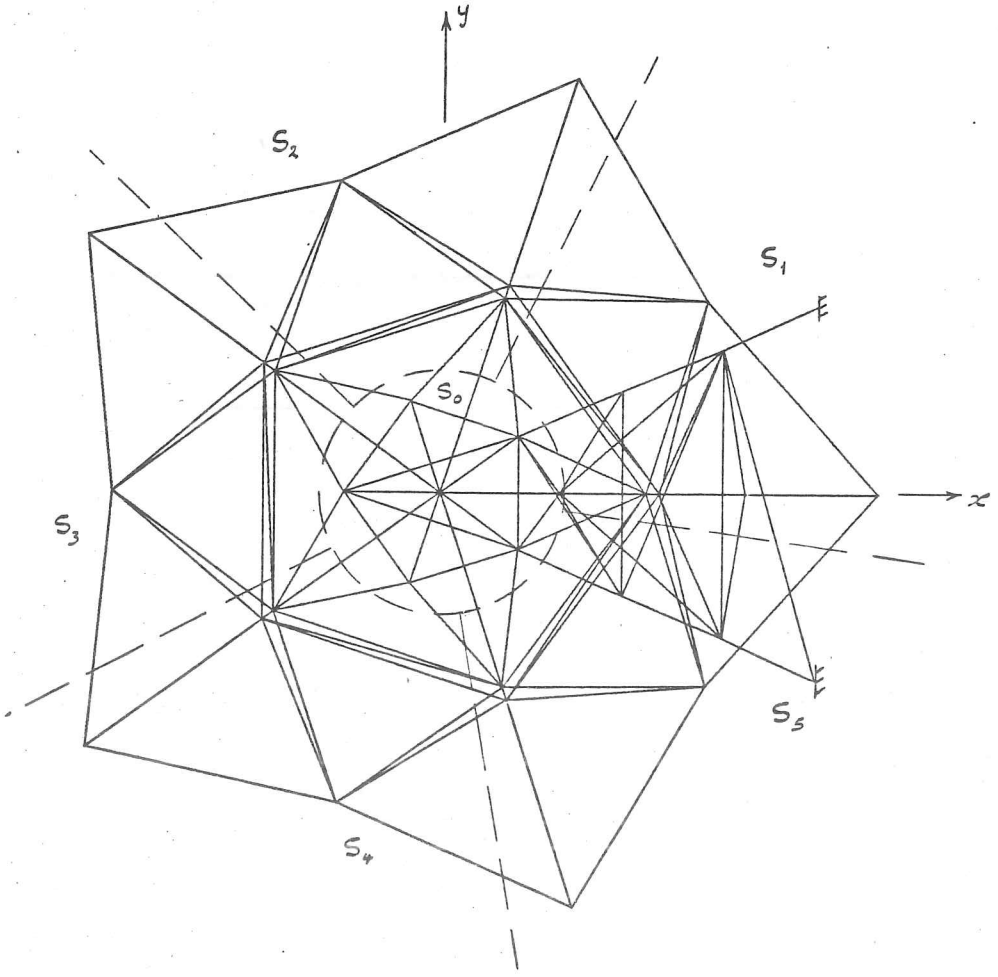

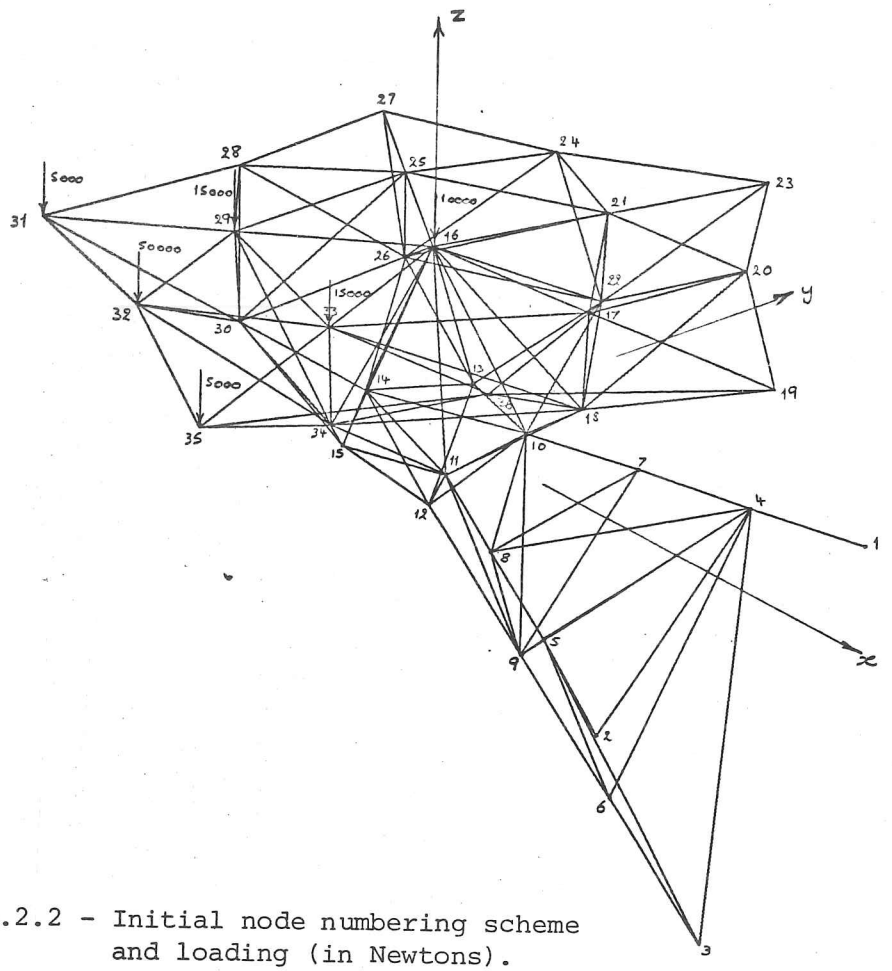

Fig.A4.2.2 - Initial node numbering scheme and loading (in Newtons).

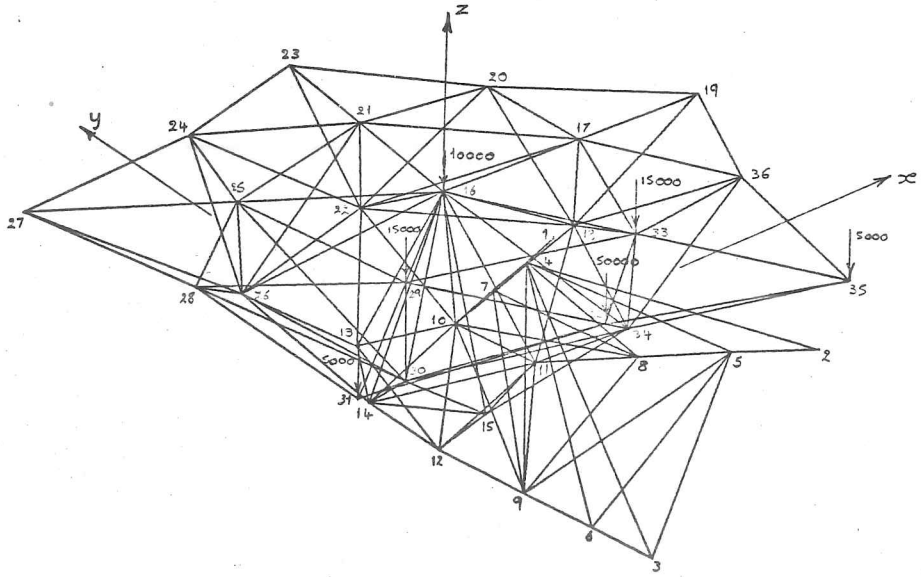

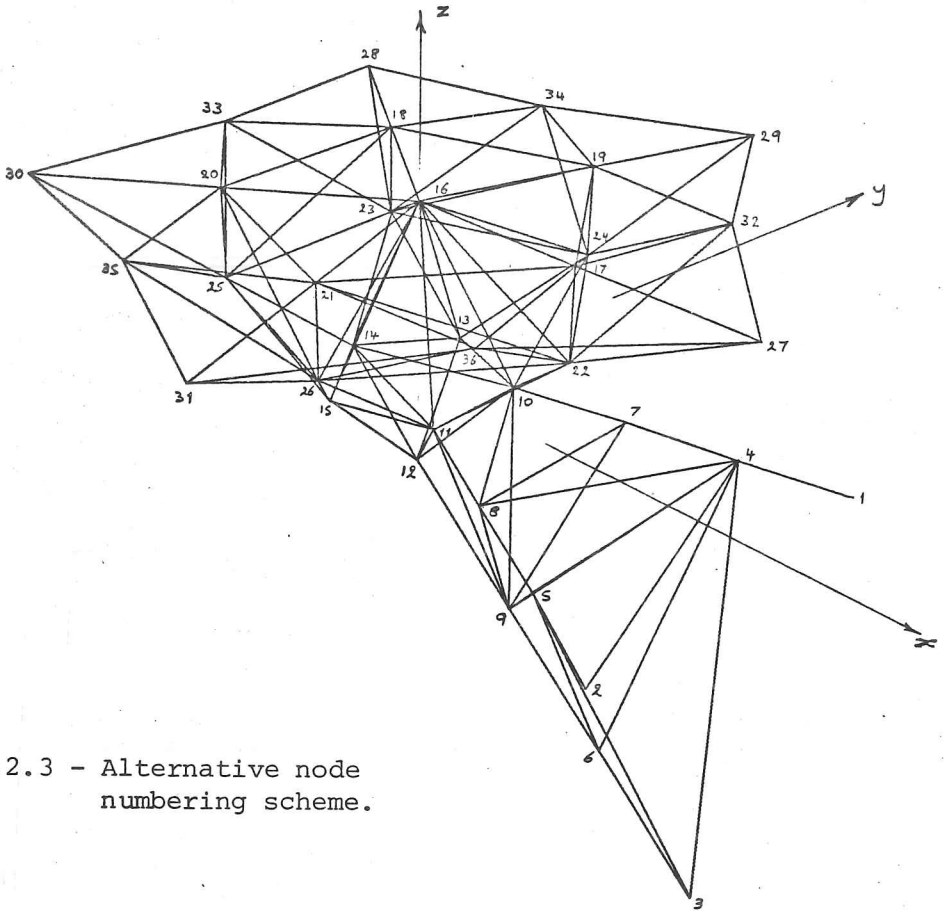

Fig.A4.2.3 - Alternative node numbering scheme.

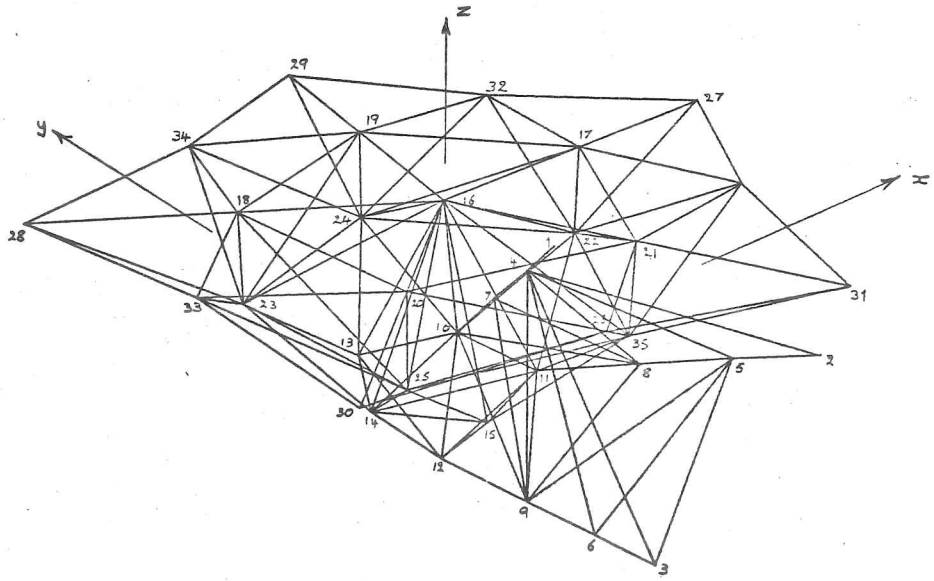

LOADING CASE ONE

NODE	X	Y	Z	NODE
1	0.00000E+01	0.00000E+01	0.00000E+01	1
2	0.00000E+01	0.00000E+01	0.00000E+01	2
3	0.00000E+01	0.00000E+01	0.00000E+01	3
4	1.23967E-04	-2.56251E-04	4.97746E-04	4
5	-3.56534E-04	-2.91101E-04	-6.84215E-04	5
6	1.71757E-04	9.41920E-04	-1.06077E-04	6
7	7.23263E-05	-3.72947E-04	4.82538E-04	7
8	-4.51408E-04	-3.69985E-04	-1.09354E-03	8
9	1.82865E-04	1.27517E-03	-3.91984E-04	9
10	5.28595E-05	-5.35578E-04	5.55600E-04	10
11	-7.99637E-04	-6.28736E-04	-1.76142E-03	11
12	-3.07560E-05	2.13799E-03	-8.90657E-04	12
13	2.08348E-04	4.66861E-05	1.15258E-03	13
14	-4.00771E-04	5.01559E-04	-1.45056E-03	14
15	-1.02805E-03	-1.54895E-05	-3.40764E-03	15
16	-1.44757E-03	-5.00279E-03	-1.01368E-03	16
CYCLIC SEGMENT 1:-				
17	-1.47445E-03	-6.27660E-03	5.94869E-05	17
18	-9.41067E-04	-3.78824E-03	5.99793E-05	18
19	-1.47319E-03	-7.52671E-03	1.12423E-03	19
20	-3.54995E-04	-6.53097E-03	4.60245E-03	20
CYCLIC SEGMENT 2:-				
17	-2.51219E-04	-5.39371E-03	3.90978E-03	17
18	2.77586E-04	-2.97592E-03	3.90787E-03	18
19	9.35866E-04	-5.77865E-03	3.83231E-03	19
20	3.50559E-04	-4.44561E-03	5.46657E-03	20
CYCLIC SEGMENT 3:-				
17	-6.98781E-04	-4.03042E-03	1.03644E-03	17
18	-2.00495E-04	-1.54668E-03	1.03315E-03	18
19	3.72733E-05	-3.02392E-03	3.15446E-03	19
20	-1.40565E-03	-3.17304E-03	-2.48174E-03	20
CYCLIC SEGMENT 4:-				
17	-2.17334E-03	-4.10426E-03	-4.79952E-03	17
18	-1.71747E-03	-1.53468E-03	-4.77646E-03	18
19	-2.97605E-03	-3.03003E-03	-8.65935E-03	19
20	-3.32598E-03	-4.70886E-03	-9.31013E-03	20
CYCLIC SEGMENT 5:-				
17	-2.69710E-03	-5.45735E-03	-5.38220E-03	17
18	-2.06443E-03	-2.99682E-03	-5.34887E-03	18
19	-3.80519E-03	-5.83597E-03	-9.76203E-03	19
20	-2.59302E-03	-6.52591E-03	-3.98263E-03	20

Table A4.2.1 - Cyclically Symmetric Analysis Results for Helipad.

NODE NO.	DISPLACEMENTS X	Y	Z	NODE NO.
4	1.24436E-04	-2.56910E-04	4.99072E-04	4
5	-3.57097E-04	-2.91835E-04	-6.85807E-04	5
6	1.72088E-04	9.44211E-04	-1.06216E-04	6
7	7.29514E-05	-3.74054E-04	4.84043E-04	7
8	-4.52179E-04	-3.71084E-04	-1.09600E-03	8
9	1.83253E-04	1.27824E-03	-3.92569E-04	9
10	5.36528E-05	-5.37042E-04	5.57621E-04	10
11	-8.00894E-04	-6.30476E-04	-1.76519E-03	11
12	-3.05455E-05	2.14317E-03	-8.91892E-04	12
13	2.09355E-04	4.62054E-05	1.15695E-03	13
14	-4.01095E-04	5.02091E-04	-1.45292E-03	14
15	-1.02977E-03	-1.61537E-05	-3.41561E-03	15
16	-1.44988E-03	-5.01685E-03	-1.01531E-03	16
17	-1.47680E-03	-6.29338E-03	5.98847E-05	17
18	-9.42403E-04	-3.79824E-03	6.03783E-05	18
19	-1.47555E-03	-7.54613E-03	1.12667E-03	19
20	-3.55004E-04	-6.54829E-03	4.61510E-03	20
21	-2.50918E-04	-5.40860E-03	3.92166E-03	21
22	2.79190E-04	-2.98421E-03	3.91975E-03	22
23	9.38601E-04	-5.79454E-03	8.85710E-03	23
24	3.52143E-04	-4.45851E-03	5.48341E-03	24
25	-6.99571E-04	-4.04247E-03	1.04094E-03	25
26	-2.00356E-04	-1.55198E-03	1.03764E-03	26
27	3.83160E-05	-3.03588E-03	3.16649E-03	27
28	-1.40794E-03	-3.18320E-03	-2.48637E-03	28
29	-2.17713E-03	-4.11642E-03	-4.81048E-03	29
30	-1.72036E-03	-1.53998E-03	-4.78738E-03	30
31	-2.98178E-03	-3.03998E-03	-8.68106E-03	31
32	-3.33234E-03	-4.72225E-03	-9.33356E-03	32
33	-2.70212E-03	-5.47234E-03	-5.39634E-03	33
34	-2.06831E-03	-3.00512E-03	-5.36296E-03	34
35	-3.81257E-03	-5.85172E-03	-9.78797E-03	35
36	-2.59768E-03	-6.54329E-03	-3.99328E-03	36

Table A4.2.2 - Conventional Finite Element Analysis Results for Helipad (Single Precision).

NODE NO.	DISPLACEMENTS X	Y	Z	NODE NO.
4	1.24438E-04	-2.56914E-04	4.99081E-04	4
5	-3.57102E-04	-2.91839E-04	-6.85818E-04	5
6	1.72088E-04	9.44227E-04	-1.06217E-04	6
7	7.29532E-05	-3.74058E-04	4.84054E-04	7
8	-4.52186E-04	-3.71088E-04	-1.09602E-03	8
9	1.83252E-04	1.27826E-03	-3.92571E-04	9
10	5.36550E-05	-5.37047E-04	5.57634E-04	10
11	-8.00905E-04	-6.30482E-04	-1.76521E-03	11
12	-3.05487E-05	2.14321E-03	-8.91898E-04	12
13	2.09361E-04	4.62053E-05	1.15698E-03	13
14	-4.01101E-04	5.02102E-04	-1.45293E-03	14
15	-1.02978E-03	-1.61517E-05	-3.41565E-03	15
16	-1.44988E-03	-5.01693E-03	-1.01532E-03	16
17	-1.47681E-03	-6.29348E-03	5.98839E-05	17
18	-9.42410E-04	-3.79830E-03	6.03783E-05	18
19	-1.47556E-03	-7.54625E-03	1.12668E-03	19
20	-3.54998E-04	-6.54840E-03	4.61516E-03	20
21	-2.50908E-04	-5.40868E-03	3.92172E-03	21
22	2.79199E-04	-2.98425E-03	3.91981E-03	22
23	9.38628E-04	-5.79442E-03	8.85724E-03	23
24	3.52158E-04	-4.45858E-03	5.48351E-03	24
25	-2.70215E-03	-5.47243E-03	-5.39642E-03	25
26	-2.06833E-03	-3.00516E-03	-5.36304E-03	26
27	-3.81261E-03	-5.85182E-03	-9.78813E-03	27
28	-2.59771E-03	-6.54339E-03	-3.99334E-03	28
29	-6.99569E-04	-4.04252E-03	1.04098E-03	29
30	-2.00331E-04	-1.55201E-03	1.03768E-03	30
31	3.83267E-05	-3.03392E-03	3.16656E-03	31
32	-1.40795E-03	-3.18325E-03	-2.48638E-03	32
33	-2.17715E-03	-4.11648E-03	-4.81053E-03	33
34	-1.72040E-03	-1.54000E-03	-4.78743E-03	34
35	-2.98180E-03	-3.04002E-03	-8.68116E-03	35
36	-3.33238E-03	-4.72232E-03	-9.33368E-03	36

Table A4.2.3 - Re-node numbered Finite Element Analysis for Helipad (Single Precision).

NODE NO.	DISPLACEMENTS X	Y	Z	NODE NO.
4	1.24414E-04	-2.56836E-04	4.98947E-04	4
5	-3.57055E-04	-2.91759E-04	-6.85686E-04	5
6	1.72073E-04	9.44037E-04	-1.06216E-04	6
7	7.29262E-05	-3.73906E-04	4.83866E-04	7
8	-4.52129E-04	-3.70937E-04	-1.09581E-03	8
9	1.83235E-04	1.27801E-03	-3.92554E-04	9
10	5.36148E-05	-5.36803E-04	5.57384E-04	10
11	-8.00761E-04	-6.30205E-04	-1.76490E-03	11
12	-3.05440E-05	2.14284E-03	-8.91831E-04	12
13	2.09298E-04	4.63703E-05	1.15651E-03	13
14	-4.01047E-04	5.02182E-04	-1.45279E-03	14
15	-1.02960E-03	-1.59741E-05	-3.41498E-03	15
16	-1.44969E-03	-5.01553E-03	-1.01524E-03	16
17	-1.47662E-03	-6.29183E-03	5.98324E-05	17
18	-9.42278E-04	-3.79726E-03	6.03264E-05	18
19	-1.47536E-03	-7.54436E-03	1.12649E-03	19
20	-3.55011E-04	-6.54669E-03	4.61400E-03	20
21	-2.50941E-04	-5.40721E-03	3.92062E-03	21
22	2.79095E-04	-2.98337E-03	3.91871E-03	22
23	9.38368E-04	-5.79286E-03	8.85493E-03	23
24	3.52011E-04	-4.45728E-03	5.48193E-03	24
25	-6.99510E-04	-4.04131E-03	1.04046E-03	25
26	-2.00343E-04	-1.55139E-03	1.03716E-03	26
27	3.82442E-05	-3.03290E-03	3.16544E-03	27
28	-1.40774E-03	-3.18219E-03	-2.48609E-03	28
29	-2.17681E-03	-4.11526E-03	-4.80964E-03	29
30	-1.72013E-03	-1.53938E-03	-4.78654E-03	30
31	-2.96131E-03	-3.03899E-03	-8.67943E-03	31
32	-3.33183E-03	-4.72101E-03	-9.33183E-03	32
33	-2.70172E-03	-5.47094E-03	-5.39525E-03	33
34	-2.06797E-03	-3.00428E-03	-5.36186E-03	34
35	-3.81195E-03	-5.85025E-03	-9.78585E-03	35
36	-2.59730E-03	-6.54168E-03	-3.99235E-03	36

Table A4.2.4 - Double Precision Conventional Finite Element Analysis Results for Helipad.

NODE NO.	DISPLACEMENTS X	Y	Z	NODE NO.
4	1.24414E-04	-2.56836E-04	4.98947E-04	4
5	-3.57055E-04	-2.91759E-04	-6.85686E-04	5
6	1.72073E-04	9.44037E-04	-1.06216E-04	6
7	7.29262E-05	-3.73906E-04	4.83866E-04	7
8	-4.52129E-04	-3.70937E-04	-1.09561E-03	8
9	1.83235E-04	1.27801E-03	-3.92554E-04	9
10	5.36148E-05	-5.36803E-04	5.57384E-04	10
11	-8.00761E-04	-6.30205E-04	-1.76490E-03	11
12	-3.05440E-05	2.14284E-03	-8.91831E-04	12
13	2.09298E-04	4.63703E-05	1.15651E-03	13
14	-4.01047E-04	5.02183E-04	-1.45279E-03	14
15	-1.02960E-03	-1.59741E-05	-3.41498E-03	15
16	-1.44969E-03	-5.01553E-03	-1.01524E-03	16
17	-1.47662E-03	-6.29183E-03	5.98325E-05	17
18	-9.42278E-04	-3.79726E-03	6.03265E-05	18
19	-1.47536E-03	-7.54437E-03	1.12650E-03	19
20	-3.55012E-04	-6.54669E-03	4.61401E-03	20
21	-2.50942E-04	-5.40721E-03	3.92062E-03	21
22	2.79095E-04	-2.98337E-03	3.91871E-03	22
23	9.38368E-04	-5.79286E-03	8.85493E-03	23
24	3.52011E-04	-4.45728E-03	5.48193E-03	24
25	-2.70172E-03	-5.47094E-03	-5.39525E-03	25
26	-2.06797E-03	-3.00428E-03	-5.36187E-03	26
27	-3.81195E-03	-5.85026E-03	-9.78586E-03	27
28	-2.59730E-03	-6.54169E-03	-3.99235E-03	28
29	-6.99511E-04	-4.04131E-03	1.04046E-03	29
30	-2.00343E-04	-1.55139E-03	1.03716E-03	30
31	3.82440E-05	-3.03290E-03	3.16544E-03	31
32	-1.40774E-03	-3.18219E-03	-2.48609E-03	32
33	-2.17681E-03	-4.11526E-03	-4.80965E-03	33
34	-1.72013E-03	-1.53938E-03	-4.78655E-03	34
35	-2.98131E-03	-3.03899E-03	-8.67943E-03	35
36	-3.33183E-03	-4.72102E-03	-9.33183E-03	36

Table A4.2.5 - Double Precision Re-node numbered Finite Element Analysis Results for Helipad.

```
HELLY-PAD ANALYSIS  -  3.7.80.
5 16 3 4 2 41 4 6 6 0
16.0 8.0 -2.0
16.0 -8.0 -2.0
16.0 0.0 -18.0
11.9 6.1 -1.3
11.9 -6.1 -1.3
10.8 0.0 -13.4
7.6 4.3 -0.6
7.6 -4.3 -0.6
5.6 0.0 -8.9
3.236 2.351 0.0
3.236 -2.351 0.0
0.0 0.0 -4.0
-1.236 3.804 0.0
-4.0 0.0 0.0
-1.236 -3.804 0.0
0.0 0.0 8.0
8.0 0.0 8.0
8.0 0.0 4.0
16.0 0.0 8.0
9.708 7.053 8.0
7 0.0 0.0 0.0
2.1E+11 0.0 0.4093 0.0205
2.1E+11 0.0 0.3661 0.0183
2.1E+11 0.0 0.3473 0.0174
2.1E+11 0.0 0.3171 0.0159
2.1E+11 0.0 0.2836 0.0142
2.1E+11 0.0 0.2589 0.0129
2.1E+11 0.0 0.0 0.0
3 6 1
6 9 1
9 12 1
1 4 2
4 7 2
7 10 2
2 5 2
5 8 2
8 11 2
2 4 3
4 5 3
3 4 3
3 5 3
4 6 3
5 6 3
4 9 3
5 9 3
7 8 3
7 9 3
8 9 3
9 10 3
9 11 3
10 11 3
10 12 3
11 12 3
4 8 3
8 10 3
10 13 4
11 15 4
13 14 4
14 15 4
12 13 4
12 14 4
12 15 4
10 14 4
11 14 4
10 16 4
13 16 4
14 16 4
15 16 4
11 16 4
17 18 5
17 19 5
18 19 5
17 20 5
18 20 5
19 20 6
10 18 4
13 14 15 11
11 18 4
10 13 14 15
16 17 5
16 16 16 16
16 18 5
16 16 16 16
20 23 6
20 21 5
20 22 5
17 21 5
18 22 5
17 22 5
1 0 5 0
16 0.0 0.0 -10000.0
4 17 0.0 0.0 -15000.0
4 19 0.0 0.0 -5000.0
4 20 0.0 0.0 -50000.0
5 17 0.0 0.0 -15000.0
5 19 0.0 0.0 -5000.0
0
3 0
1 1 1 1
2 1 1 1
3 1 1 1
```

Table A4.2.6 - Helipad Data for Cyclically Symmetric Analysis Program.

```
3 33 6 0 121
16.0 8.0 -2.0
16.0 -8.0 -2.0
16.0 0.0 -18.0
11.9 6.1 -1.3
11.9 -6.1 -1.3
10.8 0.0 -13.4
7.6 4.3 -0.6
7.6 -4.3 -0.6
5.6 0.0 -8.9
3.236 2.351 0.0
3.236 -2.351 0.0
0.0 0.0 -4.0
-1.236 3.804 0.0
-4.0 0.0 0.0
-1.236 -3.804 0.0
0.0 0.0 8.0
8.0 0.0 8.0
8.0 0.0 4.0
16.0 0.0 8.0
9.708 7.053 8.0
2.472 7.609 8.0
2.472 7.609 4.0
4.944 15.217 8.0
-3.708 11.413 8.0
-6.472 4.702 8.0
-6.472 4.702 4.0
-12.944 9.406 8.0
-12.0 0.0 8.0
-6.472 -4.702 8.0
-6.472 -4.702 4.0
-12.944 -9.406 8.0
-3.708 -11.413 8.0
2.472 -7.609 8.0
2.472 -7.609 4.0
4.944 -15.217 8.0
9.708 -7.053 8.0
2.1E+11
3 6 0.025
6 9 0.025
9 12 0.025
1 4 0.02
4 7 0.02
7 10 0.02
2 5 0.02
5 8 0.02
8 11 0.02
2 4 0.018
4 5 0.018
3 4 0.018
3 5 0.018
4 6 0.018
5 6 0.018
4 9 0.018
5 9 0.018
7 8 0.018
7 9 0.018
8 9 0.018
9 10 0.018
9 11 0.018
10 11 0.018
10 12 0.018
11 12 0.018
4 8 0.018
8 10 0.018
10 13 0.015
11 15 0.015
13 14 0.015
14 15 0.015
12 13 0.015
12 14 0.015
12 15 0.015
10 14 0.015
11 14 0.015
10 16 0.015
13 16 0.015
14 16 0.015
15 16 0.015
11 16 0.015
10 18 0.015
11 18 0.015
10 22 0.015
13 22 0.015
13 26 0.015
14 26 0.015
14 30 0.015
15 30 0.015
15 34 0.015
11 34 0.015
16 17 0.012
16 18 0.012
17 18 0.012
16 21 0.012
16 22 0.012
21 22 0.012
16 25 0.012
16 26 0.012
25 26 0.012
16 29 0.012
16 30 0.012
29 30 0.012
16 33 0.012
16 34 0.012
33 34 0.012
17 21 0.012
17 33 0.012
21 25 0.012
25 29 0.012
29 33 0.012
18 22 0.012
18 34 0.012
22 26 0.012
26 30 0.012
30 34 0.012
17 22 0.012
18 33 0.012
21 26 0.012
25 30 0.012
29 34 0.012
17 19 0.012
18 19 0.012
21 23 0.012
22 23 0.012
25 27 0.012
26 27 0.012
29 31 0.012
30 31 0.012
33 35 0.012
34 35 0.012
17 20 0.012
18 20 0.012
17 36 0.012
18 36 0.012
20 21 0.012
20 22 0.012
21 24 0.012
22 24 0.012
24 25 0.012
24 26 0.012
25 28 0.012
26 28 0.012
28 29 0.012
28 30 0.012
29 32 0.012
30 32 0.012
32 33 0.012
32 34 0.012
33 36 0.012
34 36 0.012
19 20 0.01
20 23 0.01
23 24 0.01
24 27 0.01
27 28 0.01
28 31 0.01
31 32 0.01
32 35 0.01
35 36 0.01
19 36 0.01
16 0.0 0.0 -10000.0
29 0.0 0.0 -15000.0
31 0.0 0.0 -5000.0
32 0.0 0.0 -50000.0
33 0.0 0.0 -15000.0
35 0.0 0.0 -5000.0
```

Table A4.2.7 - Helipad Data for Conventional Finite Element Analysis Program.

Appendix 4.3 - Recommendations and Suggestions for the Improvement of the Cyclic Symmetry Analysis Program

I. The node numbering for the central region and cyclic segment structure should be independent, so that changes to the number of nodes in the central region does not necessitate the renumbering of the cyclic segment nodes - and thus element data. In effect, this means starting at one for the nodes of both regions, rather than numbering the central region nodes and then continuing onto the cyclic segment nodes.

II. It should be possible for the cyclic segment structure to be reanalysed - having made some modifications to its geometry - without having to include the unchanged central region in the reanalysis.

III. The number of transformed load-stiffness-displacement systems calculated and solved should be controllable via a data input parameter, so that unnecessary transformation calculations are not carried out.

IV. Rather than storing in binary files intermediate results which are used again, they could be recalculated, thus saving on storage space and the read/write time.

V. Efficient computational methods should be used throughout the program, which take advantage of symmetry and sparseness to again reduce the store requirement and calculation time.

VI. The calculation of forces and stresses should be included along with relevant stability checks on slender members.

VII. A selection of structural elements should be included to improve the structural modelling capability of the program.

Appendix 5.1 - Allowable focal length variation of a Homologically Deforming Parabolic Antenna

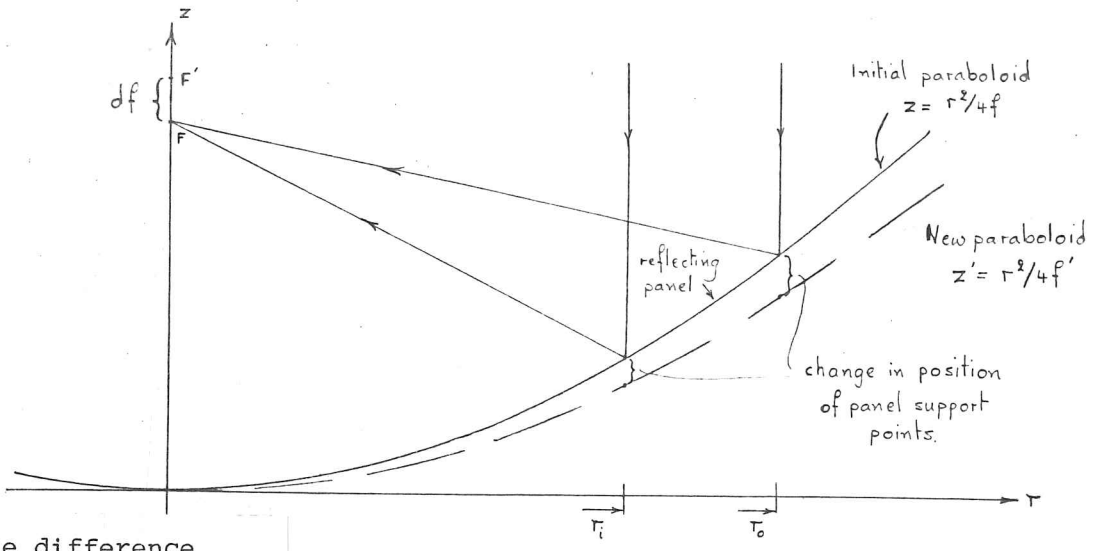

The difference between the actual panel shape and the correct panel shape will produce a surface error and this therefore must be below that specified by the observed wave length for sufficiently good operation.

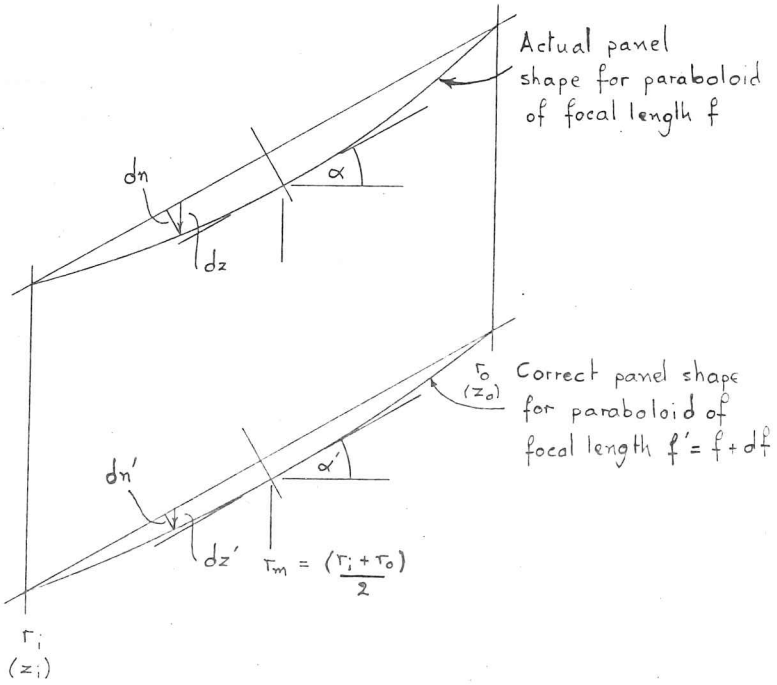

$$dn = dz \cos \alpha \quad , \text{ where } \tan \alpha = r_m/2f .$$

$$\text{Similarly } dn' = dz' \cos \alpha' \quad , \text{ where } \tan \alpha' = r_m/2f'.$$

This difference is defined as:

$$\Delta n = dn - dn' , \qquad \text{(A5.1.1)}$$

(see figures), where

$$dn = dz \cos\alpha$$

and $$dn' = dz' \cos\alpha' .$$

Now

$$dz = (z_i + (r-r_i)\tan\alpha) - z(r) ,$$

and $$dz' = (z_i' + (r-r_i)\tan\alpha') - z'(r) . \qquad \text{(A5.1.2)}$$

Thus equation (A5.1.1) becomes:

$$\Delta n = \{(z_i+(r-r_i)\tan\alpha)-z(r)\}\cos\alpha - \{(z_i'+(r-r_i)\tan\alpha')-z'(r)\}\cos\alpha' , \qquad \text{(A5.1.3)}$$

where

$$\tan\alpha = \frac{(r_i+r_o)}{4f}, \quad \cos\alpha = \frac{2f}{\sqrt{4f^2+r_m^2}}, \quad \tan\alpha' = \frac{(r_i+r_o)}{4(f+df)}$$

and $$\cos\alpha' = \frac{2(f+df)}{\sqrt{4(f+df)^2+r_m^2}} .$$

For small values of (df/f), $\cos\alpha' \approx \cos\alpha$ and $(1-1/(1+df/f)) \approx df/f$, which on substituting into equation (A5.1.3) and rearranging gives:

$$\Delta n = \left(\frac{df}{f}\right) \frac{\cos\alpha}{4f} \{r(r_i+r_o) - r_i r_o - r^2\} \qquad \text{(A5.1.4)}$$

The largest value of Δn will occur in the central panel ring where the curvature of the paraboloid surface is greatest. Thus for a 15 m diameter dish, of focal length 5.4 m, having five rings of panels whose innermost ring is defined by: $r_i = 0.5$ m and $r_o = 2.3$ m. Δn is given by:

$$\Delta n = \left(\frac{df}{f}\right) \frac{\{2.8r - 1.115 - r^2\}}{21.78} ,$$

which on substituting $r = 1.4$ m - the centre of the panel ring - gives:

$$\Delta n = 0.0372 \left(\frac{df}{f}\right)$$

as the largest value which occurs.

Now for reasonably efficient observations (i.e. $\eta_s = 0.5$ in

equation (5.4.3)) $\Delta n_{max} \leq \lambda/16$. Thus for an operating wavelength of 0.35 mm :

$$\Delta n_{max} \leq \frac{0.35\times10^{-3}}{16}$$

or $$0.0372 \left(\frac{df}{f}\right) \leq \frac{0.35\times10^{-3}}{16}$$

$$\therefore \quad \left(\frac{df}{f}\right) \leq 5.88\times10^{-4}$$

or $$df \leq 3.18 \text{ mm} \quad \text{(for } f = 5.4 \text{ m)}$$

This value of df is calculated on the assumption that there are no other surface errors present, which of course there are. This implies that a smaller limit should be placed on df . However, another assumption made, was that the focal length was correct for the horizon pointing case, so that df is the result of the difference between the horizon and zenith pointing homology paraboloid focal lengths. In practice, the actual reflecting surface could be made to have a focal length between the two, thus reducing df (by a half if the mean value of f and f' is used). The calculated limit for df is therefore of the right order in practice.

For the 15 m diameter three panel ring dish design considered in chapter six, where $r_i = 0.5$ m , $r_o = 3.525$ m and $f = 5.4$ m ,

$$\Delta n_{max} = \left(\frac{df}{f}\right) \frac{\{4.025\times2.0125 - 1.7625 - (2.0125)^2\}}{21.972}$$

$$\therefore \quad \Delta n_{max} = 0.104 \left(\frac{df}{f}\right) .$$

Thus for a minimum observable wavelength of 0.4 mm :

$$\left(\frac{df}{f}\right) \leq \frac{0.4\times10^{-3}}{16\times0.104} \text{ m}$$

$$\therefore \quad df \leq 1.3 \text{ mm} .$$

Appendix 5.2 - Best Fit Paraboloid and r.m.s. Deviation

5.2.1 - Signal path length change minimization

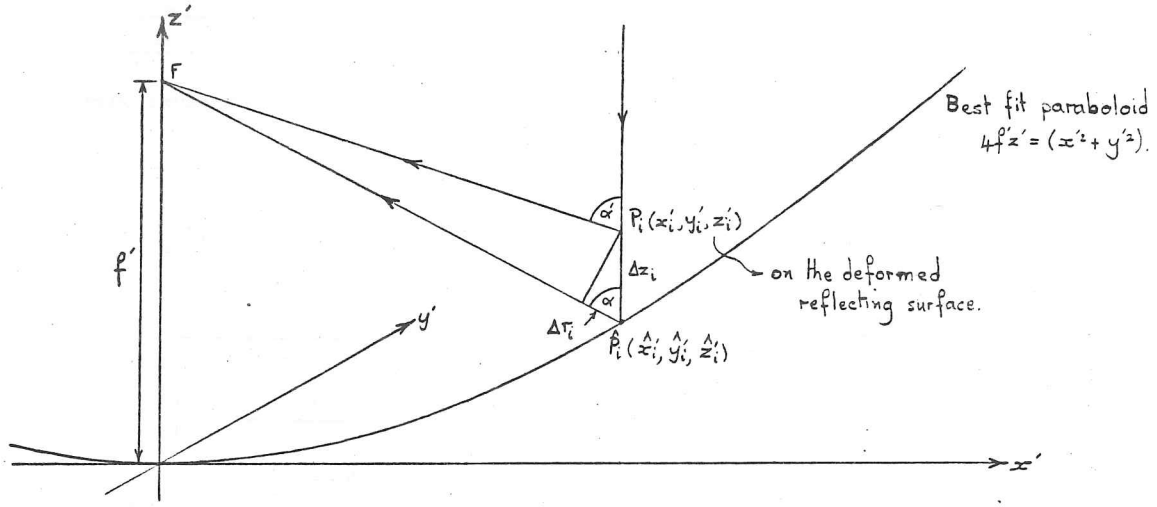

Fig.A5.2.1 - The change in path length of a signal reflected at P_i and $\hat{P}_i$.

The best fit paraboloid is defined as the one which minimizes the sum of the signal path length changes squared.

Let P_i be a point on the deformed reflecting surface and let $\hat{P}_i$ be a point, in the same signal path, but on the best fit paraboloid $4f'z' = (x'^2+y'^2)$. If $\Delta r = F\hat{P}_i - FP_i$, then the change in path length Δp of a signal reflected at point $\hat{P}_i$ rather than at point P_i is given by:

$$\Delta p_i = \Delta z_i + \Delta r_i \qquad \text{(A5.2.1)}$$

Now for small values of Δz (compared to r_i);

$$\Delta r_i = \Delta z_i \cos \alpha ,$$

or $$\Delta r_i = \Delta z_i \sin(\pi/2 - \alpha) ,$$

and from figure A5.2.1 $\sin(\pi/2 - \alpha) = \left(\frac{f' - \hat{z}_i}{r_i}\right)$,

thus $$\Delta r_i = \left(\frac{f' - \hat{z}_i}{r_i}\right) \Delta z_i , \qquad \text{(A5.2.2)}$$

which on substituting into equation (A5.2.1) gives:

$$\Delta p_i = \Delta z_i + \left(\frac{f'-\hat{z}_i}{r_i}\right)\Delta z_i \quad . \qquad \text{(A5.2.3)}$$

On rearranging this equation we get:

$$\Delta p_i = \left(\frac{f'+r_i-\hat{z}_i}{r_i}\right)\Delta z_i \quad . \qquad \text{(A5.2.4)}$$

Now because of the path length of any reflected signal is the same we can say that:

$$2f' = f' + r_i - \hat{z}_i \quad , \qquad \text{(A5.2.5)}$$

which on substituting into equation (A5.2.4) gives:

$$\Delta p_i = \frac{2f'}{r_i}\Delta z_i$$

$$\text{or} \qquad \Delta p_i = \frac{2f'\Delta z_i}{(f'+z_i)} \quad , \qquad \text{(A5.2.6)}$$

since $r_i = f' + \hat{z}_i$, from equation (A5.2.5).

Since in practice $f' - f$ (where f is the initial focal length) must be small, f' may be replaced by f in equation (A5.2.6). Similarly, $\hat{z}_i$ may be replaced by z_i (the initial z value). Equation (A5.2.6) therefore becomes:

$$\Delta p_i = 2\left(\frac{1}{1+(x_i^2+y_i^2)/4f^2}\right)\Delta z_i \qquad \text{(A5.2.7)}$$

The best fit paraboloid is then found by minimizing $\sum_{i=1}^{n} (\Delta p_i)^2$.

The axes of the best fit paraboloid, (x',y',z') , are assumed to have a translational and rotational displacement from the initial (undeformed) paraboloid axes (x,y,z) , see figure A5.2.2. These consist of an origin shift in the x and z directions, and a rotation of ϕ about the y axis in the x-z axes plane.

The coordinate transformation from the (x,y,z) axes to the (x',y',z') axes is then given by:

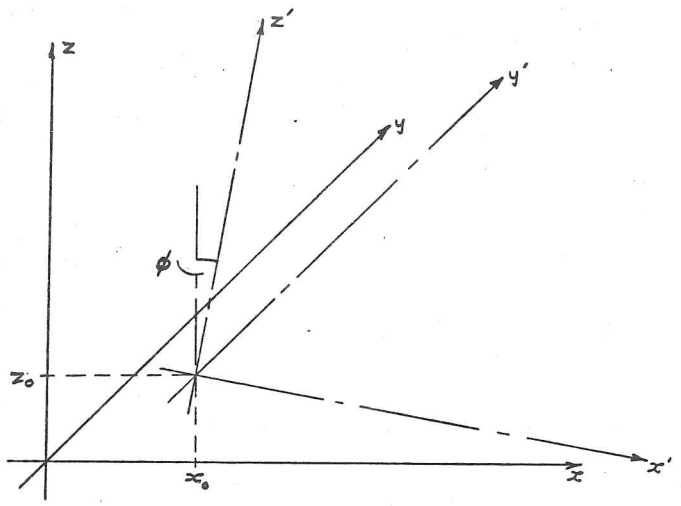

Fig.A5.2.2 - Best fit paraboloid axes in relation to the initial axes.

$$x' = (x-x_o)\cos\phi - (z-z_o)\sin\phi ,$$
$$y' = y , \qquad \text{(A5.2.8)}$$
$$z' = (x-x_o)\sin\phi + (z-z_o)\cos\phi ,$$

which for small values of x_o , z_o and ϕ may be simplified to:

$$x' = (x-x_o) - z\phi ,$$
$$y' = y , \qquad \text{(A5.2.9)}$$
$$z' = x\phi + (z-z_o)$$

by ignoring second order terms in x_o , z_o and ϕ .

The distance, Δz , between a point on the deformed surface and a point on the best fit paraboloid, in the same signal path is given by:

$$\Delta z_i = \hat{z}'(x_i',y_i') - z_i' , \qquad \text{(A5.2.10)}$$

(see figure A5.2.1), where $\hat{z}_i'(x_i',y_i')$ is the value computed from the equation for the best fit paraboloid, $4f'z' = (x'^2+y'^2)$, and z_i' is the actual z-coordinate of the point P_i' on the deformed surface relative to the (x',y',z') axes. Thus the square of the path length change of a signal reflected at point P_i is given by:

$$(\Delta p_i)^2 = \left(\frac{2}{1+(x_i^2+y_i^2)/4f^2}\right)^2 \{z'(x_i',y_i') - z_i'\}^2$$

or
$$(\Delta p_i)^2 = \left(\frac{2}{1+(x_i^2+y_i^2)/4f^2}\right)^2 \left\{\frac{(x_i'^2+y_i'^2)}{4f'} - z_i'\right\}^2 . \qquad \text{(A5.2.11)}$$

Applying the co-ordinate transformation defined by equation (A5.2.9), equation (A5.2.11), in terms of the original (x,y,z) axes, becomes:

$$(\Delta p_i)^2 = \left(\frac{2}{1+(x_i^2+y_i^2)/4f^2}\right)^2 \left\{\frac{[(x_i-x_o-z_i\phi)^2+y_i^2]}{4f'} - [x_i\phi+z_i-z_o]\right\}^2 , \qquad \text{(A5.2.12)}$$

which, by ignoring second order terms in x_o, z_o and ϕ may be simplified to:

$$(\Delta p_i)^2 = \left(\frac{2}{1+(x_i^2+y_i^2)/4f^2}\right)^2 \left\{\frac{(x_i^2+y_i^2)}{4f'} - \left(\frac{x_o}{2f'}+\phi\right)x_i - \frac{x_i z_i \phi}{2f'} - z_i + z_o\right\}^2 . \qquad \text{(A5.2.13)}$$

By dividing x_i, y_i, z_i, x_o and z_o by f, equation (5.2.13) can be converted to the non-dimensional form:

$$(\Delta p_i)^2 = \left(\frac{8}{4+(\bar{x}_i^2+\bar{y}_i^2)}\right)^2 \left\{\frac{(\bar{x}_i^2+\bar{y}_i^2)}{4f'} f^2 - \left(\frac{\bar{x}_o f}{2f'}+\phi\right)\bar{x}_i f - \frac{\bar{x}_i \bar{z}_i \phi f}{2f'} - \bar{z}_i f + \bar{z}_o f\right\}^2 , \qquad \text{(A5.2.14)}$$

where $\bar{x}_i = x_i/f$, $\bar{y}_i = y_i/f$, $\bar{z}_i = z_i/f$, $\bar{x}_o = x_o/f$ and $\bar{z}_o = z_o/f$.

The best fit parabola will now be developed for the two cases of zenith and horizon pointing.

Zenith Pointing - The deformation of a zenith pointing dish is assumed to be such that only change in focal length and a vertical shift of the initial paraboloid origin takes place. Thus, x_o and ϕ are assumed to be zero. Equation (A5.2.14) can therefore be simplified to:

$$(\Delta p_i)_z^2 = \left(\frac{8}{4+(\bar{x}_i^2+\bar{y}_i^2)}\right)^2 \left\{\frac{(\bar{x}_i^2+\bar{y}_i^2)}{4f'} f^2 - \bar{z}_i f + \bar{z}_o f\right\}^2 . \qquad \text{(A5.2.15)}$$

By putting $\alpha_z = \frac{f}{4f'}$, $\beta_z = \bar{z}_o$ and $\omega_i = \left(\frac{8}{4+(\bar{x}_i^2+\bar{y}_i^2)}\right)$ equation (A.5.2.15) may be rewritten as:

$$(\Delta p_i)_z^2 = \omega_i^2 f^2 (\alpha_z(\bar{x}_i^2+\bar{y}_i^2) - \bar{z}_i + \beta_z)^2 . \qquad \text{(A5.2.16)}$$

The function to be minimized is therefore given by:

$$\sum_{i=1}^{n} (\Delta p_i)_z^2 = f^2 \sum_{i=1}^{n} \omega_i^2 (\alpha_z(\bar{x}_i^2+\bar{y}_i^2) - \bar{z}_i + \beta_z)^2 , \qquad \text{(A5.2.17)}$$

where n is the number of surface panel support points in the structure. Applying the calculus method of minimization, the function will be a minimum when the following conditions are satisfied:

$$\frac{\partial \Sigma}{\partial \alpha_z} (\Delta p_i)_z^2 = f^2 \sum_{i=1}^{n} 2\omega_i^2 (\alpha_z(\bar{x}_i^2+\bar{y}_i^2) - \bar{z}_i + \beta_z)(\bar{x}_i^2+\bar{y}_i^2) = 0 ,$$

$$\text{and} \quad \frac{\partial \Sigma}{\partial \beta_z} (\Delta p_i)_z^2 = -f^2 \sum_{i=1}^{n} 2\omega_i^2 (\alpha_z(\bar{x}_i^2+\bar{y}_i^2) - \bar{z}_i + \beta_z) = 0 , \qquad \text{(A5.2.18)}$$

which on rearranging becomes:

$$\alpha_z \sum \omega_i^2 (\bar{x}_i^2+\bar{y}_i^2)^2 + \beta_z \sum \omega_i^2 (\bar{x}_i^2+\bar{y}_i^2) = \sum \omega_i^2 \bar{z}_i (\bar{x}_i^2+\bar{y}_i^2) ,$$

$$\alpha_z \sum \omega_i^2 (\bar{x}_i^2+\bar{y}_i^2) + \beta_z \sum \omega_i^2 = \sum \omega_i^2 \bar{z}_i . \qquad \text{(A5.2.19)}$$

On solving for α_z and β_z, f' and z_o may be found from:

$$f' = \frac{f}{4\alpha_z} \quad \text{and} \quad z_o = f\beta_z . \qquad \text{(A5.2.20)}$$

Horizon Pointing - The deformation of a horizon pointing dish is assumed to be such that only an angular displacement of the paraboloid axis and a translational displacement of the origin (along the x-axis) occurs. Thus it is assumed that z_o is zero and that $f' = f$. Equation (A5.2.14) can therefore be simplified to:

$$(\Delta p_i)_H^2 = \left(\frac{8}{4+(\bar{x}_i^2+\bar{y}_i^2)}\right)^2 \left\{\frac{(\bar{x}_i^2+\bar{y}_i^2)}{4} f - \left(\frac{\bar{x}_o}{2}+\phi\right)\bar{x}_i f - \frac{\bar{x}_i \bar{z}_i \phi f}{2} - \bar{z}_i f\right\}^2 . \qquad \text{(A5.2.21)}$$

Again, by putting $\alpha_H = -\left(\frac{\bar{x}_o}{2}+\phi\right)$, $\beta_H = \frac{-\phi}{2}$ and $\omega_i = \left(\frac{8}{4+(\bar{x}_i^2+\bar{y}_i^2)}\right)$ equation (A5.2.21) may be rewritten as:

$$(\Delta p_i)_H^2 = \omega_i^2 f^2 \{\alpha_H \bar{x}_i + \beta_H \bar{x}_i \bar{z}_i + \frac{1}{4}(\bar{x}_i^2+\bar{y}_i^2) - \bar{z}_i\}^2 . \qquad \text{(A5.2.22)}$$

The function to be minimized is therefore given by:

$$\sum_{i=1}^{n} (\Delta p_i)_H^2 = f^2 \sum_{i=1}^{n} \omega_i^2 (\alpha_H \bar{x}_i + \beta_H \bar{x}_i \bar{z}_i + \frac{1}{4}(\bar{x}_i^2 + \bar{y}_i^2) - \bar{z}_i)^2 \quad . \qquad \text{(A5.2.23)}$$

Applying the calculus method of minimization, the above function will be a minimum if the following conditions are satisfied:

$$\frac{\partial \Sigma}{\partial \alpha_H} (\Delta p_i)_H^2 = f^2 \sum_{i=1}^{n} 2\omega_i^2 (\alpha_H \bar{x}_i + \beta_H \bar{x}_i \bar{z}_i + \frac{1}{4}(\bar{x}_i^2 + \bar{y}_i^2) - \bar{z}_i) \bar{x}_i \bar{z}_i = 0 \quad , \qquad \text{(A5.2.24)}$$

and $$\frac{\partial \Sigma}{\partial \beta_H} (\Delta p_i)_H^2 = f^2 \sum_{i=1}^{n} 2\omega_i^2 (\alpha_H \bar{x}_i + \beta_H \bar{x}_i \bar{z}_i + \frac{1}{4}(\bar{x}_i^2 + \bar{y}_i^2) - \bar{z}_i) \bar{x}_i \bar{z}_i = 0 \quad .$$

which on rearranging become:

$$\alpha_H \sum \omega_i^2 \bar{x}_i^2 + \beta_H \sum \omega_i^2 \bar{x}_i^2 \bar{z}_i = -\frac{1}{4} \sum \omega_i^2 (\bar{x}_i^2 + \bar{y}_i^2) \bar{x}_i + \sum \omega_i^2 \bar{x}_i \bar{z}_i \quad , \qquad \text{(A5.2.25)}$$

$$\alpha_H \sum \omega_i^2 \bar{x}_i^2 \bar{z}_i + \beta_H \sum \omega_i^2 \bar{x}_i^2 \bar{z}_i^2 = -\frac{1}{4} \sum \omega_i^2 (\bar{x}_i^2 + \bar{y}_i^2) \bar{x}_i \bar{z}_i + \sum \omega_i^2 \bar{x}_i \bar{z}_i^2 \quad .$$

On solving for α_H and β_H, ϕ and x_o may be found from:

$$\phi = -2\beta_H \qquad \text{and} \qquad x_o = -2f(\alpha_H + \phi) \quad . \qquad \text{(A5.2.26)}$$

The best fit parabolas for the zenith and horizon pointing cases are thus given by:

$$4f'z = x^2 + y^2 + 4f'z_o \qquad \text{(A5.2.27)}$$

and $$4fz = x^2 + y^2 - 2x_o x - 2\phi xz \quad ,$$

respectively.

5.2.2 - r.m.s. deviation

The r.m.s. deviation of the deformed surface from the best fit paraboloid is defined as the average of $(\Delta p_i)^2$ over all the surface support points, and is thus given by:

$$\sigma^2_{r.m.s.} = \frac{\sum_{i=1}^{n} \omega_i^2 \Delta z_i^2}{n} \quad , \qquad \text{(A5.2.28)}$$

where $\omega_i = \left(\frac{8}{4+(\bar{x}_i^2+\bar{y}_i^2)}\right)$,

$\Delta z_i = f(\alpha_z(\bar{x}_i^2+\bar{y}_i^2) - \bar{z}_i + \beta_z)$ for the zenith pointing case,

$\Delta z_i = f(\alpha_H \bar{x}_i + \beta_H \bar{x}_i \bar{z}_i + \frac{1}{4}(\bar{x}_i^2+\bar{y}_i^2) - \bar{z}_i)$ for the horizon pointing case,

and n is the number of surface support points.

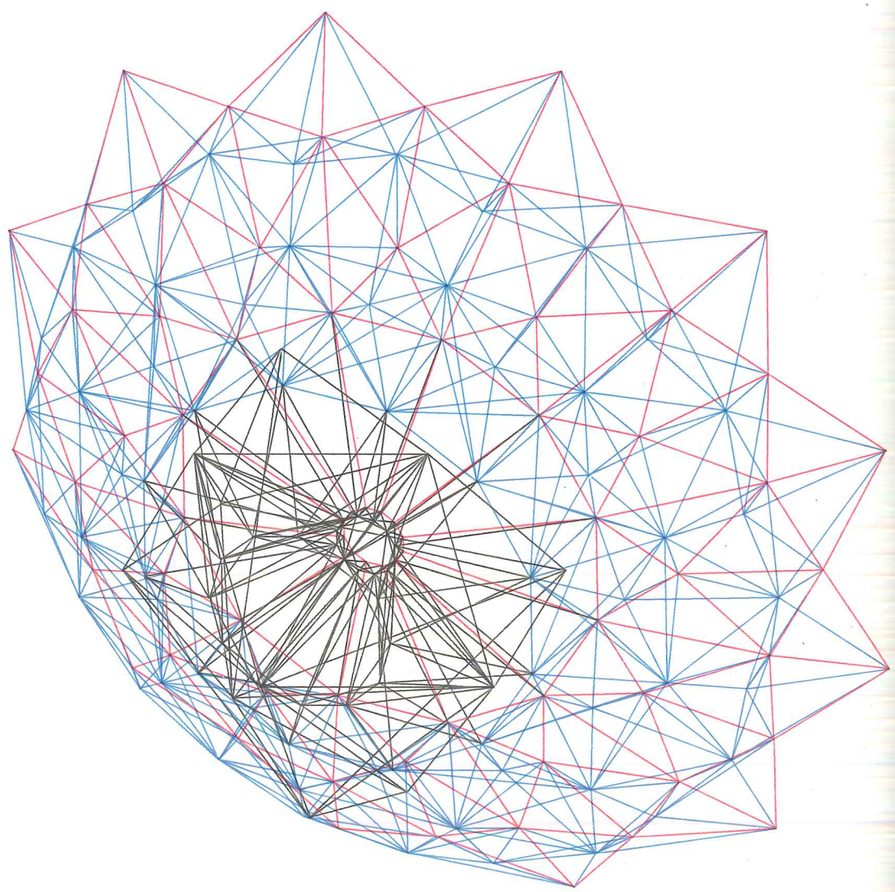

Fig.A6.1.1 - A cyclically symmetric surface supporting dish structure mounted on a four point off-axis system via a central barrel.

Appendix 6.1 - The Initial Telescope Structure Design

One of the main reasons for specifying a cassegrain type of arrangement for the telescope (which is also the case for the British 15 m millimetre wave telescope) is so that the electronic receiving and amplification equipment can be placed at the centre of the structure - where it is more easily supported and more easily accessible. In order to do this a hole has to be made in the centre of the primary reflecting dish and also a 'clear' space behind it to accommodate the electronics. This rules out a structure design which is supported at two points on the paraboloid axis - like the Bonn dish. To get over this problem a system of four off-axis points is used to support a central 'barrel' to which the cyclically symmetric dish structure is connected - see figure A6.1.1. The four point barrel supports are themselves held by the elevation circle structure and axis arms - see figure A6.1.2a and b.

Another advantage of using this central barrel support system is, that by making the diameter of the barrel larger at the bottom than at the top, the congestion, which otherwise tends to occur with large numbers of radial ribs connected on the axis, is greatly reduced.

The cyclically symmetric dish structure consists of twelve radial ribs with twelve half ribs between them in the outer two panel rings. Each primary rib is connected to the central barrel and to its immediate neighbours - see figure A6.1.2a and b.

The geometry of the cyclically symmetric dish structure is largely governed by the positions of the reflecting panel support points. Each of the sixty panels supported in this case are mounted at three points on their perimeter. These are arranged so that there are six support points per cyclic segment - see figure A6.1.3.

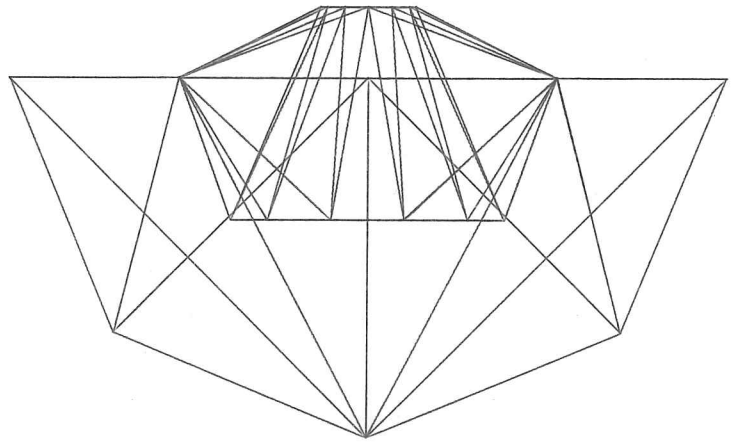

Fig.A6.1.2a - Central barrel and elevation mounting structure.

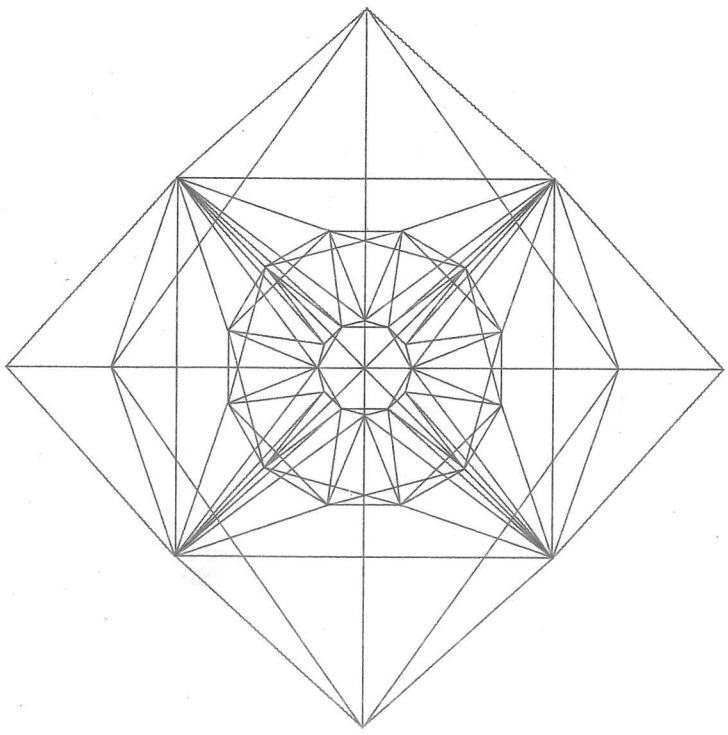

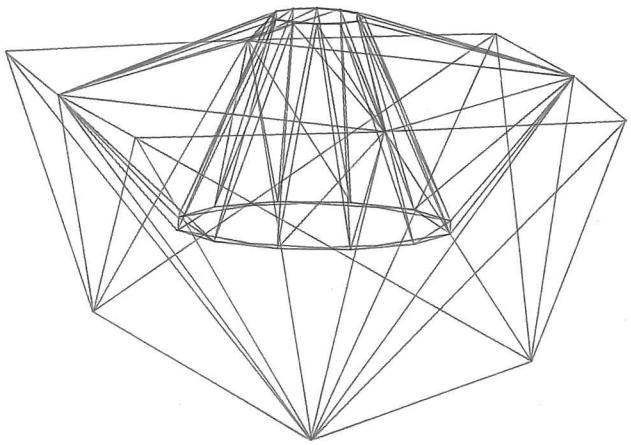

Fig.A6.1.2b

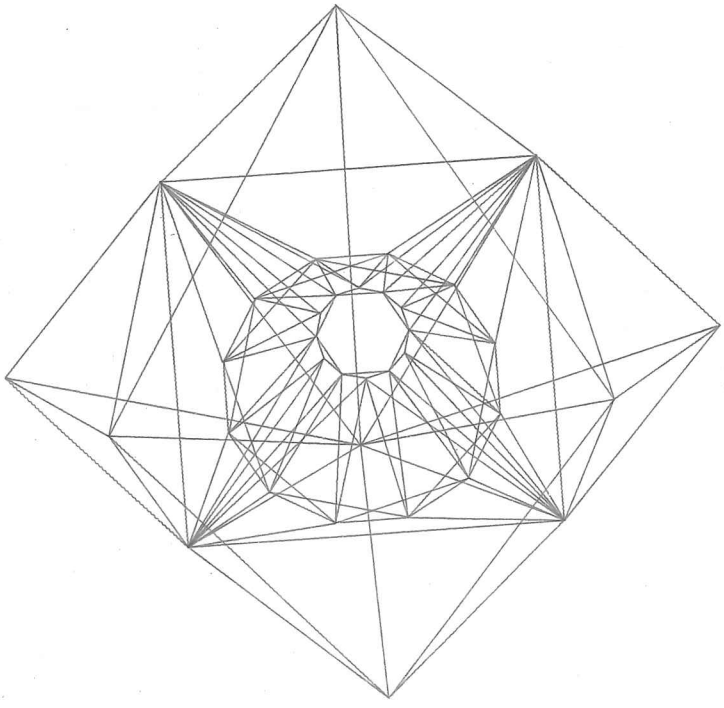

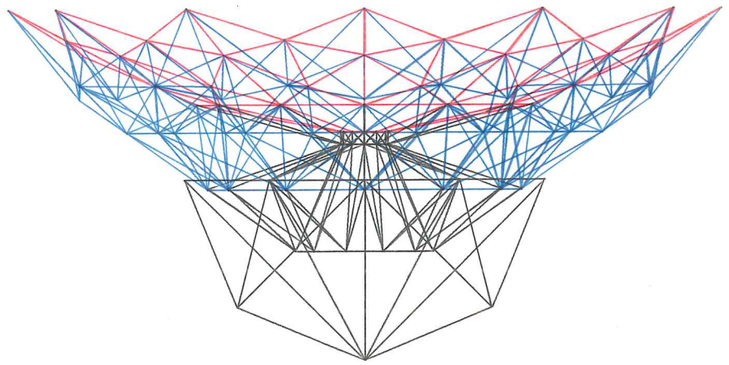

Fig.A6.1.3 - Complete structure.

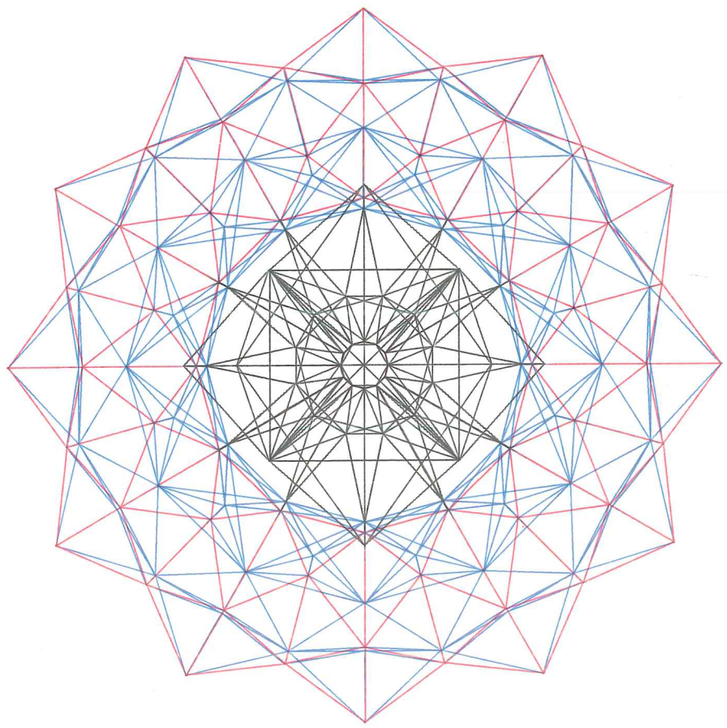

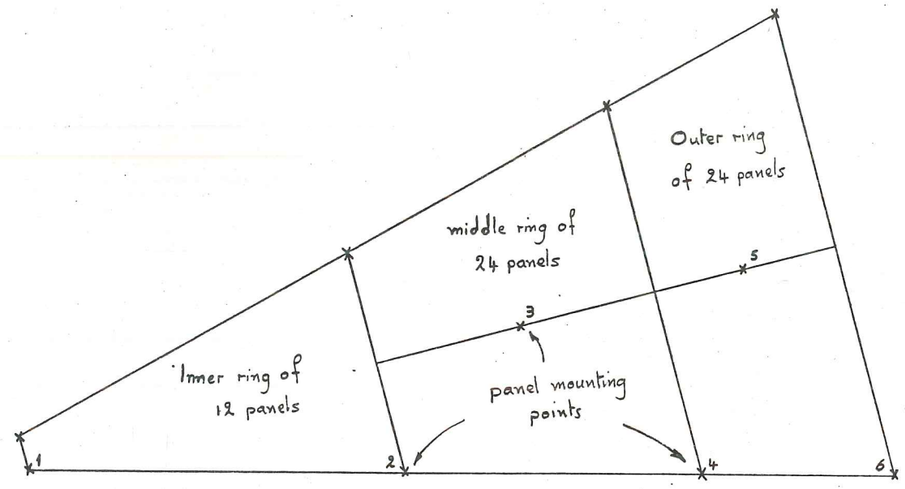

Fig.A6.1.4 - Arrangement of panel mounting points for one cyclic segment.

From the panel mounting arrangement shown in figure A6.1.4, it can be seen that the position of the mounting points is governed by the size and shape of the panels. Now the size of the panels dictates the value of the panel loading taken at each point and it has been found that the smoother the variation of loading over the six points, the easier it is to obtain good homological behaviour. Thus, by careful design, the panel loading for the arrangement shown above, can be made to be equal for support points 2 to 5 and half the value at points 1 and 6 – so producing the smoothest possible arrangement of panel loads.

Appendix 6.2 - Computer Generated Stereo Pictures

In order to produce an image of a three-dimensional object on a two-dimensional surface one of the three dimensions must be ignored. This is also what happens on the retina of the human eye! Now by viewing a three-dimensional object from two slightly different positions, and comparing the two images produced, information about the third dimension can be obtained - which is how our brain forms the three-dimensional images we have of our surroundings. Thus, by presenting each eye with a single two-dimensional picture which is suitably different from that seen by the other eye, we can trick our brain into thinking it is receiving the images produced by viewing a real three-dimensional object, and so form a three-dimensional image.

By using a digital plotter, driven by a computer, it is possible to produce the two slightly different pictures necessary to form a 'stereo pair' quickly and accurately. Each picture is obtained by drawing the two-dimensional projection of the perspective view seen by each eye - see figure A6.2.1. In this case, the perspective viewing routine FROM3*, provided by the GINO graphics package, is used - see box A6.2.2.

Examples of stereo-pairs produced in this way are included in the pocket at the end of this volume.

---

*GINO-F User Manual Issue 2 - CAD Centre, Madingley Road, Cambridge.

x, y and z are the picture axes and α_x, α_y and α_z the rotation of the picture axes about the GINO axes X_g, Y_g and Z_g.

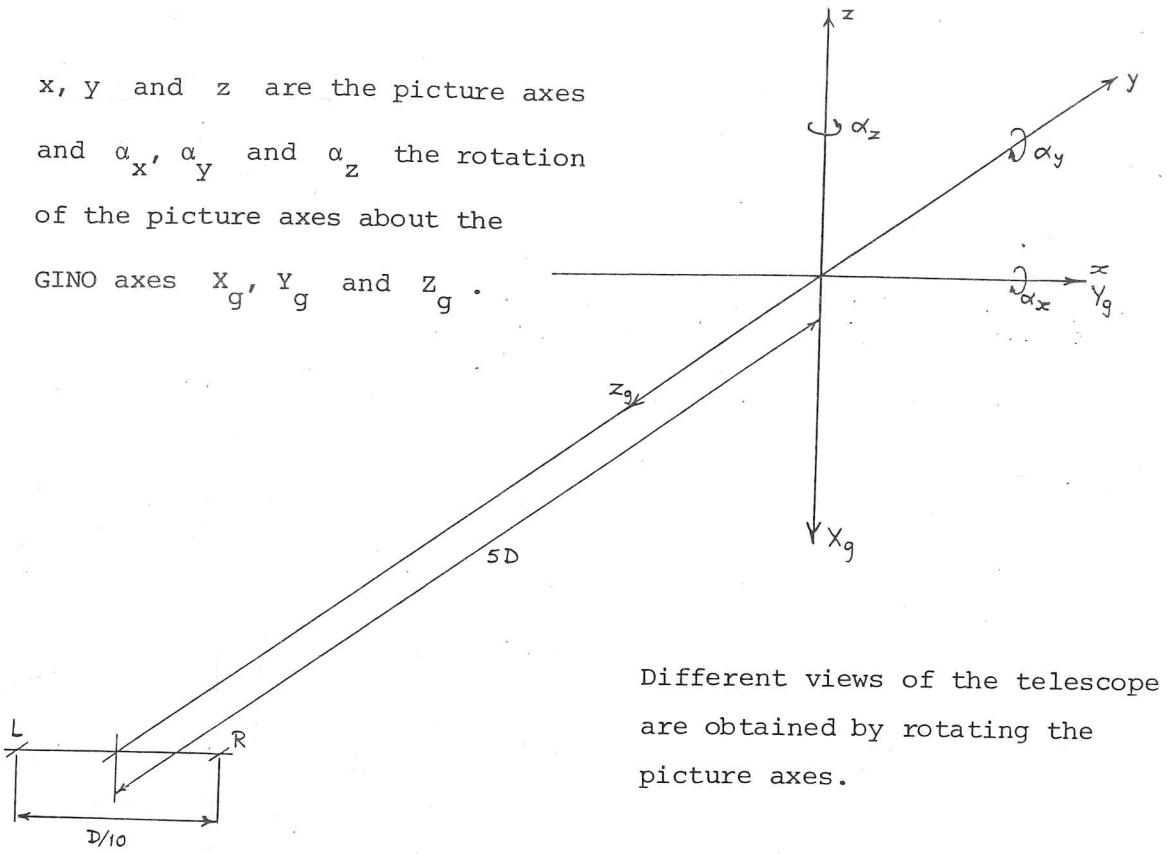

Different views of the telescope are obtained by rotating the picture axes.

Fig.A6.2.1 - Perspective Views for Stereo Pair Generation.

Each picture is produced full size and then scaled down to fit on an A5 sheet of paper - see examples. (D is the telescope diameter.)

```
CALL FROM3(0.0,-D/20,5D)   - Left view point.
CALL ROTSET(αx,αy,αz)      - Rotate structure to desired position.
CALL PICY                  - Draws perspective view.
CALL RESET                 - Cancels rotations.
CALL FROM3(0.0,D/20,5D)    - Right view point.
CALL ROTSET(αx,αy,αz)
CALL PICY
```

Box.6.2.2 - Program subroutine calling sequence used to produce stereo pairs of a given view.

Appendix 6.3 - A Semi-Rigid Joint Model

6.3.1 - Joint model definition

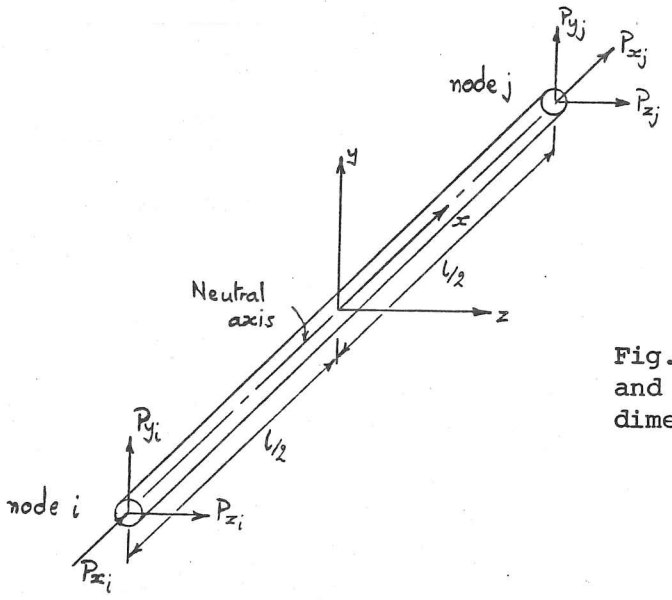

Fig.A6.3.1 - Co-ordinate axes and end-loads for a three-dimensional tubular element.

The load-displacement relationship for a three-dimensional line element defined with respect to its local co-ordinate system is given by [*]:-

$$\underline{P}_i = \underline{K}_{ii}\underline{d}_i + \underline{K}_{ij}\underline{d}_j$$
$$\underline{P}_j = \underline{K}_{ji}\underline{d}_i + \underline{K}_{jj}\underline{d}_j \qquad \text{(A6.3.1)}$$

For a tubular element which possesses only axial strength and some shear strength depending on its slenderness ratio, the stiffness matrices defined in equation (A6.3.1) are given by:

$$\underline{K}_{ii} = \underline{K}_{jj} = \begin{bmatrix} AE/L & 0 & 0 \\ 0 & 12kEI/L^3 & 0 \\ 0 & 0 & 12kEI/L^3 \end{bmatrix}$$

and $\underline{K}_{ij} = \underline{K}_{ji} = -\underline{K}_{ii}$

---

* Livesley, R.K. - Matrix Methods of Structural Analysis, 2nd Ed., Pergamon Press, 1975, pp.32.

where E = Youngs modulus,

A = Cross-sectional area of element,

I = Second moment of area of element cross-section,

L = Length of element,

and $k = \frac{1}{2}$ - to produce the semi-rigid lateral stiffness components,

where r_g = radius of gyration of the element cross-section.

Equation (A6.3.1) may thus be rewritten in the form:

$$\begin{aligned} \underline{P}_i &= \underline{K}_{ii}\underline{d}_i - \underline{K}_{ij}\underline{d}_j \\ \underline{P}_j &= -\underline{K}_{ij}\underline{d}_i + \underline{K}_{ii}\underline{d}_j \ . \end{aligned} \qquad \text{(A6.3.2)}$$

Transforming into global co-ordinate space equation (A6.3.2) becomes:

$$\begin{aligned} \underline{P}'_i &= \underline{\underline{T}}\underline{K}_{ii}\underline{T}^T\underline{d}'_i - \underline{\underline{T}}\underline{K}_{ij}\underline{T}^T\underline{d}'_j \\ \underline{P}'_j &= -\underline{\underline{T}}\underline{K}_{ij}\underline{T}^T\underline{d}_i + \underline{\underline{T}}\underline{K}_{ii}\underline{T}^T\underline{d}'_j \end{aligned} \qquad \text{(A6.3.3)}$$

where $\underline{P}'_i$, $\underline{P}'_j$, $\underline{d}'_i$ and $\underline{d}'_j$ are the global load and displacement vectors for nodes i and j respectively, and $\underline{T}$ is the co-ordinate transformation matrix.

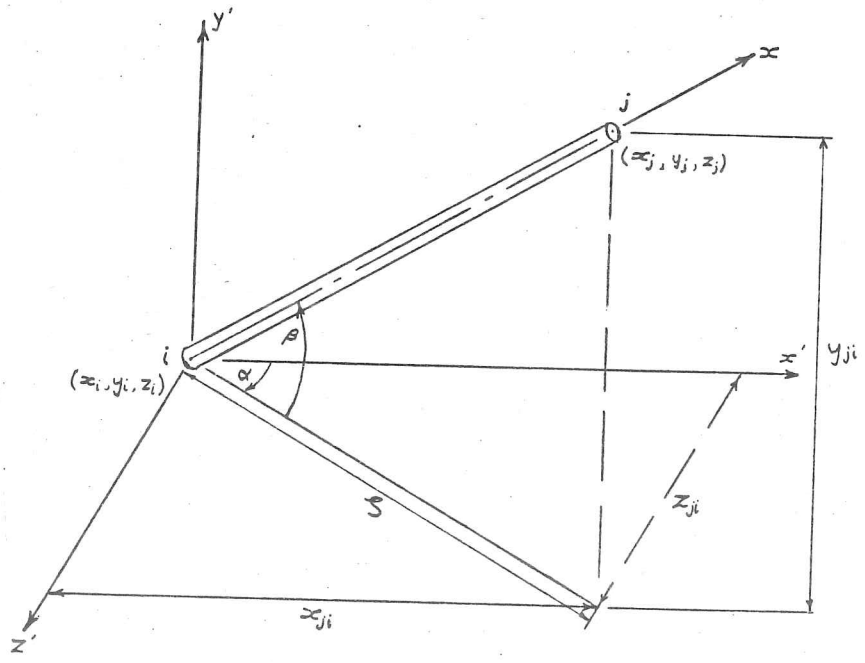

Fig.A6.3.2 - Co-ordinate transformation.

From figure A6.3.2 the transformation matrix $\underline{T}$ can be defined as:

$$\underline{T} = \begin{bmatrix} x_{ji}/L & -x_{ji}y_{ji}/L\zeta & -z_{ji}/\zeta \\ y_{ji}/L & \zeta/L & 0 \\ z_{ji}/L & -y_{ji}z_{ji}/L\zeta & x_{ji}/\zeta \end{bmatrix} \quad \text{for} \quad \zeta > 0$$

$$\text{or} \quad \underline{T} = \begin{bmatrix} 0 & -1 & 0 \\ 1 & 0 & 0 \\ 0 & 0 & 1 \end{bmatrix} \quad \text{for} \quad \zeta = 0 \quad \text{and} \quad y_{ji} > 0 \qquad \text{(A6.3.4)}$$

$$\text{or} \quad \underline{T} = \begin{bmatrix} 0 & 1 & 0 \\ -1 & 0 & 0 \\ 0 & 0 & 1 \end{bmatrix} \quad \text{for} \quad \zeta = 0 \quad \text{and} \quad y_{ji} < 0$$

where $x_{ji} = x_j - x_i$, $y_{ji} = y_j - y_i$, $z_{ji} = z_j - z_i$

and $\zeta = \sqrt{z_{ji}^2 + x_{ji}^2}$.

6.3.2 - Joint model experiment

To compare the displacement behaviour of a pin-joint, rigid joint and semi-rigid joint model, the displacement behaviour of a simple cantilever structure is considered - see figure A6.3.3. All members are of length L cross-section area A , section radius of gyration r_k and Youngs modulus E . The loads $\underline{P}_3$, $\underline{P}_4$ and $\underline{P}_5$ are in the proportion

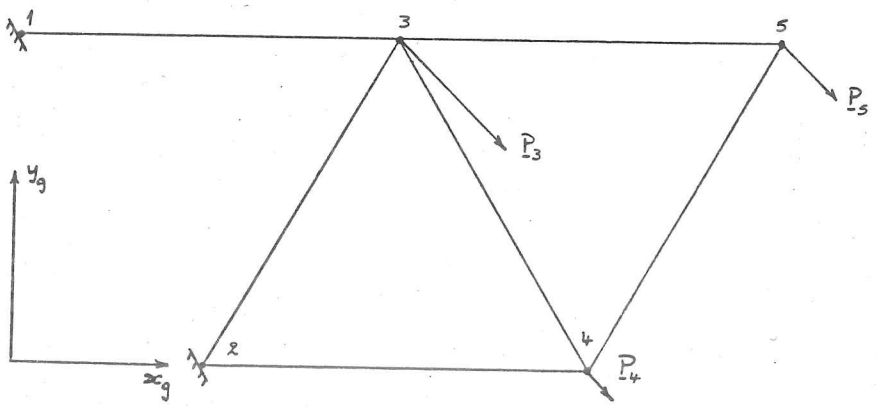

Fig.A6.3.3 - Joint model test structure.

$\underline{P}_3 : 5\underline{P}_4 : 2\underline{P}_3$ - to represent the typical loading on one radial rib of a telescope structure.

The Load-Displacement relationship for each joint, relative to the global co-ordinate system (x_g, y_g) is given by:

$$\underline{P}_i = \underline{\underline{TK}}_{ii}\underline{T}^T\underline{d}_i - \underline{\underline{TK}}_{ik}\underline{T}^T\underline{d}_j$$

$$\underline{P}_j = -\underline{\underline{TK}}_{ji}\underline{T}^T\underline{d}_i + \underline{\underline{TK}}_{jj}\underline{T}^T\underline{d}_j$$

where $\underline{P}_i$, $\underline{P}_j$, $\underline{d}_i$ and $\underline{d}_j$ are the global load and displacement vectors respectively for nodes i and j, and $\underline{T}$ is the local to global co-ordinate transformation matrix.

For the pin-joint model:

$$\underline{K}_{ii} = \underline{K}_{jj} = \underline{K}_{ij} = \underline{K}_{ji} = \begin{bmatrix} AE/L & 0 \\ 0 & 0 \end{bmatrix}$$

and $\underline{P}_i = \begin{bmatrix} P_x \\ P_y \end{bmatrix}_i$, $\underline{P}_j = \begin{bmatrix} P_x \\ P_y \end{bmatrix}_j$, $\underline{d}_i = \begin{bmatrix} d_x \\ d_y \end{bmatrix}_i$ and $\underline{d}_j = \begin{bmatrix} d_x \\ d_y \end{bmatrix}_j$

For the rigid-joint model:

$$\underline{K}_{ii} = \begin{bmatrix} EA/L & 0 & 0 \\ 0 & 12EJ/L^3 & 6EI/L^2 \\ 0 & 6EJ/L^2 & 4EI/L \end{bmatrix}, \quad \underline{K}_{jj} = \begin{bmatrix} EA/L & 0 & 0 \\ 0 & 12EI/L^3 & -6EI/L^2 \\ 0 & -6EJ/L^2 & 4EI/L \end{bmatrix}$$

and $\underline{K}_{ij} = \underline{K}_{ji}^T = \begin{bmatrix} EA/L & 0 & 0 \\ 0 & 12EI/L^3 & -6EI/L^2 \\ 0 & 6EI/L^2 & 4EI/L \end{bmatrix}$

and $\underline{P}_i = \begin{bmatrix} P_x \\ P_y \\ m \end{bmatrix}_i$, $\underline{P}_j = \begin{bmatrix} P_x \\ P_y \\ m \end{bmatrix}_j$, $\underline{d}_i = \begin{bmatrix} d_x \\ d_y \\ 0 \end{bmatrix}_i$ and $\underline{d}_j = \begin{bmatrix} d_x \\ d_y \\ 0 \end{bmatrix}_j$

For the semi-rigid joint model:

$$\underline{K}_{ii} = \underline{K}_{jj} = \underline{K}_{ij} = \underline{K}_{ji} = \begin{bmatrix} EA/L & 0 \\ 0 & 6EI/L^3 \end{bmatrix}$$

and $\underline{P}_i = \begin{bmatrix} P_x \\ P_y \end{bmatrix}_i$, $\underline{P}_j = \begin{bmatrix} P_x \\ P_y \end{bmatrix}_j$, $\underline{d}_i = \begin{bmatrix} d_x \\ d_y \end{bmatrix}_i$ and $\underline{d}_j = \begin{bmatrix} d_x \\ d_y \end{bmatrix}_j$

The results of varying the slenderness ratio (L/r_g) are presented in figures 6.3.1a,b,c of chapter 6.

UNIVERSITY
LIBRARY
CAMBRIDGE

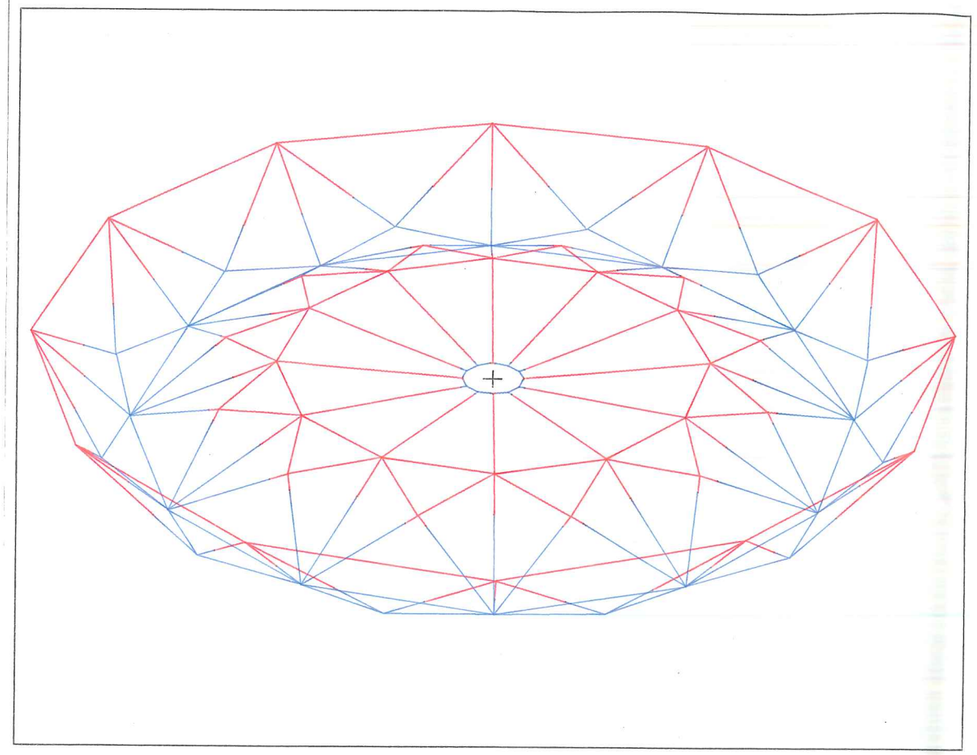

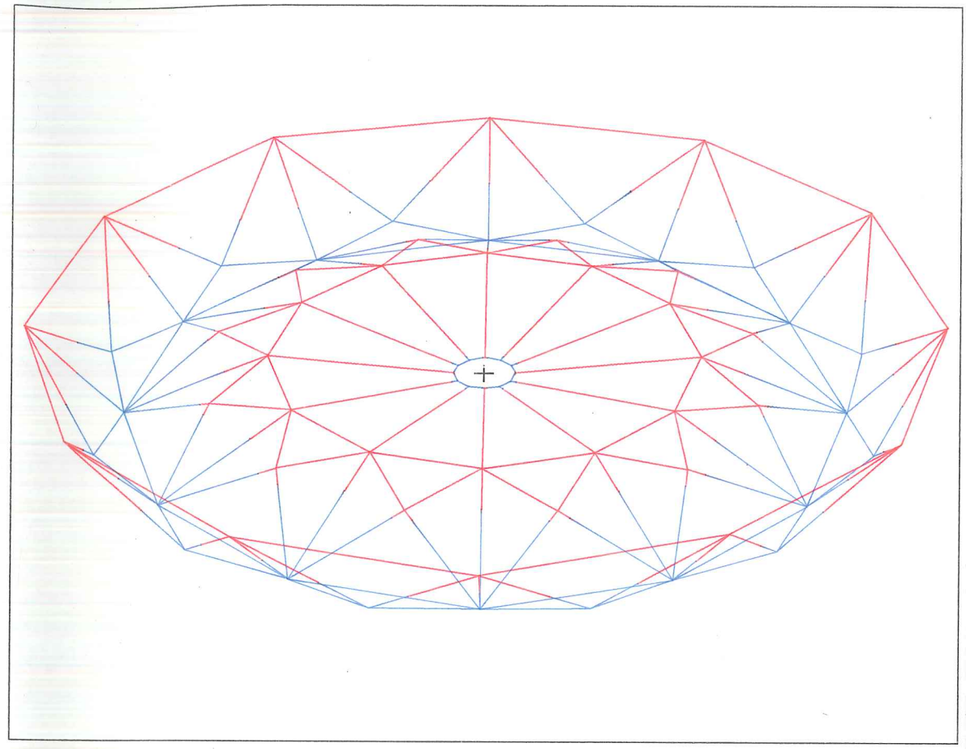

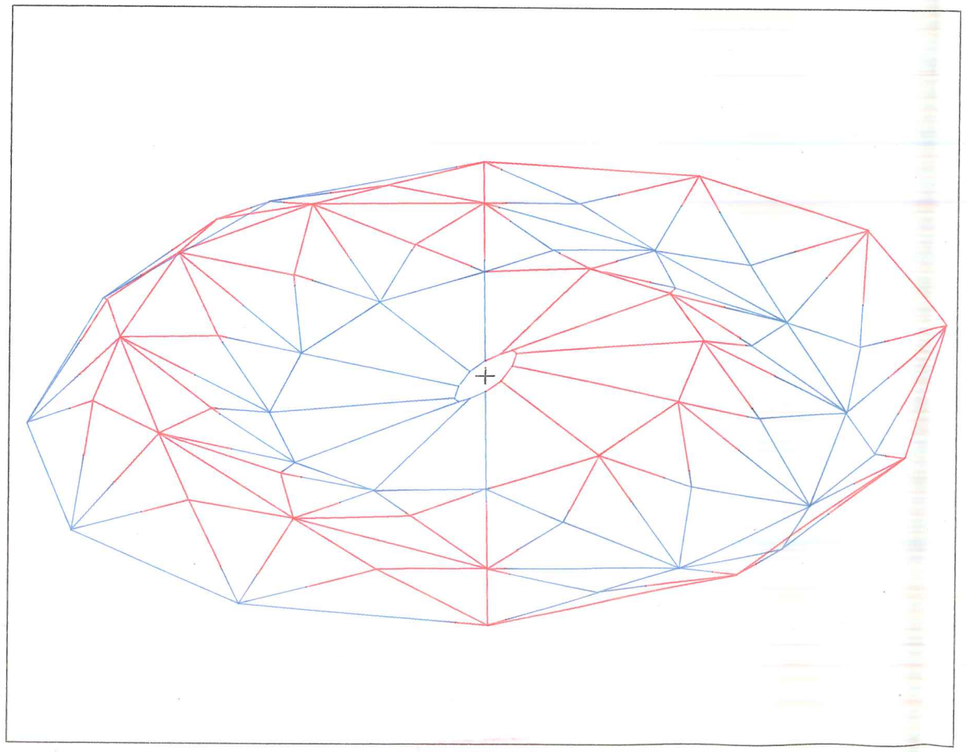

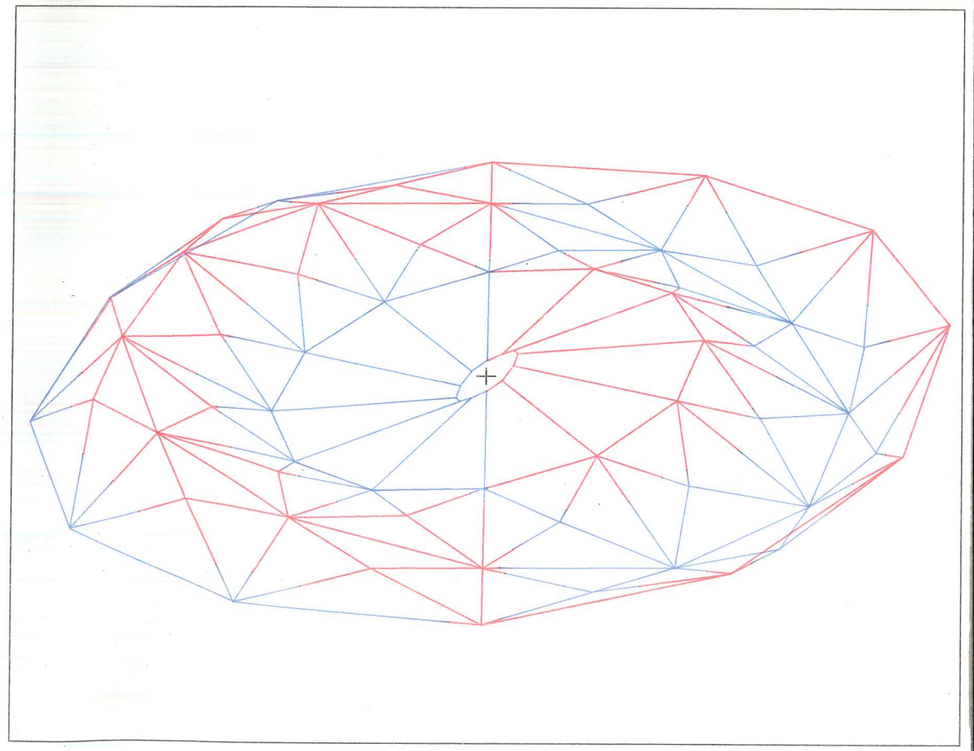

Stereo pairs of the homology deviation surfaces given in fig.6.5.1.

UNIVERSITY
LIBRARY
CAMBRIDGE

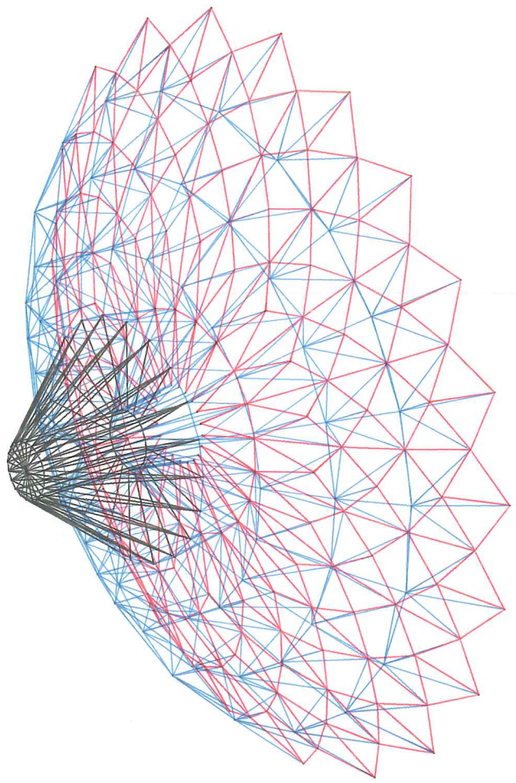

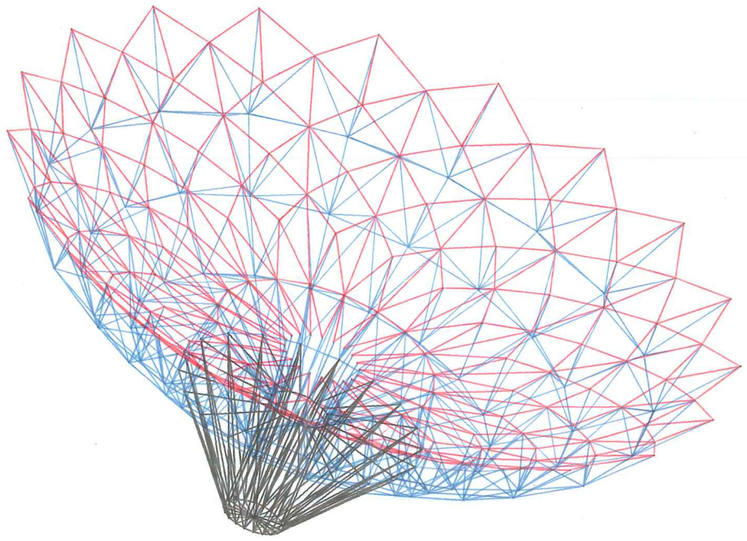

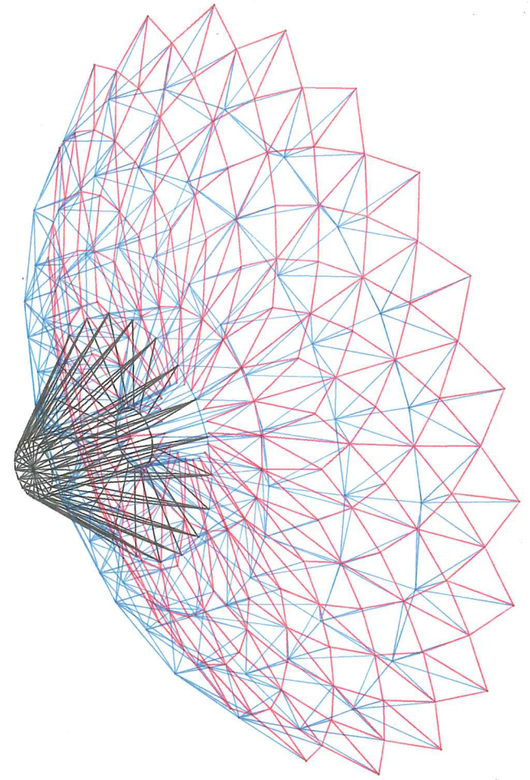

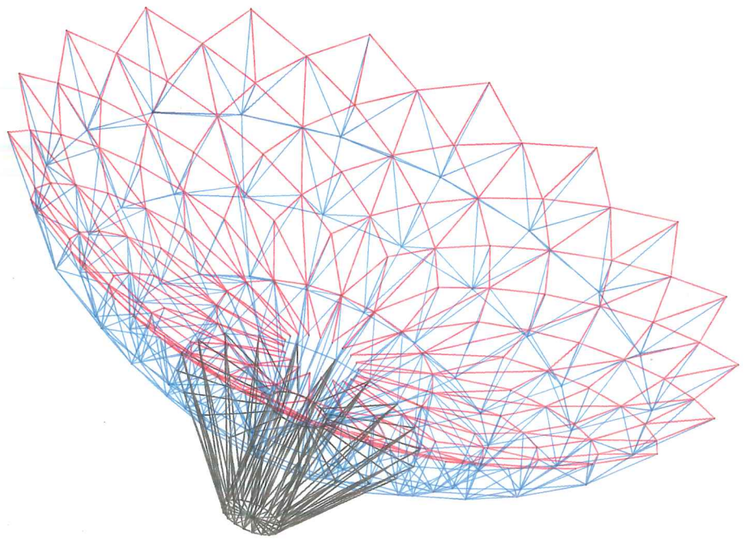

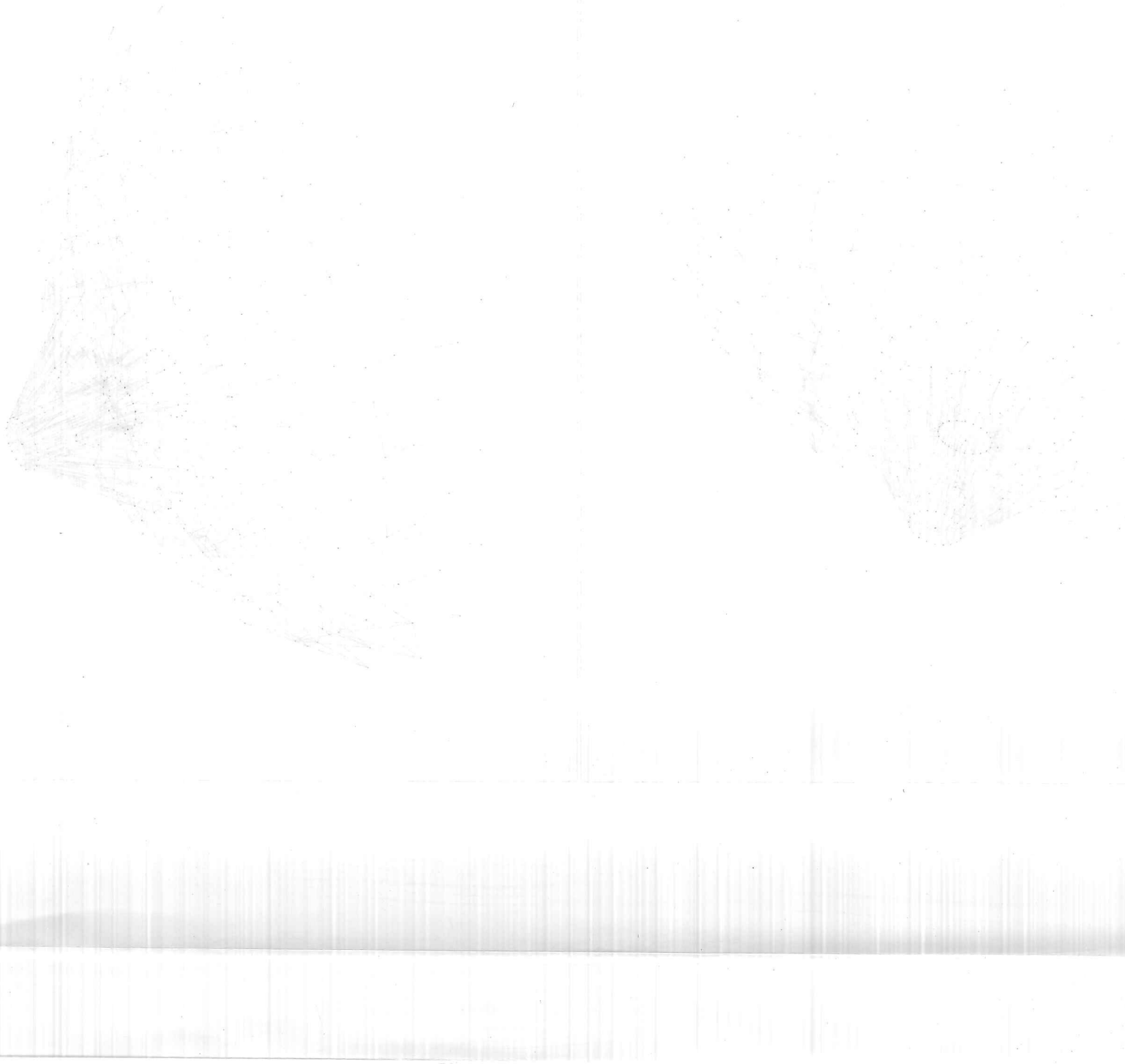

Stereo pairs of an early version of the U.K. Millimetre Wave Telescope Structure.

UNIVERSITY
LIBRARY
CAMBRIDGE

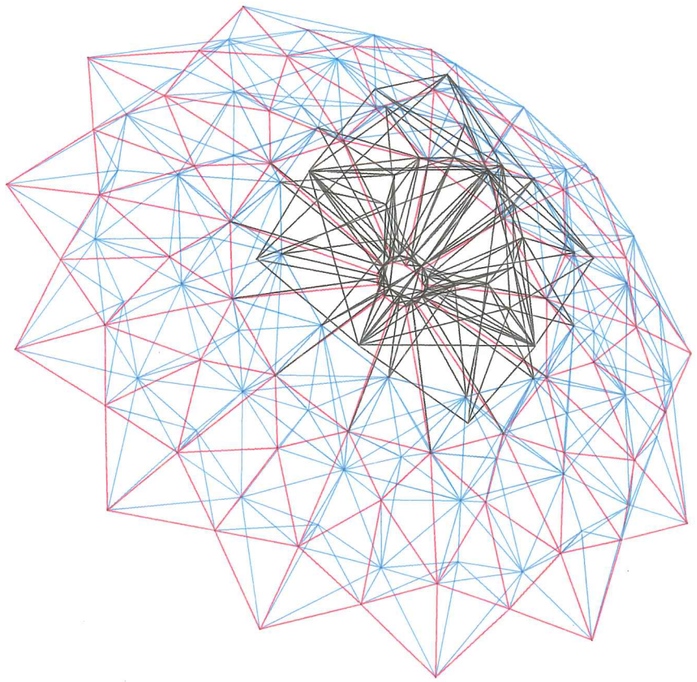

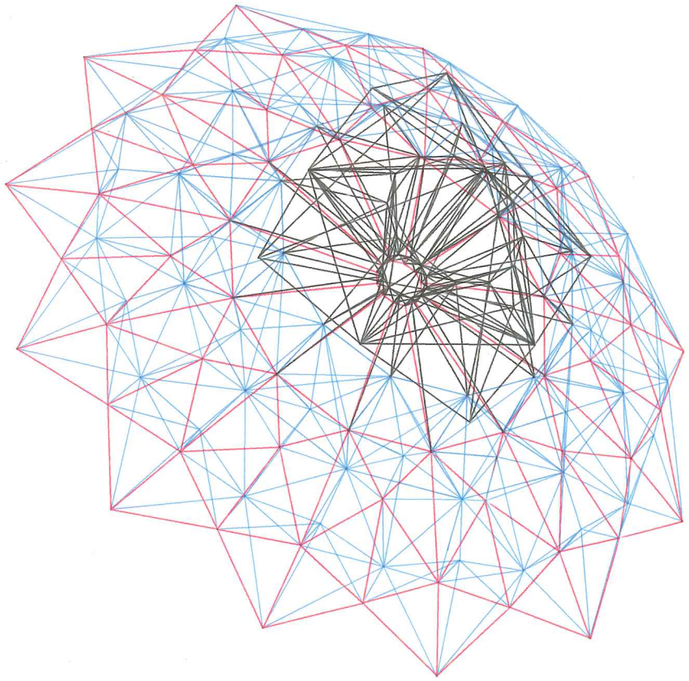

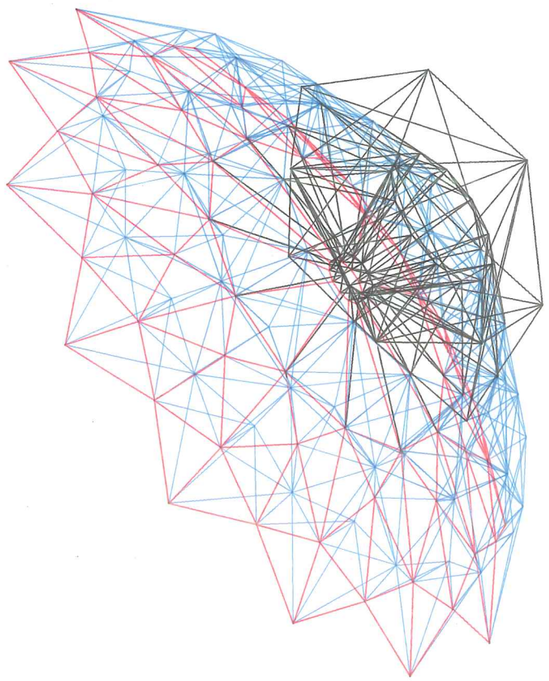

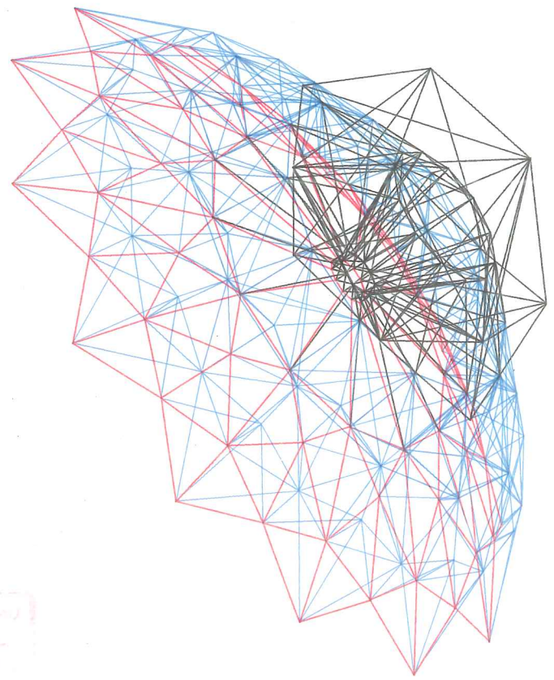

Stereo pairs of the two views given in fig.6.1.2 (and the same as those in fig.6.2.1).

UNIVERSITY
LIBRARY
CAMBRIDGE

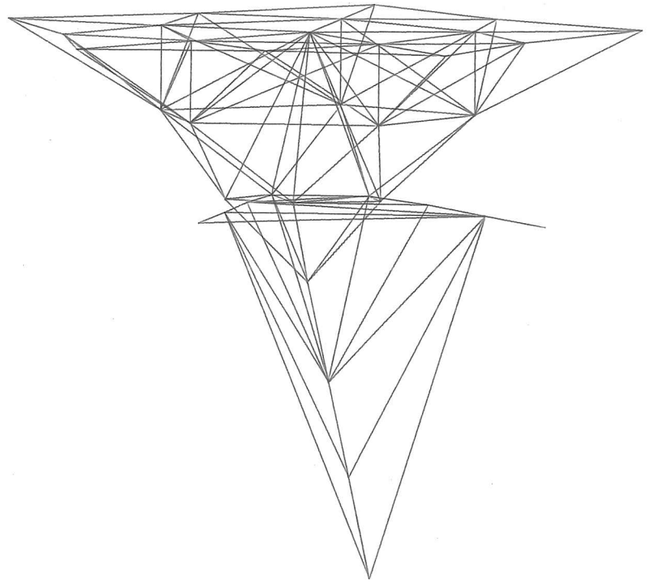

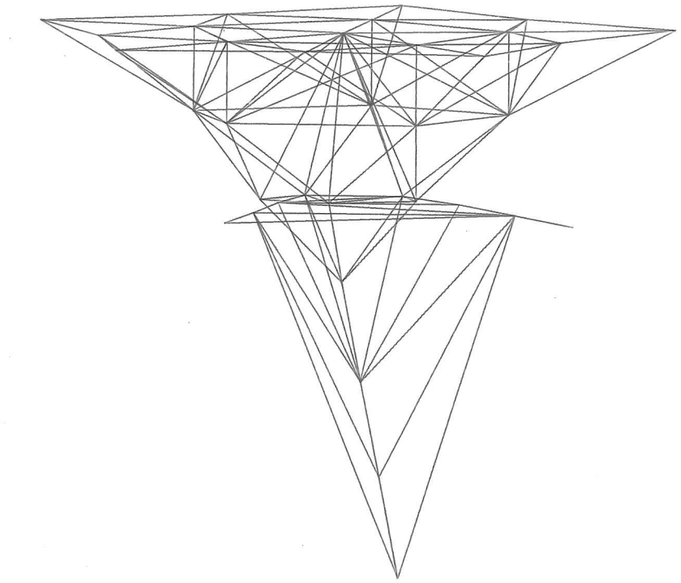

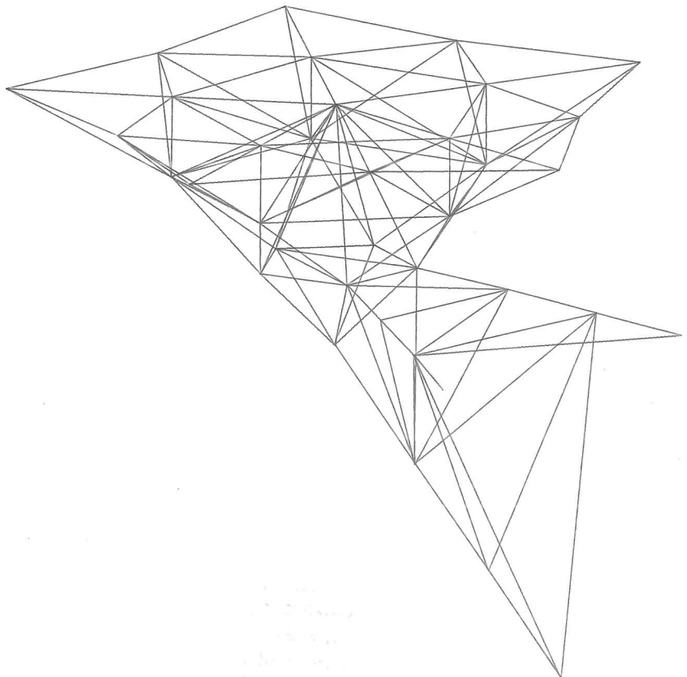

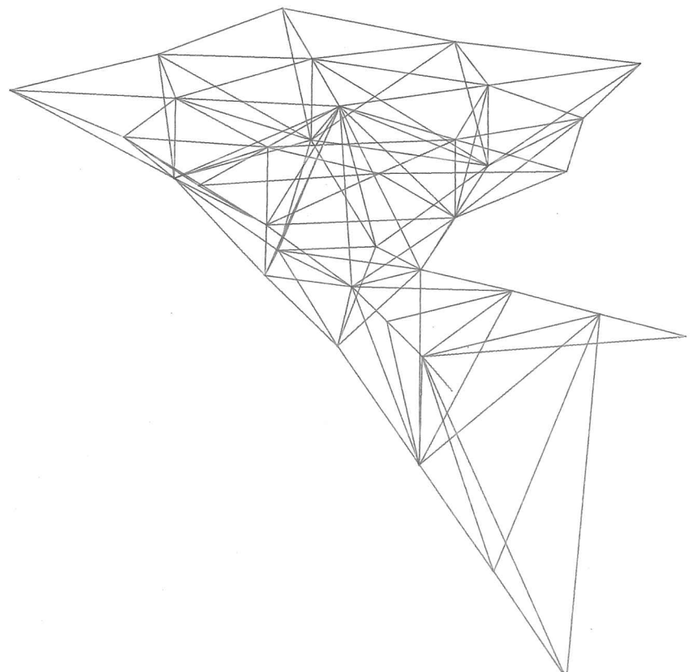

Stereo pairs of the Helipad Structure described in Chapter 4 and Appendix 4.2.

UNIVERSITY
LIBRARY
CAMBRIDGE